University of Southern Queensland

Faculty of Health, Engineering and Sciences

Modelling and analysis of multi-junction photovoltaic cells using MATLAB/Simulink for the improvement of conversion efficiency.

A dissertation submitted by

Anthony Laurent

in fulfilment of the requirements of

ENG4111 and 4112 Research Project

towards the degree of

Bachelor of Engineering (Honours) (Electrical)

Submitted November, 2016

Abstract

Multijunction solar cells (MJSCs) are a more efficient photovoltaic solar cell technology than the conventional single junction alternative. When used in conjunction with concentrator technology MJSCs can provide conversion efficiencies upwards of 40% - due to a better conversion response to a broader light spectrum. Iterative design methodology can be applied to derive models of conversion efficiency in MJSCs by adapting existing single junction solar cell (SJSC) modelling practices. However this can be a very time consuming process, given the abundance of literature regarding conversion efficiency in SJSCs

This dissertation provides several criteria to consider when designing MJSC conversion efficiency models, by addressing two research questions: (1) how is the conversion efficiency of MJSCs simulated within the Matlab/Simulink environment?, (2) and which of the existing SJSC modelling practices are more/less adaptable for simulating MJSCs in the Simulink environment.

The first part of the literature review outlines the peer reviewed literature regarding SJSC model practices and discusses the results of the project simulation tests. The second part of the review (1) outlines the literature on MJSC architecture related to model design, (2) proposes an iteration of a SJSC model that simulates the conversion efficiency in MJSCs and (3) discusses the results of the proposed model tested under Simulink simulation.

The simulation results confirmed that, as expected, the double diode model provides more accurate results than the single diode model, with respect to changes in temperature and changes in irradiance. The simulation results confirmed that the proposed model correctly simulated the conversion efficiency in MJSCs with respect to irradiance, but failed to correctly simulate the conversion efficiency in MJSCs with respect to temperature.

This paper offers insight into appropriate and inappropriate SJSC modelling techniques to consider when applying iterative design methodology to design a model that correctly simulates MJSC conversion efficiency within the Matlab/Simulink environment.

University of Southern Queensland

Faculty of Health, Engineering and Sciences

ENG4111 & ENG4112 Research Project

Limitations of Use

The Council of the University of Southern Queensland, its Faculty of Health, Engineering & Sciences, and the staff of the University of Southern Queensland, do not accept any responsibility for the truth, accuracy or completeness of material contained within or associated with this dissertation.

Persons using all or any part of this material do so at their own risk, and not at the risk of the Council of the University of Southern Queensland, its Faculty of Health, Engineering & Sciences or the staff of the University of Southern Queensland.

This dissertation reports an educational exercise and has no purpose or validity beyond this exercise. The sole purpose of the course pair entitled “Research Project” is to contribute to the overall education within the student’s chosen degree program. This document, the associated hardware, software, drawings, and other material set out in the associated appendices should not be used for any other purpose: if they are so used, it is entirely at the risk of the user.

Certification

I certify that the ideas, designs and experimental work, results, analyses and conclusions set out in this dissertation are entirely my own effort, except where otherwise indicated and acknowledged.

I further certify that the work is original and has not been previously submitted for assessment in any other course or institution, except where specifically stated.

Anthony Laurent

Student Number : 0061021918

Acknowledgements

It would not have been possible to complete this dissertation, let alone my undergraduate studies, if my lovely wife Kristen had not been so unflinchingly supportive. My two fantastic kids and loving parents also deserve a very heart-felt thanks

Many thanks to my Principal Supervisor, Dr Narottam Das, for providing me with this research opportunity - I have learned a great deal throughout this project. I would like to express my sincerest gratitude to my project Co-supervisor, Mr Andreas Helwig, whose guidance and support will not be forgotten by myself or Kristen. I am also grateful to Dr Les Bowtell and Associate Professor Alexander Kist for their support towards the successful completion of this dissertation.

Table of Contents

Table of Figures

List of Tables

Nomenclature

a	ideality factor for the diffusion current component of diode (D1 model)
a1	ideality factor for the diffusion current component of diode 1 (D2 model)
a2	ideality factor for the rccombination current component of diode 2 (D2 model)
D1	Single diode model
D2	Double diode model
Eg	bandgap energy (eV)
FF	fill factor
Gc	actual measured irradiance of the PV cell
Gstc	reference irradiance under standard test conditions (1000 W/m2)
I	total current that is generated by the cell, minus losses
Iph	the photon generated current
Iph_stc	photocurrent under STC conditions, and can be approximated by Isc_stc
I_{RS}	the voltage across the series resistances
Irs	the recombination current, is used to determine the saturation current.
Is	the diode saturation current for the D1 model - measured under reverse bias dark conditions and usually referred to as the reverse saturation current, saturation current or leakage current
I_{s1}	the first diode dark/reverse saturation current for the D2 model - measured under reverse bias dark conditions and usually referred to as the reverse saturation current, saturation current or leakage current
I_{s2}	the second diode saturation current for the D2 model - measured under reverse bias dark conditions and usually referred to as the reverse saturation current, saturation current or leakage current
Isc	the short circuit current, or when voltage is zero
Isc_stc	Isc measured under STC
J	current density. When comparing the characteristics of a device, the current can be normalised to the respective area of the device.

k	Boltzmann’s constant, 1.381*10(-23)
K_I	temperature coefficient for the short circuit current (mA / °K)
K_V	temperature coefficient for the open circuit voltage (mV / °K)
λ	photon wavelength
λ_{BG}	bandgap wavelength
MJSC	multi-junction solar cell
Ns	the number of cells in the PV cell module
Pe	the sum of ideality factor a1 and ideality factor a2.
P_{in}	input power (W)
VI curve	Voltage current curve. Often denoted in the literature as IV curve
VP curve	Voltage power curve. Often denoted in the literature as PV curve
P_{mpp}	power at the maximum power point (W)
q	the charge of an electron, 1.602*10(-19)
SJSC	single junction solar cell
STC	Standard test conditions (Gstc = 1000 W/m2 and Tstc = 25°C)
V	total voltage generated by each cell
V_D	voltage across the PV cell diode,
V_{oc_stc}	open current voltage measured under STC conditions
Vt	the Temperature dependant voltage for Ns cells (at any temperature)
R_P	represents the shunt losses within the PV cell
R_S	represents the series losses within the PV cell
T_C	the actual measured temperature of the PV cell (°C)
T_{STC}	the reference temperature under standard test conditions (25°C / 298°K)

Chapter 1: Introduction

1.1. Context

The conventional single junction solar cell is made of two bands of oppositely charged semiconductor materials separated by a third neutral band material. Photons of a particular wavelength will permeate the solar cell to the lower positively charged band, and according to Bohr's Atomic Model, will collide into the band-atoms with such force that the atom-electrons are excited (knocked free) from their valence.

In an ideal solar cell the electron is forced into the negatively charged conduction band to remain separated from its valence hole by the neutral band. This process becomes useful when an external conduction wire bridges the bands such that an electrical current is produced by the action of the electron-hole pair recombination.

Multijunction solar cells (MJSCs) respond to a range of photon wavelengths and provide a greater conversion efficiency. And as the production of MJSCs becomes more commonplace, iterative design methodology will play a greater role in design, by enabling the adaption of proven SJSC modelling practices to model conversion efficiency in MJSCs.

1.2. Problem Specification

The first problem is to determine how single junction solar cell (SJSC) conversion efficiency is modelled in Simulink. A literature review will be conducted to investigate the differences between single diode models and double diode models.

The second problem is to determine which of the SJSC modelling practices are more/less adaptable when modelling conversion efficiency in MJSCs. A further literature review will be conducted to propose an iterative Simulink model that will simulate the conversion efficiency of several proven MJSCs.

1.3. Aim and objectives

The main aim of this dissertation was to provide a standardised D2 equivalent circuit model to the conversion efficiency in MJSCs and to identify a range of existing SJSC modelling practices that are more/less adaptable for simulating the conversion efficiency of MJSCs within the Simulink environment.

The modelling techniques reviewed and tested in this paper aim to provide students and researchers a set of criteria that will assist in designing a model to identify which multijunction semiconductor materials convert photons to DC current more efficiently.

1.4. Dissertation Overview

Chapter 1 contains a brief introduction with regards to the project context, problem specifications and project aims.

Chapter 2 contains a brief introduction to several topics including conventional SJSCs, P-N junction diodes, bandgap energy models. A literature review of SJSC subjects include photodiode characteristics, conventional solar cell characteristics and D1 and D2 models. A literature review of MJSC subjects includes structures that influence modelling techniques, loss mechanisms related to MJSCs and provides a chart to assist analysing SJSC and MJSC characteristics.

Chapter 3 contains the project methodology. A Simulink simulation method is proposed for comparing the accuracy of D1 and D2 SJSCs with regards to conversion efficiency, and a Simulink simulation method is proposed for modelling the conversion efficiency of MJSCs

Chapter 4 provides a discussion on the results of the comparative simulation between D1 and D2 SJSCs with regards to conversion efficiency and contains a discussion on the results of the MJSC conversion efficiency simulations.

Chapter 5 contains the project conclusions and outlines the project outcomes, provides a discussion on how the project findings can benefit research, reflections on the project and identifies areas of further research.

Chapter 2: Literature Review

Chapter 2 contains a brief introduction to several topics including conventional SJSCs, P-N junction diodes, bandgap energy models. A literature review of SJSC subjects include photodiode characteristics, conventional solar cell characteristics and D1 and D2 models. A literature review of MJSC subjects includes structures that influence modelling techniques, loss mechanisms related to MJSCs and provides a chart to assist analysing SJSC and MJSC characteristics.

Single junction solar cells (SJSC)

2.1. The conventional single junction silicon solar cell

When defined in a very broad context, a conventional silicon PV cell can be considered as a dual semiconductor diode/device made of a continuous crystalline Silicon (Si) structure. The device converts the sun's light (irradiance) into energy, in the form of direct current (DC) (Chin, Salam & Ishaque 2015).

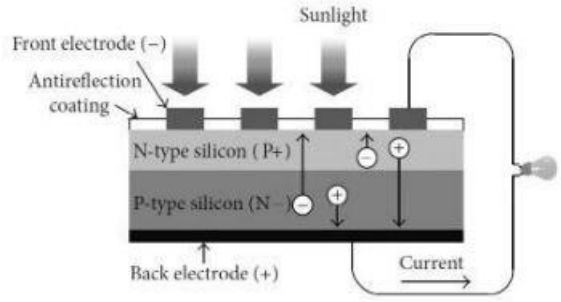

Figure 1: Conventional single junction PV cell. Image from (Chin, Salam & Ishaque 2015).

Figure 1 shows one representation/model that succinctly encompasses the fundamental behaviour of a single Si PV cell. A phenomenon, commonly termed the photoelectric effect, occurs within the p-n junction, where sun light photons of a particular wavelength are absorbed into the PV cell (Chin, Salam & Ishaque 2015), creating a forced reaction whereby an electron is excited from its valence and allowed to flow as current through the external wire conductor.

Although Figure 1 provides a succinct overview of the conventional silicon PV cell, it lacks the sophistication to describe the conversion efficiency limitations of the crystalline silicon PV semiconductor material.

The modelling in this paper will be based on compact modelling where device characteristics are described by measuring equivalent circuit models consisting of of lumped components.

In a single diode (D1) model, for example, photons are represented by a DC current source and the bulk behaviour of the solar cell is represented by an ideal diode. The double diode (D2) model allows for an extra layer of complexity, where the second diode represents the behaviour of the solar cell depletion region, hence, there will be some discussion and research of atomic concepts.

However it is not within the scope of this paper to model the atomic concepts in detail. Physical parameters such as cell thickness, junction thickness, and doping concentrations are ignored, and it is assumed that bandgap energies are ideal and the characteristic behaviour is predictable.

Likewise, the modelling of atomic parameters such as carrier concentrations, diffusivity and recombination rates are not within the scope of this paper, as the design considerations for such related behaviour is generally represented by including a second diode to represent the solar cell depletion region.

2.1.1. The P-N junction diode

Most of the measurable characteristics of a solar cell can be explained by the characteristic behaviours of a P-N junction diode and and its junction bandgap energy.

When the anode terminal of a P-N junction diode is connected to the positive terminal of a battery and the cathode terminal is connected to ground, the diode is said to be forward biased will conduct current to the battery ground. When the anode and cathode terminals are interchanged, the diode is said to be reversed biased and will insulate the current from reaching ground

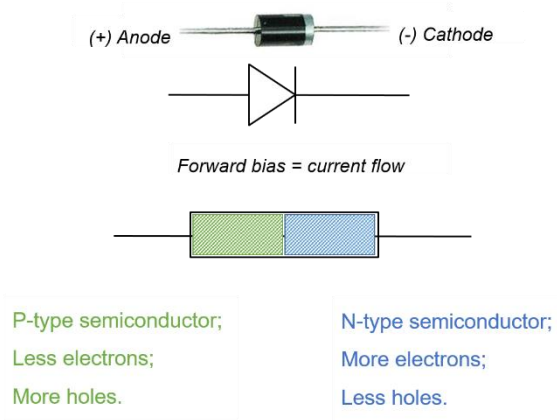

Figure 2: Various representations of a P-N junction diode.

The forward and reverse control of current flow is due to the interaction between the applied electric field of the battery and the built in electric field of the PN junction. When the potential across the diode reaches 0.6 - 0.7V in forward bias, the applied field exceeds the built in field and current flows. When the potential across the diode is in reverse bias, the applied field will then add to the built in field and block the current.

The conventional solar cell utilises the very same P-N junction current control characteristic to convert the suns photons to DC current and much of the observable behaviour in a PN junction and PV solar cell, can be described by the bandgap energy model.

2.1.2. Bandgap energy model

The bandgap model is a very useful tool when designing PV solar cells as it succinctly describes the correlation between material selection and conduction potential. Figure 3 shows an atom with orbiting electrons with specific energy levels, or shells, which are represented by discrete electron volt (eV) energy lines.

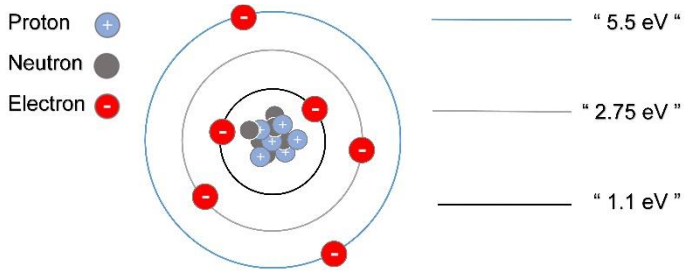

Figure 3: Atom showing three orbitals and their respective energies.

The greater the electron distance from the nucleus – the higher its energy level. When several atoms of the same element bond, the electron shells overlap and the electrons are shared between the atoms and the energy levels are no longer discrete (Figure 4a).

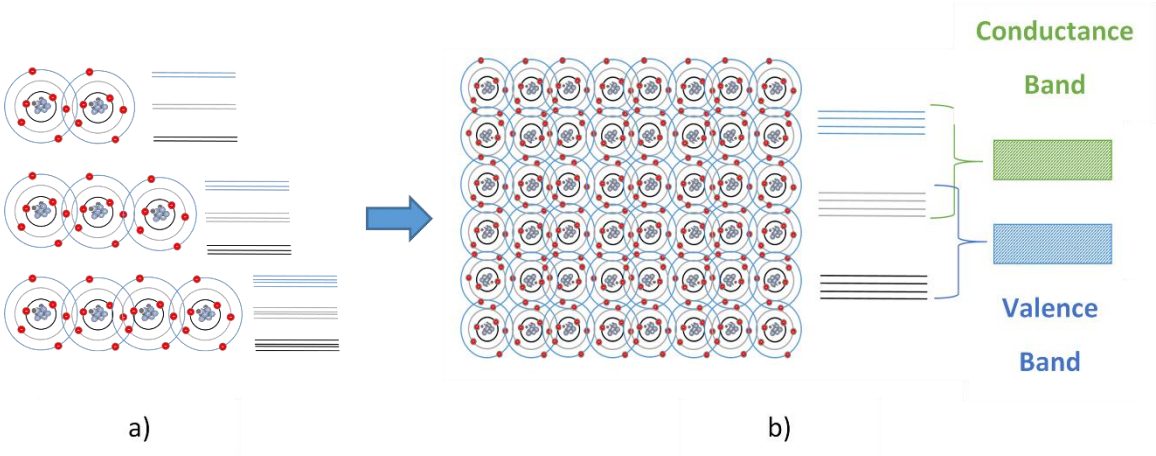

Figure 4: The electrons shells of a) several atoms, and b) countless atoms.

There are countless atoms in solid materials and the effect is magnified so the many overlapping electron energy levels start to spread and energy band ranges emerge (Figure 4b):

- The the lower energy band, known as the valence band, is indicative of the range of valence electron energies for that particular solid.
- The the upper energy band, known as the conduction band, is indicative of electron energies required to induce electron conduction in that particular material.
- The gap/distance between the two bands is indicative of the amount of photon energy required to force an electron from its valence energy state to – the conduction energy state.

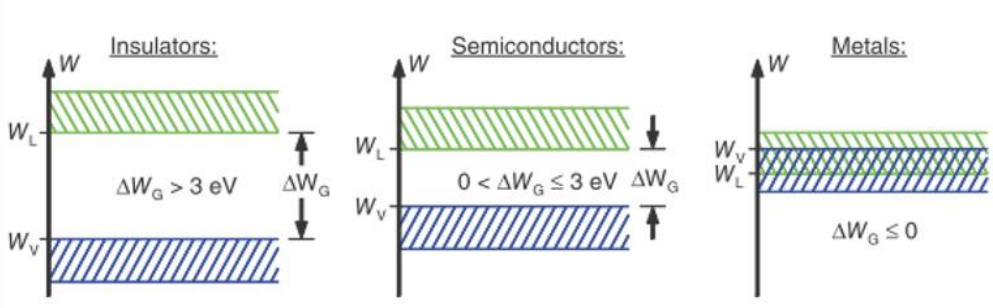

Figure 5: Material state bandgap energies. Image taken form (Mertens & Roth 2014).

Figure 5 denotes the energy difference between the upper band and lower band as W_G. Electrons within the valence shells of conduction materials require no extra energy to change from a valence electron to a free electron. Electrons within the valence shells of insulation materials usually require more than 3ev of energy to clear the bandgap, however this amount of energy would severely compromise the material. Electrons within the valence shells of semiconductor materials require anywhere in the range of 0 to 3ev to clear the bandgap.

It is the ability - to determine the which of the semiconductor materials provide a better conversion response to a broader light spectrum - that makes it possible to design MJSCs with a higher conversion efficiency.

2.2. The photodiode based solar cell model

Given that the solar cell is a photodiode device, then it makes sense that it can be characterised by a diode based equivalent circuit model.

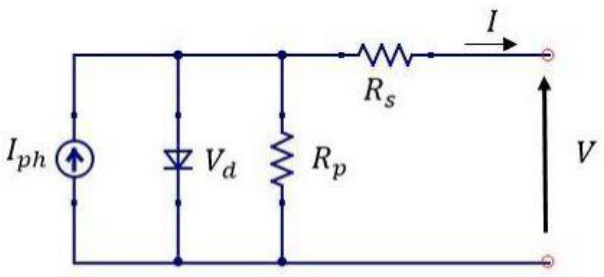

Figure 6: Single diode equivalent circuit.

The following parameters are contained within the equivalent circuit:

- The current source (Iph) that represents the photoelectric effect due to sunlight;
- An ideal diode (Vd) parallel to Iph, representing an ideal PV junction within the solar cell;
- A parallel resistor (Rp) representing the shunt losses within the PV cell;
- A series resistor (Rs) representing the series losses within the PV cell;
- Total current (I), the current that is generated by the cell, minus losses;
- Total voltage (V), the voltage across the load

As circuit theory dictates, equivalent circuit output current (I) will increase if the series resistance is very low to nil and the parallel resistance is very high to infinity. Hence, the characteristic equation for the single diode model, including shunt and series losses, is given by:

$$I = I_{ph} - I_s\left(exp\left(\frac{V+IR_s}{a \cdot V_t}\right) - 1\right) - \frac{V+IR_s}{R_p} \qquad \textit{Equation 1}$$

The photo current is represented by Iph, and the diode current is represented by the transient part of the expression and its co-efficient Is, and the current due to resistances are represented by the fraction/real part of the expression.

2.3. Ideal photodiode and characteristic curves

In 1961 William Shockley and Hans Queisser published a paper containing the derivation of an ideal diode equation (W. Shockley 1961) which provides a means to predict the behaviour of a diode by utilising its super positional qualities. When the diode is exposed to light the electron and hole charges in the p-n junction are separated, generating a forward biased current (González-Longatt 2005). The VI characteristics can be described by subtracting the short circuit current from the 'non illuminated' ideal diode equation (Equation 2 on page 8), and although the diode is reverse biased under dark conditions, the characteristic curve is exactly the same as an illuminated diode.

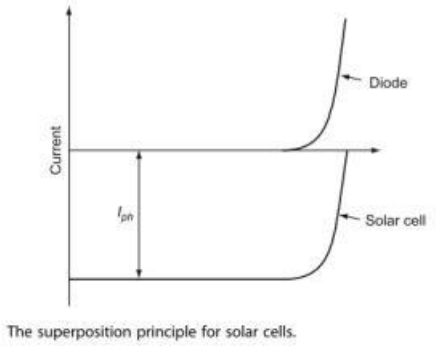

Figure 7: Diode curve characteristics Image from (Markvart & Castañer 2012) .

Figure 7 contains a diagram taken from (Markvart & Castañer 2012):

i. The characteristic of an ideal diode in the dark is represented by the top "Diode" curve;

ii. The characteristic of the diode when exposed to light is represented by the lower "Solar cell" curve;

Consider the single diode equivalent circuit shown in Equation 1, where I_{ph} represents the current generated under sunlight and Id is the current generated when there is no sunlight. Therefore the total current, I, is simply the difference between the diode generated current under light and the diode generated current in the dark (as the two currents flow in opposite directions) (Jha 2009).

The electrical characteristics of the source parallel diode is made up of a real current part and a transient part. The transient/real relationship is more accurately described by William Shockley's ideal diode equation, where I_D is the current through the diode:

$$I_D = I_s\left(exp\frac{q \cdot V_d}{a \cdot k \cdot T_c} - 1\right) \qquad \textit{Equation 2}$$

Where: *Is* is the diode's saturation current,

Vd is the diode voltage;

q is the charge of an electron, 1.602e-19;

Tc is the temperature in Kelvin;

k is Boltzmann's constant, 1.381e-23 and

a is a diode ideality constant/factor.

The saturation current will increase as temperature increases (Mertens & Roth 2014), however, the magnitude will be less severe - depending on the quality of the materials within the solar cell. A perfect diode with perfect materials will have an ideality constant (a) equal to 1, meaning that the diode obeys the ideal diode equation perfectly and there is no unwanted electron-hole-pair recombination. However some degree of unwanted recombination is inevitable (Alharbi & Kais 2015) and a silicon PV cell diode will typically have an ideality factor between 1.2 and 1.7.

The ideality factor is closely linked to the effect of temperature on a device, so that when a diode with a higher ideality factor is exposed to a higher temperature - will 'turn on' faster.

2.3.1. Solar cell characteristics

The characteristic curves of a solar cell very much follow photodiode characteristic curve principles, however convention dictates that the diode characteristics shown in Figure 7 are to be represented in the first quadrant being that the solar cell is producing power (Mertens & Roth 2014). The diagram in Figure 7. shows a negative current and a positive voltage, hence the current axis is inverted in the Figure 8 diagram.

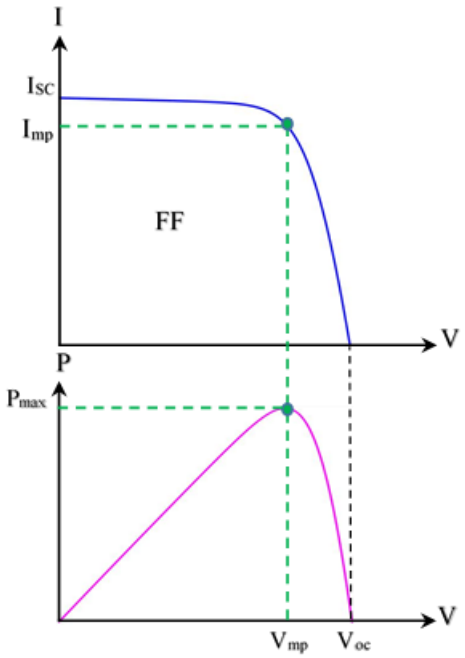

Figure 8: Characteristic curves of a solar cell diode.

Much like the ideal diode characteristic curve, the characteristic equation (Equation 2) also applies to the solar cell characteristic curves and allows for derivation of useful solar cell parameters. The following sub sections apply basic electrical analysis techniques to describe several important solar

cell parameters, the solar cell characteristic curves, and the solar cell characteristic equation (Equation 2).

2.3.1.1 Short circuit current

Figure 8 shows that the short circuit current occurs when the solar cell is shorted, voltage is equal to zero and the current is at its maximum value. Assuming that the solar cell is ideal, parallel resistance is infinite and losses are ignored, then when the cell is shorted there is no current through the diode (Figure 6) and it can be said that:

i. when the solar cell voltage equals zero, I_{SC} equals I_{ph},

ii. and hence, I_{SC} is proportional to irradiance.

Irradiance proportionality then provides some insight into semiconductor material selection with respect to solar cell design and bandgap energy. The lower the energy of the semiconductor bandgap, then the higher the solar cell efficiency will be (W. Shockley 1961), so it can be said that:

iii. lower bandgap energies absorb a greater quantity of photons,

iv. hence I_{SC} increases as the energy of the bandgap decreases.

2.3.1.2 Open circuit voltage

Figure 8 shows on both axis' that when solar cell current equals zero, the solar cell voltage is at its maximum open circuit voltage (V_{OC}). V_{OC} can be found from the ideal form of Equation 3 by setting I equals to zero, I_{ph} equals I_{SC} and solving for V_{OC}:

$$V_{OC} = a \cdot V_t \cdot \ln\left(\frac{I_{SC}}{I_S} + 1\right) \qquad \textit{Equation 3}$$

Where: V_t is the temperature dependant voltage (V),

Isc is the the short circuit current (A),

and I_S is the saturation current.

Area is the srface area of the solar cell (m),

The expression contains a natural logarithm, which indicates that the open circuit voltage is less dependant on irradiance than the short circuit current is (Mertens & Roth 2014):

i. and hence, V_{OC} is proportional to the natural log of irradiance.

As with I_{SC}, V_{OC} is an interesting parameter in terms of bandgap material selection, as V_{OC} is a function of bandgap energy (W. Shockley 1961) and as such:

ii. V_{OC} increases as bandgap energy increases,

iii. and as V_{OC} increases, efficiency increases until the current starts to drop.

2.3.1.3 Fill factor and maximum power

The fill factor, denoted by FF in Figure 8, is a graphical tool that provides a ratio that represents the quality of a power cell. Generally speaking, a less rounded VI characteristic curve will provide a higher fill factor and represents a high quality solar cell. The fill factor is described by:

$$Fill\ Factor = FF = \frac{V_{mpp} \cdot I_{mpp}}{V_{OC} \cdot I_{SC}} = \frac{P_{mpp}}{V_{OC} \cdot I_{SC}} \qquad \textit{Equation 4}$$

Where: *Pmpp* is the power at the maximum power point (W),

Vmpp is the maximum voltage (V),

Impp is the maximum current (A),

Voc is the the open current voltage (V),

Isc is the the short circuit current (A),

It is difficult to improve the fill factor of a poor quality cell, but it is not difficult to degrade the fill factor of a good solar cell if the series resistance high - due device contacts. The FF can also be approximated by the following expression (Mertens & Roth 2014):

$$FF = \frac{1+\ln\left(\frac{V_{OC}}{V_t}+0.72\right)}{\frac{V_{OC}}{V_t}+1} \qquad \textit{Equation 5}$$

Where: V*t* is the temperature dependant voltage (V),

The maximum power point of a solar cell (Figure 8) is the point where the maximum current and maximum voltage s graphically intersect to give the greatest fill factor area.

2.3.1.4 Efficiency

Solar cell efficiency provides a means to quantify the power output of a PV cell as a percentage/ratio of the suns input (Tanvir Ahmad* March 2016). A cell with a low efficiency requires a greater area to produce a given power, needs more natural resources and will have a higher relative cost to manufacture compared to more efficient cell.

$$Single\ junction\ cell\ efficiency = \eta_{SJSC} = \frac{P_{mpp}}{P_{in}} = \frac{V_{oc} \cdot I_{sc} \cdot FF}{\left(\frac{Area(mm^2)}{1000}\right)} \cdot 100 \qquad \textit{Equation 6}$$

Where: *Pin* is the solar cell input power (W)

Pmpp is the power at the maximum power point (W),

Voc is the the open current voltage (V),

Isc is the the short circuit current (A),

FF is the fill factor,

Area is the surface area of the solar cell (m),

2.3.2. Parasitic series resistance (R_S) losses

The series resistance (Rs) primarily represents losses due to (1) current through the solar cell emitter and base, (2) resistance within the metal contact material and (3) the resistance caused at the interface between the metal contacts and the solar cell semiconductor materials.

Series resistance is normally considered to occur as a result of poor design and reduces the characteristic fill factor. The effect of a changing series resistance on the characteristic VI and VP curves is shown in Figure 9.

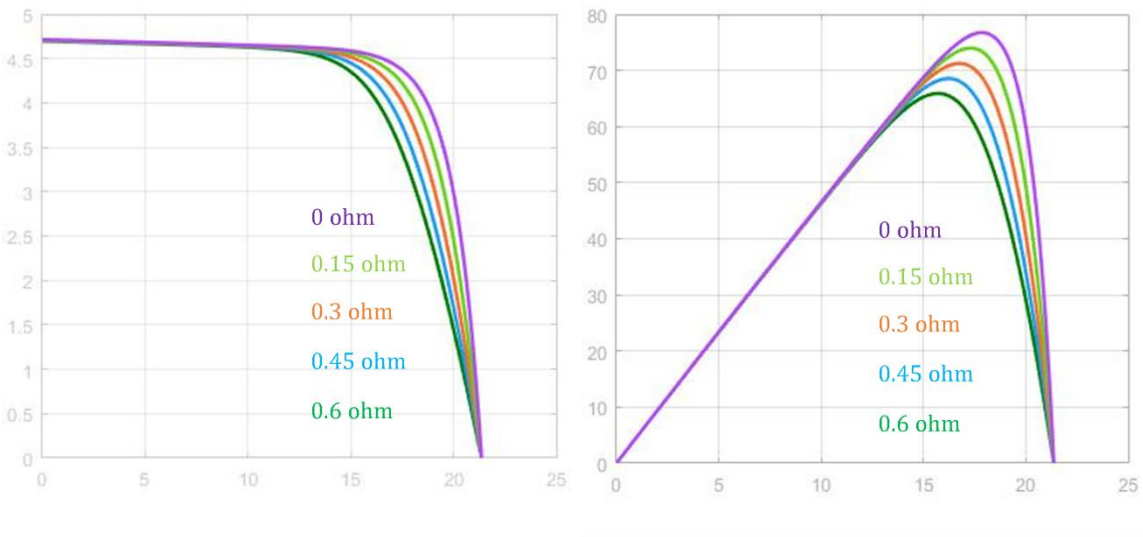

Figure 9: The effect of changing Rs on the SJSC VI & VP curves.

Consider Figure 9 and note the following observations with respect to each graph:

- The y-axis of the LHS graph represents the cells short circuit current *(I_{SC})*,
- The y-axis of the RHS graph represents the cells power *(P)*,
- The x-axis of each graph represents the cells open circuit cvoltage *(V_{OC})*,
- The series resistance has no effect on the cell short circuit current (I_{SC}) or the cell open circuit voltage (V_{OC}).
- The cell fill factor increases as the series resistance tends to zero,
- A linear increase in resistance provides a generally linear reduction in the maximum power point (MPP).

2.3.3. Parasitic shunt/parallel resistance (R_P) losses

Losses due to shunt/parallel resistance is generally due to manufacturing defects, transportation defects and damage due to careless installation.

Cracked or scratched cells provide an alternate current path, reducing the amount of current flowing through the solar cell junction culminating in a lower voltage potential across the solar cell. The effects of a changing shunt resistance on the characteristic VI and VP curves is shown in Figure 10.

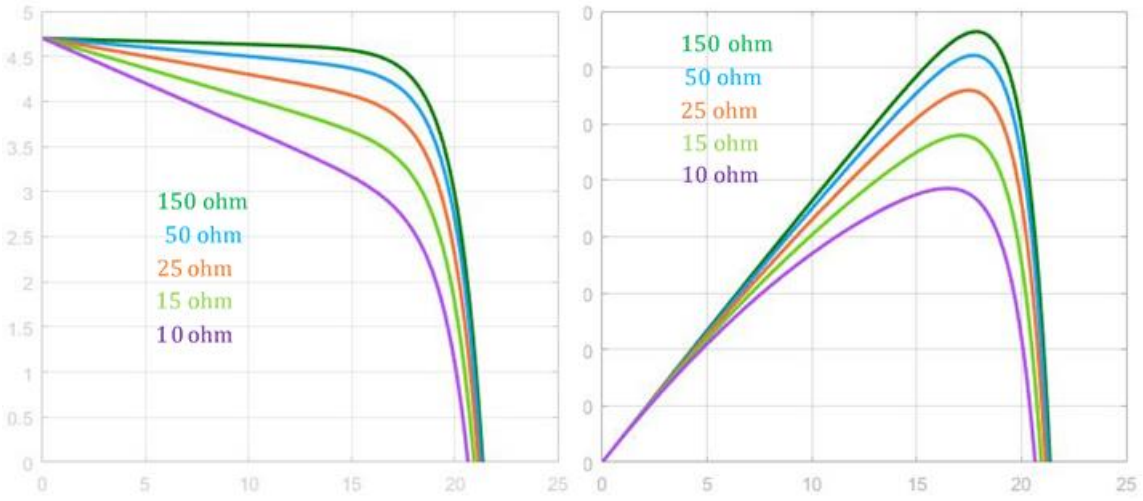

Figure 10: The effect of changing values of RP, on VI & VP characteristic curves.

Consider Figure 10 and note the following observations with respect to each graph:

- The y-axis of the LHS graph represents the cells short circuit current *(I_{SC})*,
- The y-axis of the RHS graph represents the cells power *(P)*,
- The x-axis of each graph represents the cells open circuit cvoltage *(V_{OC})*,
- Assuming that the series resistance is zero, then it can be said that the shunt resistance has no effect on the short circuit current (I_{SC}).
- However, the shunt resistance will reduce the cell's open circuit voltage (V_{OC}) as the shunt approaches zero.
- The cell fill factor increases as the shunt resistance tends to infinity,
- A linear increase in resistance does not provide linear increase in the maximum power point (MPP), that is, lower values of shunt resistance leads to a much lower solar cell conversion efficiency.

2.3.4. The effect of temperature and irradiance

Temperature is a primary concern when designing for PV cell efficiency, as an increase in temperature results in a marked loss in efficiency due to large losses in open circuit voltage, slight increase in short circuit current - not withstanding.

An increase in irradiance is obviously beneficial to a solar cells output power, as the short circuit current (I_{SC}) will increase linearly as irradiance increases. However efficiency does not have a linear response, as it is dependant on the inverse (log) voltage exponent shown in Equation 1. The

irradiance affects all parameters of the solar cell including I_{SC}, V_{OC}, the fill factor (FF), and both forms of resistance. The effects of temperature and the effect of irradiance are discussed at length in Chapter 3.2 of this report.

2.3.5. Inherent limitations for cell efficiency

Much of the advancement in new PV cell technology is driven by the limitations imposed on existing technologies due to the theoretical limit for a materials conversion efficiency. In Shockley's 1961 paper, he discusses the theoretical limit for the (conversion) efficiency of p-n junction PV cells and proves the upper obtainable efficiency for a single solar cell, with a single material and a single bandgap to be 33%.

The upper obtainable efficiency for a single solar cell contained the following assumptions:

i. Only auger and band to band recombination occurs;

ii. All photons with energy greater than the bandgap are absorbed, and all electron hole pairs have thermalisation loss;

iii. No losses occur when charge carriers are collected and transported.

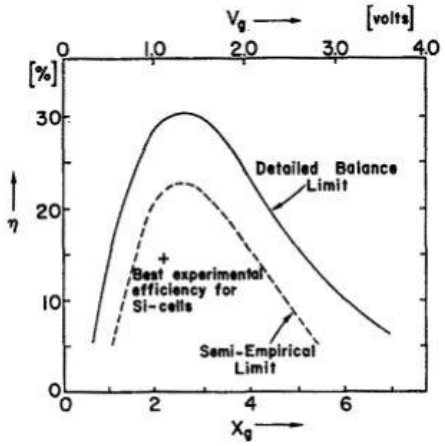

Figure 11: Early theoretical and experimental efficiencies. Image from (W. Shockley 1961).

The slowing rate of advancement in Si technology means that the return on investment in silicon PV efficiency research will continue to diminish

It would appear that MJSCs may be able to circumvent this limitation by simply adding more junctions, however, ultimate efficiency and the thermodynamic limit provides that as the number of junctions approach infinity, efficiency approaches zero.

2.3.6. The solar spectrum

The solar spectrum is standardised to provide a reference for comparing conversion efficiencies across all manner of PV cells and PV cell models. The AM1.5 global spectrum has been ratified for non-concentrate models, and allows for a global mid latitude of 48.2 degrees to the normal (equator).

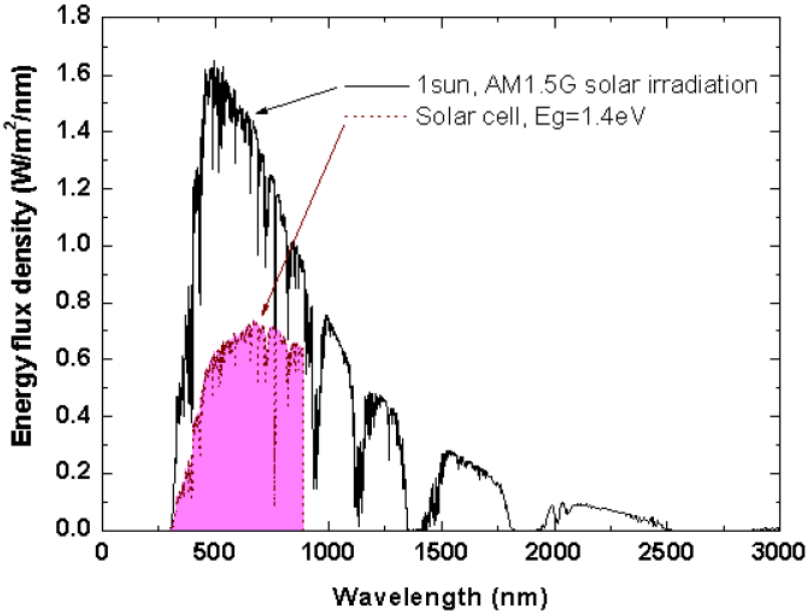

Figure 12: Spectrum utilisation of a 1.4ev bandgap. Image from (Tanabe 2009)

The integrated power for the AM1.5 spectrum equates to 1000 watts per square metre, hence, a 1 cm2 solar cell with a conversion efficiency of 10% would produce 10 mW of power.

There are various atmospheric and detritus that will absorb the particular photon frequencies so that the wavelengths are not recorded at ground level, and these can be observed in the spectrum as dramatic drops in values of spectral irradiance, as seen by the indents in the Figure 12 AM1.5 solar irradiation line.

2.4. The conventional silicon PV cell band gap

As previously discussed, the bandgap model provides a powerful tool when designing PV cells, furthermore, the model characterises the inverse relationship between the wavelength of light and the energy of a photon. The sun provides a range of photon energies between approximately 0.4 to

3.1 eV, and the P-N junction bandgap of a Si PV cell can be considered as the level of the solar spectrum, that the material absorbs most efficiently (Buonassisi 2013).

The diagram in Figure 13 is an amalgamation of two separate diagrams – taken from (Chin, Salam & Ishaque 2015) and (Jha 2009). The conventional Si PV cell has been modified to show a more detailed representation of the cell junction showing the bandgap that exists between the crystalline N-type silicon (conduction band) and the crystalline P-type silicon (valence band) (Green 1982). The energy band is commonly denoted by Eg, and is often referred to as the "band-gap" or the "forbidden layer/gap".

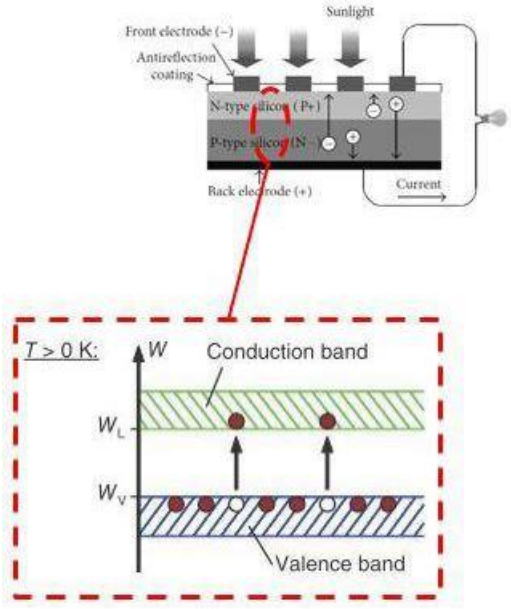

Figure 13: PV cell bandgap. Image from (Mertens & Roth 2014) and (Chin, Salam & Ishaque 2015)

Consider that the sunlight radiating onto the device injects a photon (of some wavelength) that permeates the conduction band and band gap. The photon will be absorbed in the valence band at some depth and an excitation reaction will occur at the absorption site where the energy of the photon will generate an electron hole pair (Green 1982) within the valence band substrate. Consider that a silicon atom in the valence band is struck by a photon of a particular length, the photon will cause an electron to be knocked free from the atom with enough force to clear the the band gap and settle within the conduction band (Figure 13). The result of the photon hole-pair interaction provides a potential difference between the two bands across the energy gap, and ideally, the only way for the electron-hole-pair to recombine is to flow (as current) through the external conductor.

The photon requires a higher energy state than the p-n junction band gap to ensure that the negatively charged electron will traverse the band gap to reside in the n-type band. It is then considered as a minority carrier (with respect to the negative-type (n-type) silicon) and the original

atom is considered to be a vacancy/hole that is analogous to a positively charged particle (Green 1982).

The Si PV cell p-n junction has an optimum bandgap energy (Eg) of approximately 1.12 electron volts (eV). That is to say, that the p-type Si semi-conductor material will absorb photons with some limited range of energy greater than 1.12 eV and any photons that are above or below this range are considered wasted.

The bandgap energy property is not unique to only Si semiconductor materials and there are many semiconductor materials that provide an optimum bandgap, for a range frequencies in the solar spectrum. Alternative band-gap energies will be discussed further when discussing multi-junction PV solar cells (MJSC).

2.4.1. Bandgap related loss mechanisms

Parasitic resistance losses are discussed on page 12 of this report, however a closer review of bandgap related loss mechanisms is warranted to provide a clearer understanding of why recombination occurs and what mechanisms are to be considered with regards to lumped recombination current (*Irs*) and to give some insight into recombination mechanisms involved in multijunction cell design.

Examples of common loss mechanisms that occur in and around cell junctions between bandgaps and photons , are represented in the Figure 14 diagram (Foozieh Sohrabi 2013).

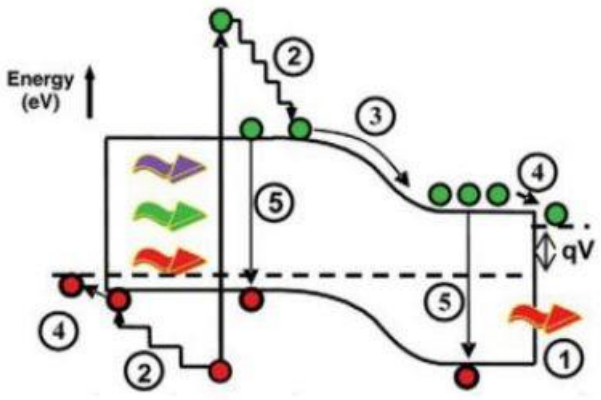

Figure 14: Bandgap loss mechanisms. Image from (Foozieh Sohrabi 2013).

Photons and bandgaps can be considered in terms of wavelength or energy so that:

- When a bandgap is expressed in terms of energy it is denoted by Eg. The corresponding matching wavelength for that bandgap energy is denoted by λg;

- When a photon is expressed in terms of wavelength it is denoted by λph. If that photon is expressed in terms of energy, it is denoted by Eph.

The loss mechanisms represented in Figure 14, occur as a result of the following:

i. Transmission losses (λph > λg) (Eph < Eg)
   Optical losses encompass such losses as reflection, shading and transmission losses. The bandgap wavelength (λg) is the wavelength of a photon that is most efficiently absorbed by the semiconductor material of a single solar cell p-n junction (Mertens & Roth 2014). Transmission loss occurs when the photon wavelength (λph) is greater than λg , hence the photon will not have enough energy (Eph) to force an electron across the bandgap to the conduction band. Transmission loss is illustrated by (1) in Figure 14, an image taken from (Foozieh Sohrabi 2013).

ii. Thermalisation losses (λph < λg) (Eg > Eph)
   Thermalisation loss occurs when λph is less than λg and the Eph is greater than Eg. Although the photon has successfully created an electron hole pair that remains separated in the correct bands, there is excess energy loss to the lattice via phonons as heat energy during thermal equalisation, as illustrated by (2) in Figure 14.

iii. Electrical and Ohmic losses
   Electrical losses occur due to cell contact design; and ohmic losses can occur due to the Schottky contact effect on any metal (plate) and semiconductor (material) interface (Mertens & Roth 2014). The Schottky contact effect is illustrated by (3) and (4) in Figure 14, where the a p-n junction type mechanism occurs at the interface and reduces the overall potential of the device.

iv. Recombination losses.
   Recombination losses occur in the base, emitter and bandgap regions and usually via one of three mechanisms:

   a. Band to band (radiative) recombination where an electron from the conductance band recombines with a hole in the valence band to release a photon. This is illustrated by (5) in Figure 14;

   b. Auger recombination where an electron from the conductance band recombines with a hole in the valence band, however the collision produces another electron (rather than a photon) that is released to the conductance band (McEvoy, Castaner & Markvart 2012);

   c. Shockley-Read-Hall recombination occurs in semiconductors that have been doped with impurities. An electron or hole may be drawn to an intermittent energy level

within the bandgap due to a impure material defect, where it may recombine to form a photon or a phonon (Sah, Noyce & Shockley 1957).

A graphical representation of the unavoidable and intrinsic losses that occur during energy conversion in a single junction Si PV cell is shown in Figure 15, an image taken from (McEvoy, Castaner & Markvart 2012).

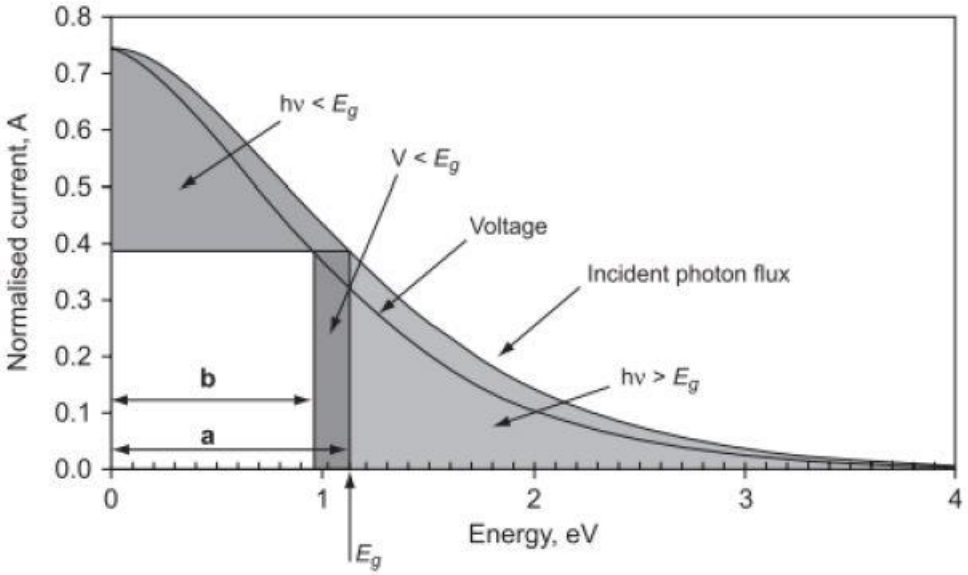

Figure 15: Representative PV energy losses. Image from (McEvoy, Castaner & Markvart 2012).

Although the graph is not to scale, the energy verse current plot represents the losses from an ideal Si cell with a bandgap of 1.12 eV that has been measured under standard test conditions. The losses include:

- Transmission losses, denoted by the (hv < Eg) shaded region, represent approximately 18.5% of the total losses;
- Thermalisation losses, denoted by the (hv > Eg) shaded region, represent approximately 47% of the total losses;
- Recombination losses, denoted by the (V < Eg) shaded region; represent approximately 1.5% of the total losses;

2.5. The single diode (D1) model

As already discussed in this paper, the conventional single junction Si PV cell can be represented by using the standard single single diode model, shown here in Figure 16.

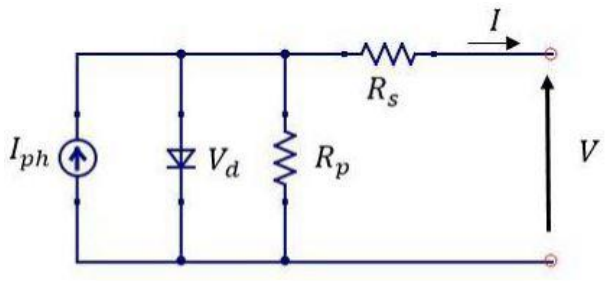

Figure 16: Single diode equivalent circuit

For the single diode model SJSC, the assumption that there are no recombination losses within the p-n junction insulation (depletion) region (Ishaque, Salam & Syafaruddin 2011), hence the ideality constant (a) is modelled as unchanging in the transient part of the diode current. The value of a diode's ideality is somewhat empirical - and opinions vary on selecting an appropriate value – however a value between 1.2 and 1.7 is acceptable in most cases (Villalva, Gazoli & Filho 2009).

Short circuit current (Isc), series and shunt resistances (Rs and Rp), saturation current (Is) and the diode ideality factor, a, are the five parameters required for the single diode model. The cell is analysed under the standard test conditions (STC) where solar a spectrum of AM1.5, irradiance of 1000 W/m2 and cell temperature of 25 degrees Celsius are provided (Hyvarinen & Karila 2003).

The characteristic equation for the single diode model is found by subtracting the diode current (I_D) and the shunt current (I_{Rp}) from the photoelectric current (Iph) to solve for the current through the series resistance, or cell current output (I):

$$I = I_{ph} - I_D - I_{Rp} \qquad \textit{Equation 7}$$

The first expression on the RHS of Equation 7 is for the photon generated current (Iph), which is dependant on both irradiance and temperature and given by:

$$I_{ph} = \left[I_{sc\_STC} + K_I\,(T_c - T_{stc})\right] \cdot \left(\frac{G_c}{G_{stc}}\right)$$ *Equation 8*

Where:: *Isc* is the short circuit current, or when voltage is zero,

K_I is the temperature coefficient for the short circuit current (mA / °C), obtained from the manufacturers datasheet,

Tc is the actual measured temperature of the PV cell (°C),

Tstc is the reference temperature under standard test conditions (25°C / 298°K),

Gc is the actual measured irradiance of the PV cell,

Gstc is the reference irradiance under standard test conditions (1000 W/m2);

The second expression in Equation 7 is the diode current (I_D), and can be substituted with Shockley's ideal diode equation (Equation 2) and considered in terms of a PV cell:

$$I_D = I_s\left(exp\frac{q \cdot V_d}{a \cdot k \cdot T_c} - 1\right) = I_s\left(exp\frac{V + IR_s}{a \cdot V_t} - 1\right)$$ *Equation 9*

Where: *Vd* is the diode voltage,

q is the charge of an electron, 1.602*10(-19),

Tc is the temperature in Kelvin,

k is Boltzmann's constant, 1.381 * 10(-23),

a is a diode ideality constant, where a =1 if the diode is perfectly efficient,

V is the total voltage generated by each cell,

IR_S is the voltage across the series resistances.

The first new term in Equation 9 is the temperature dependant voltage, which is given by:

$$\mathrm{V}_t = \frac{N_s \cdot k \cdot T_c}{q}$$ *Equation 10*

Where: *Ns* is the number of series connected cells per module.

The second new term in Equation 9 is the saturation current (*Is*), which can be derived depending on the approach taken. This section of this paper will assume that Is is to include the bandgap energy (Eg) in the expression for the saturation current, which is given by:

$$I_s = I_{rs}\left(\frac{T_c}{T_{stc}}\right)^3 \cdot exp\left(\left(\frac{q \cdot E_g}{a \cdot k}\right)\left(\frac{1}{T_{stc}} - \frac{1}{T_c}\right)\right) \qquad \textit{Equation 11}$$

Irs is another new term – that represents recombination current:

$$I_{rs} = \frac{I_{ph\_stc}}{exp\left(\frac{V_{oc\_stc}}{a \cdot V_{tstc}}\right) - 1} = \frac{I_{sc\_stc}}{exp\left(\frac{V_{oc\_stc}}{a \cdot V_{tstc}}\right) - 1} \qquad \textit{Equation 12}$$

Where:

- I_{sc_stc} is short circuit current as measured under STC conditions,
- I_{ph_stc} is the photocurrent as measured under STC conditions, (approximated by *Isc_stc*),
- V_{oc_stc} is the open current voltage measured under STC conditions,
- *a* is the diode ideality factor, and
- V_{tstc} is the temperature dependant voltage for Ns cells under STC conditions.

Note that the inclusion of Irs in the saturation current (Is) effectively computes the saturation current twice to eliminate the diode diffusion factor (Bellia, Youcef & Fatima 2014).

Therefore, the single diode (D1) model of the output current of a PV cell module, is given by:

$$I = I_{ph} - I_s\left[\exp\left(\frac{q(\mathrm{V}+\mathrm{I}\cdot R_s)}{a \cdot N_s \cdot \mathrm{k} \cdot T_c}\right) - 1\right] - \frac{V + I \cdot R_s}{R_p}$$

$$= I_{ph} - I_s\left[\exp\left(\frac{\mathrm{V}+\mathrm{I}\cdot R_s}{a \cdot \mathrm{V}_t}\right) - 1\right] - \frac{V + I \cdot R_s}{R_p} \qquad \textit{Equation 13}$$

2.6. The double diode (D2) model

Although the single diode model is arguably the most popular PV model, its accuracy diminishes at lower voltages and lower irradiances (Chin, Salam & Ishaque 2015). The double diode (D2) model includes a second diode that allows for the losses that occur during recombination in the depletion region (Mahmoud et al. 2012).

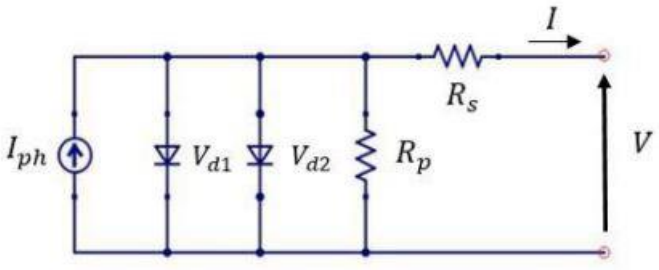

Figure 17: Double diode equivalent circuit.

The saturation current in the second diode is generally accepted as being equal to the first diode saturation current, however the ideality factor varies, as the ideality factor is really a function of voltage across the device. The first diode is often allocated an *a1* of 1, and the second diode will have an *a2* equal or greater than 1.2 (Ishaque 2011) and (Mahmoud et al. 2012).

The derivation of the D2 model relationships are simply an extension of the D1 relationships. The characteristic equation for the double diode model is found by subtracting the both diode currents (Id1 and Id2) and shunt current from the photoelectric current to solve for the current through the series resistance:

$$I_{ph} - (I_{d1} + I_{d2}) - I_{Rp} - I = 0 \qquad \textit{Equation 14}$$

$$I = I_{ph} - (I_{d1} + I_{d2}) - I_{Rp} \qquad \textit{Equation 15}$$

Sub in the ideal diode current and use the voltage divider rule to find the current through the shunt, hence providing expression for the PV cell characteristic equation. Hence, the double diode (D2) model of the output current of a PV cell module, is given by:

$$I = I_{ph} - I_{s1}\left[\exp\left(\frac{q(\mathrm{V}+\mathrm{I}\cdot R_s)}{a1\cdot N_s\cdot \mathrm{k}\cdot T_c}\right) - 1\right] - I_{s2}\left[\exp\left(\frac{q(\mathrm{V}+\mathrm{I}\cdot R_s)}{a2\cdot N_s\cdot \mathrm{k}\cdot T_c}\right) - 1\right] - \frac{V+I\cdot R_s}{R_p}$$

$$I = I_{ph} - I_{s1}\left[\exp\left(\frac{\mathrm{V}+\mathrm{I}\cdot R_s}{a1\cdot V_t}\right) - 1\right] - I_{s2}\left[\exp\left(\frac{\mathrm{V}+\mathrm{I}\cdot R_s}{a2\cdot V_t}\right) - 1\right] - \frac{V+I\cdot R_s}{R_p} \qquad \textit{Equation 16}$$

Where:

I_{ph}	is the photon generated current,
I_{s1}	is the first diode saturation current,
I_{s2}	is the second diode saturation current,
q	is the charge of an electron, 1.602*10^(-19),
V	is the total voltage generated by each cell,
I_{RS}	is the voltage across the series resistances,
a_1	is the first diode ideality factor,
a_2	is the second diode ideality factor,
N_S	is the number of cells in the PV cell module,
k	is Boltzmann's constant, 1.381 * 10^(-23),
T_C	is the actual measured temperature of the PV cell (°C),
R_P	represents the shunt losses within the PV cell,
V_{tc}	is the Temperature dependant voltage for Ns cells (at any temperature).

The photocurrent and temperature dependant voltage expressions are identical to the D1 model, and the saturation currents vary - only in quantity - to allow for the number of diodes and respective ideality factors.

Hence, the D2 saturation currents are given by:

$$I_{s1} = I_{rs1}\left(\frac{T_c}{T_{stc}}\right)^3 \cdot exp\left(\left(\frac{q\cdot E_g}{a1\cdot k}\right)\left(\frac{1}{T_{stc}} - \frac{1}{T_c}\right)\right)$$

$$I_{s2} = I_{rs2}\left(\frac{T_c}{T_{stc}}\right)^3 \cdot exp\left(\left(\frac{q\cdot E_g}{a2\cdot k}\right)\left(\frac{1}{T_{stc}} - \frac{1}{T_c}\right)\right) \qquad \textit{Equation 17}$$

and the respective recombination currents are given by:

$$I_{rs_1} = \frac{I_{ph\_stc}}{\exp\left(\frac{V_{oc\_stc}}{a_1 \cdot V_t}\right)-1} = \frac{I_{sc\_stc}}{\exp\left(\frac{V_{oc\_stc}}{a_1 \cdot \frac{Ns \cdot k \cdot T_c}{q}}\right)-1}$$

$$I_{rs_2} = \frac{I_{ph\_stc}}{\exp\left(\frac{V_{oc\_stc}}{a_2 \cdot V_t}\right)-1} = \frac{I_{sc\_stc}}{\exp\left(\frac{V_{oc\_stc}}{a_2 \cdot \frac{Ns \cdot k \cdot T_c}{q}}\right)-1}$$

Equation 18

2.7. Alternative approaches to modelling diode saturation current

There are many considerations when determining appropriate modelling techniques for conventional Si PV cells. There is a large body of work dedicated to extracting modelling parameters to provide accurate estimation, however, there is no systematic documentation within the literature, so a comprehensive and accurate benchmarking system is not yet available (Chin, Salam & Ishaque 2015).

Whilst conducting the literature review, the modelling techniques were tested against expected characteristics and results did not always correlate between similar papers. On further review it became apparent that there are two distinct and predominant forms of translational equations when calculating the saturation current.

2.7.1. The Kv form saturation current.

The first predominant approach to modelling saturation current will be referred to as the Kv form of modelling. The Kv form is important to this dissertation as it is the form that is used when modelling the validation data. Features include:

a. The Kv form of saturation current modelling is used in papers such as (Ishaque 2011), (Ishaque, Salam & Syafaruddin 2011), (Ishaque, Salam & Taheri 2011) and (Jena & Ramana 2015);

b. This form uses an alternative computational method that simplifies the saturation current equation and incorporates the recombination current into the primary equation for saturation;

c. The bandgap energy is ignored when modelling the saturation current of the device;

d. The saturation current also includes a coefficient of voltage per Kelvin that does not commonly appear in the alternative predominate approach.

e. The single diode (D1) model in the Kv form will be referred to as the ***D1_Kv*** model.

f. The double diode (D2) model in the Kv form will be referred to as the ***D2_Kv*** model.

In the D1_Kv model - saturation current is given by Equation 19:

$$I_s = \frac{I_{sc\_stc}+K_I\cdot(T_c-T_{stc})}{\left[\exp\left(\frac{V_{oc\_stc}+K_V\cdot(T_c-T_{stc})}{a\cdot V_t}\right)-1\right]} = \frac{I_{sc\_stc}+K_I\cdot(T_c-T_{stc})}{\left[\exp\left(\frac{V_{oc\_stc}+K_V\cdot(T_c-T_{stc})}{a\cdot\frac{Ns\cdot k\cdot T_c}{q}}\right)-1\right]} \qquad \textit{Equation 19}$$

Where: K_I is the temperature coefficient for the short circuit current (mA / °K),

K_V is the temperature coefficient for the open circuit voltage (mV / °K),

a is the ideality factor of the diode, which is found analytically to be between 1.2 and 2.0.

In the D2_Kv model, the saturation current is given by Equation 20:

$$I_{s1} = I_{s2} = \frac{I_{sc\_stc}+K_I\cdot(T_c-T_{stc})}{\left[\exp\left(\frac{V_{oc\_stc}+K_V\cdot(T_c-T_{stc})}{\left(\frac{a1+a2}{P_e}\right)\cdot V_{tc}}\right)-1\right]} = \frac{I_{sc\_stc}+K_I\cdot(T_c-T_{stc})}{\left[\exp\left(\frac{V_{oc\_stc}+K_V\cdot(T_c-T_{stc})}{\left(\frac{a1+a2}{P_e}\right)\cdot\frac{Ns\cdot k\cdot T_c}{q}}\right)-1\right]} \qquad \textit{Equation 20}$$

Where : *a1*, is the ideality factor of diode 1 is assumed to be unity,

a2, is the ideality factor of diode 2 is assumed to be two,

Pe is the sum of a1 and a2.

The D2_Kv model gives both saturation currents equal magnitude to remove the need for computational iteration, and *a1* is assumed to be unity whilst *a2* is assumed to be any value up to 1.7, and somewhat flexible above a value of 1.2 (Ishaque 2011).

2.7.2. The Eg form saturation current

The second predominant approach to modelling saturation current will be referred to as the Eg form of modelling. The Eg form is important to this dissertation as it is the form that is used required when modelling solar cells with multiple junctions.. Features include:

a. The Eg form of saturation current modelling is used in such papers as (Das, Wongsodihardjo & Islam 2013), (Das, Wongsodihardjo & Islam 2015), (Lineykin, Averbukh & Kuperman 2014) and (Villalva, Gazoli & Filho 2009).

b. This form of saturation current derivation implements translational that include the bandgap energy of the device within the expression for the saturation current.

c. The single diode (D1) model in the Eg form will be referred to as the ***D1_Eg*** model.

d. The double diode (D2) model in the Eg form will be referred to as the ***D2_Eg*** model.

In the D1_Eg model – saturation current is given by Equation 11, first introduced on page 23:

$$I_s = I_{rs}\left(\frac{T_c}{T_{stc}}\right)^3 \cdot exp\left(\left(\frac{q \cdot E_g}{a \cdot k}\right)\left(\frac{1}{T_{stc}} - \frac{1}{T_c}\right)\right)$$

In the D2_Eg model – saturation current is given by Equation 17, first introduced on page 25:

$$I_{s1} = I_{rs1}\left(\frac{T_c}{T_{stc}}\right)^3 \cdot exp\left(\left(\frac{q \cdot E_g}{a1 \cdot k}\right)\left(\frac{1}{T_{stc}} - \frac{1}{T_c}\right)\right)$$

$$I_{s2} = I_{rs2}\left(\frac{T_c}{T_{stc}}\right)^3 \cdot exp\left(\left(\frac{q \cdot E_g}{a2 \cdot k}\right)\left(\frac{1}{T_{stc}} - \frac{1}{T_c}\right)\right)$$

2.7.3. Exponential coefficient for parasitic resistances

Another modelling technique that did not correlate with the literature when tested against expected characteristics, was the use of an exponential coefficient for parasitic resistances. Eg form models appeared to respond more accurately when $R_S(T)$ and $R_P(T)$ were multiplied by an exponential to the value of negative K_V, the coefficient of temperature.

This modelling technique is found in the associated documentation for the single solar cell library block within Simulink (MathWorks 2015).

The temperature dependant resistances are given in the D1_Eg and D2_Eg models by:

$$R_P(\mathrm{T}) = R_P\left(\frac{T_c}{T_{stc}}\right)^{-K_V}$$ *Equation 21*

$$R_S(\mathrm{T}) = R_S \left(\frac{T_c}{T_{stc}}\right)^{-K_V}$$ *Equation 22*

Where: Rp is the extracted value for shunt resistance,

Rs is the extracted value for series resistance and

Kv is the voltage coefficient of temperature given in the manufacturer data sheet.

The temperature dependant resistances are given in the D1_Kv and D2_Kv models by:

$$R_P(\mathrm{T}) = R_P \left(\frac{T_c}{T_{stc}}\right)^{0}$$ *Equation 23*

$$R_S(\mathrm{T}) = R_S \left(\frac{T_c}{T_{stc}}\right)^{0}$$ *Equation 24*

Where: Rp is the extracted value for shunt resistance, and

Rs is the extracted value for series resistance.

The zero exponent in Equation 23 and Equation 24 effectively cancels the exponent, as the Kv form has Kv included in Equation 19 for the D1 model and in Equation 20 for the D2 model.

2.8. Cells and modules

PV module voltage is determined by the number of series connected solar cells, PV current from the module is dependant on the size and efficiency of the solar cells. In this paper, the nomenclature for a number of series connected cells is Ns, and the nomenclature for a number of parallel connected cells is Np. Therefore the calculations for current will take the number of parallel cells into account, and the calculations for voltage will take the number of series cells into account:

Total short circuit current $= (I_{SC})(N_P)$,

Total short circuit current at the maximum power point $= (I_{mpp})(N_P)$,

Total open circuit voltage $= (V_{OC})(N_S)$,

Total open circuit voltage at the maximum power point $= (V_{mpp})(N_S)$,

Unless stated otherwise, it is assumed that there are no parallel connected cells included in this paper. Ns will be included in all temperature dependant voltage relationships, where Ns = 1, when there is a single cell.

Multijunction solar cells (MJSC)

2.9. The multi-junction solar cell

A multi-junction solar cell (MJSC) can be defined, in very simple terms, as a solar cell that contains two or more single junction semiconductors - layered on top of each other to enable absorption of a wider range of solar spectrum photons. The schematic representation of a triple junction solar cell in Figure 18, taken from (Friedman 2010), shows the photon distribution as a function of junction bandgap energy.

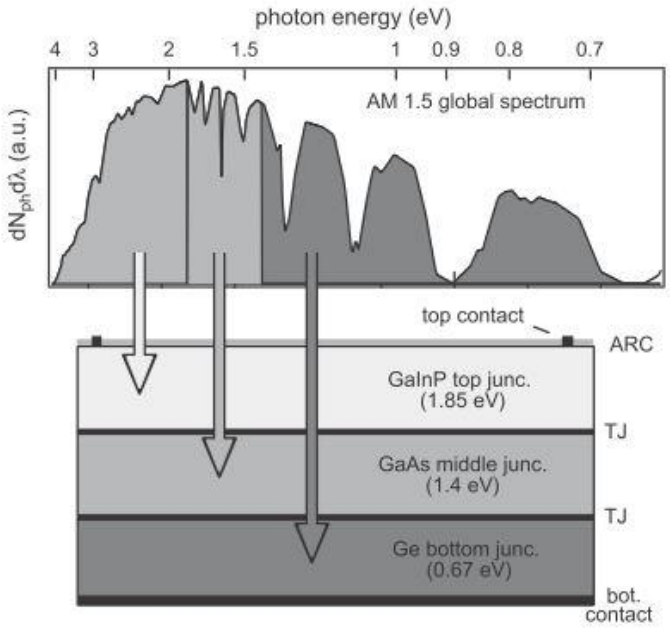

Figure 18: Schematic representation of a MJSC. Image from (Friedman 2010).

The single junction PV device is particularly vulnerable to transmission losses, thermalisation losses and surface recombination losses - all of which are intrinsic to p-n junction devices, as the semiconductor material is limited to a specific range of energy, hence, a limited range of photon absorption.

The MJSC has layer of semiconductor materials of different bandgaps with the highest bandgap energy on the upper surface, to the lowest bandgap energy material on the bottom surface. In Figure 18, photons that have a bandgap energy higher than 1.85 eV, will be be able to excite electron-hole pair separation in the gallium indium phosphide (GaInP) semiconductor material. Photons with longer wavelengths, and an energy greater than 1.4 eV, will excite electron-hole pair separation in the gallium arsenide (GaAs) semiconductor material. Finally, the photons that have the longest wavelength, and an energy greater than 0.67 eV, will excite electron-hole pair separation in the germanium (GaAs) semiconductor material.

The result is that the MJSC increases quantity of photons converted into useful energy, and reduces losses related to wasted photon energy.

2.10. MJSC architecture related modelling techniques

2.10.1. Production methods

There are two predominant methods of manufacturing MJSCs, (1) by mechanically stacking prefabricated single junction cells, or (2) by monolithically depositing individual layers of crystalline semiconductor onto a wafer substrate via a process, known as epitaxial growth (Cotal et al. 2009).

Mechanical stacking can be difficult to do efficiently, as the sub cell configuration is bulky, requiring relatively complex circuitry and the integrated contacts can complicate inefficiencies due to heat dispersion.

As a result, the monolithic method of production is widely considered the norm, with metal organic chemical vapour deposition (MOCVD) being a common method used to mass produce MJSC's (Tanabe 2009). This paper will focus on modelling of monolithically produced MJSCs.

2.10.2. Semiconductor band gap energy and lattice constant

Semiconductors can be characterised by the band gap energy of the material and the crystal lattice constant of the material structure - an indication of the spacing between crystal atoms (Das, Al Ghadeer & Islam 2014).

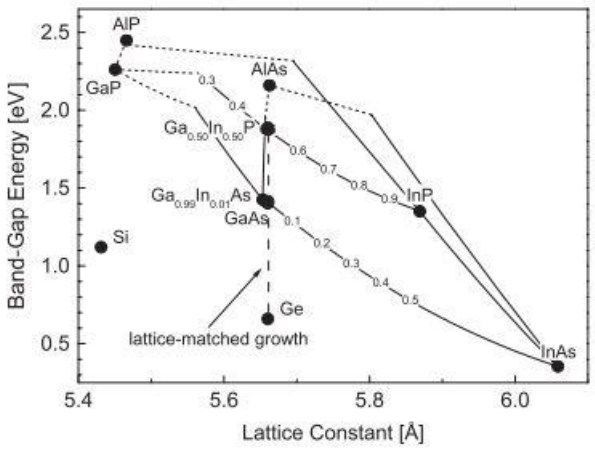

Figure 19: Bandgap as a function of lattice constant. Image taken from (Friedman 2011).

Figure 19, taken from (Friedman 2011), shows the bandgaps of some of the more commonly used III-V Group Alloy semiconductors, plotted as a function of their individual lattice constant. The bandgaps with a higher photon absorption(direct bandgaps) are indicated by solid lines and the bandgaps with a lower photon absorption (indirect bandgaps) are indicated by broken lines.

Note that the figure includes the bandgap combination of one of the most commonly used triple-junction solar cell's GaInP/GaInAs/Ge (Friedman 2011). The GaInP/GaInAs/Ge cell is an example of a lattice matched system, where the semiconductor crystal lattice constants of adjacent solar cell layers are closely matched to reduce recombination due to dislocation at the layer interface (cracking or deformation). Matched systems are generally simpler to implement compared to mismatched systems, however, there are limited combinations. With an ideal dual bandgap energy's of 1.1 and 1.7 (eV) - it is possible to harvest at a 36% efficiency, however there are no affordable III-IV group compounds that can provide a bandgap of 1.1 eV so other more commonly found materials are used to provide the nearest bandgap energy to 1.1 (eV) as possible (Bhattacharya & Foo 2010).

MJSC layers with mismatched systems are becoming more common place and there are a greater range of less-precise bandgap energies to choose from, however, the different lattice constants form dislocations and subsequent recombination. Therefore strategies such as epitaxial buffer structures are implemented between layers to allow for a gradual change in lattice constant values to reduce and contain the high ratio of dislocation in mismatched materials (Bett et al. 2013).

Table 1: Basic crystal structure parameters for commonly used MJSC semiconductors.

Material		*Basic parameters at 300K*		
		Lattice Constant (A)	Bandgap energy (eV)	Crystal Structure
Aluminium gallium arsenide	AlGaAs	5.653	1.42 – 2.16	Zinc blende (FCC)
Gallium antimode	GaSb	6.096	0.726	Zinc blende (FCC)
Gallium arsenide	GaAs	5.653	1.424	Zinc blende (FCC)
Gallium indium phosphide	GaInP	5.869		Zinc blende (FCC)
Gallium phosphide	GaP	5.451	2.26	Zinc blende (FCC)
Germanium	Ge	5.658	0.66	Diamond (FCC)
Silicon	Si	5.431	1.12	Diamond (FCC)

The band gap energy and lattice constant values for the commonly used MJSC materials is shown in Table 1.

The distribution of the spectrum region over more than one band gap is also a challenge when matching the current of each series connected layer, given that the maximum current output of the device is the layer with the minimum output. Consider that the Ge sub-cell of a (GaInP/GaInAs/Ge) multijunction cell will generate approximately twice the amount of current than the adjacent GaInAs cell (Bedair & Samberg 2013). Even though the lattice match is very good, the less than optimal current match between the second and third layers restricts the total cell potential efficiency.

2.11. Loss mechanisms related to MJSC architecture

The epitaxial process used to manufacture monolithic MJSCs greatly influences parasitic series resistances and recombination losses. The modelling of individual junction resistance and tunnelling is outside the scope of this paper, however a basic understanding why tunnel junctions are required is warranted.

2.11.1. Tunnel junctions

Epitaxial growth of monolithic MJSCs results in a series of layered structures with an interface between each single junction layer and one set of contacts at the top and bottom of the cell. However, the series 'connected' interfaces produce a high resistance between each sub-cell layer resulting in electrical properties similar to that of a reverse biased diode (Cotal et al. 2009).

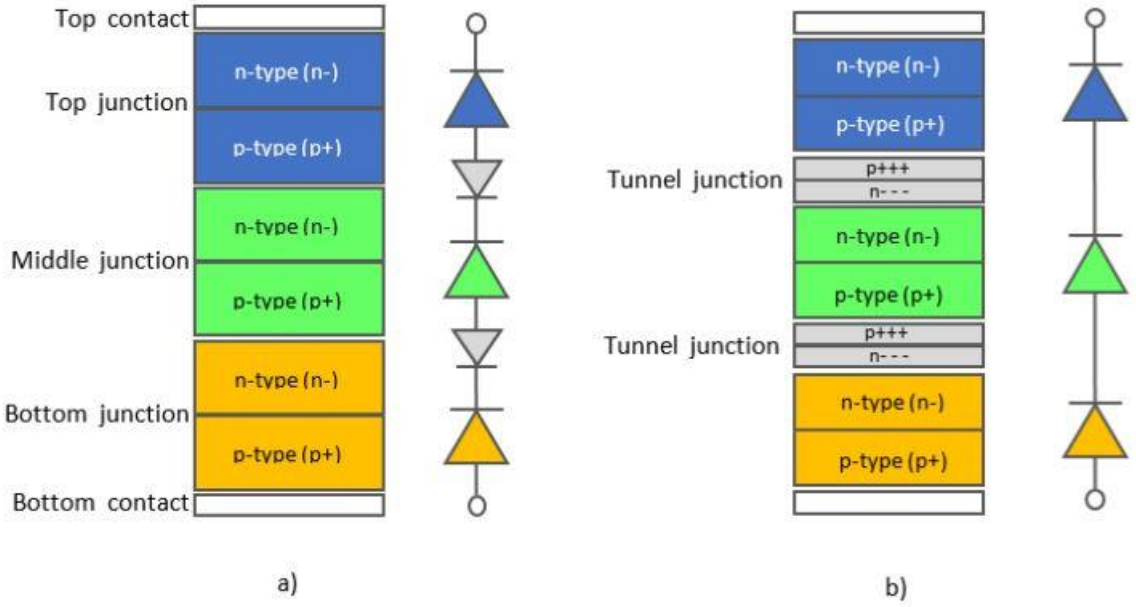

Figure 20: MJSC without/with tunnel junctions. Image adapted from (Cotal et al. 2009).

The image in Figure 19 was adapted from an image in (Cotal et al. 2009), and depicts:

a) A triple junction solar cell ***without*** a tunnel junctions between each interface;

b) And a triple junction solar cell ***with*** a tunnel junction between each interface.

In Figure 20a), each of the three layered single junctions are forward biased and as the crystalline layers are deposited on top of each other during manufacturing, an undesirable reverse biased effect is created due to the alternate p-n junction pattern at the interface. The resulting effect will cause a reverse biased effect and the flow of current will be blocked at the interface.

The forward to reverse biasing problem is resolved by including a tunnel junction at the interface of each layer, as demonstrated in Figure 20b), where the same MJSC includes a tunnel junction between each single junction layer. This layer contains heavily doped semiconductor material and is grown at the surface of each interface, to allow the photons to travel between each cell layer by tunnelling directly through each interface (Cotal et al. 2009).

2.12. Proven multi-junction solar cells

The most common dual-junction MJSC contains the III-V group alloys of Indium Gallium Phosphide (InGaP) and Gallium Arsenide (GaAs) where each bandgap is closely lattice matched (Das, Wongsodihardjo & Islam 2015). The detailed schematic (Figure 21), taken from (Jain & Hudait 2012) shows the various band-gap, tunnel substrate and buffer alloy compositions, as well as the specific InGaP and GaAs bandgap energies of a typical InGaP/GaAs dual-MJSC.

The InGaP/GaAs dual MJSC is monolithically grown via epitaxial growth with an expected efficiency of 30.8%. Table 2 lists some of the cell performance characteristics, and according to papers by (Jain & Hudait 2012), (Kayes et al. 2014) and (Tanabe 2009) - the dual-junction MJSC has an experimental efficiency ranging between 27% to 31%.

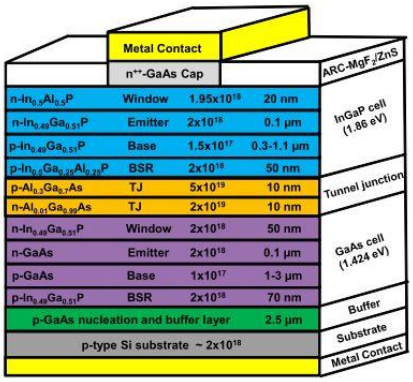

Figure 21: Double junction diode. Image taken from (Jain & Hudait 2012)

Table 2: Dual MJSC InGaP/GaAs performance characteristics.

InGaP/GaAs dual MJSC performance characteristics:			
InGaP (eV)	*1.86*	*Spectrum*	*AM(1.5*
GaAs (eV)	*1.42*	*Irradiance (W/m^2)*	*1000*
Efficiency (%)	*30.8*	*Area (cm^2)*	*1.0*
		Matched lattice constant (Tanabe 2009)	*5.64*
Recorded Data:	*(Kayes et al. 2014)*	*(Takamoto et al. 1997) as cited in (Jain & Hudait 2012)*	*(Algora et al. 2007) as cited in (Jain & Hudait 2012)*
V_{oc} (V)	*2.547*	*2.48*	*2.52*
J_{sc} (mA/cm^2)	*14.3*	*14.22*	*12.70*
Fill Factor	*84.7*	*85.6*	*85*
Efficiency (η)	*30.8*	*30.28*	*27.2*

The majority of the literature reviewed in this paper tended towards the most common triple-junction MJSC as having an upper layer of Indium Gallium Phosphide (InGaP), a middle layer of Indium Gallium Arsenide (InGaAs) and a substrate layer of Germanium (Ge) (Das, Wongsodihardjo & Islam 2015), (Hussain et al. 2016), (Rezk & Hasaneen 2015), (King et al. 2007).

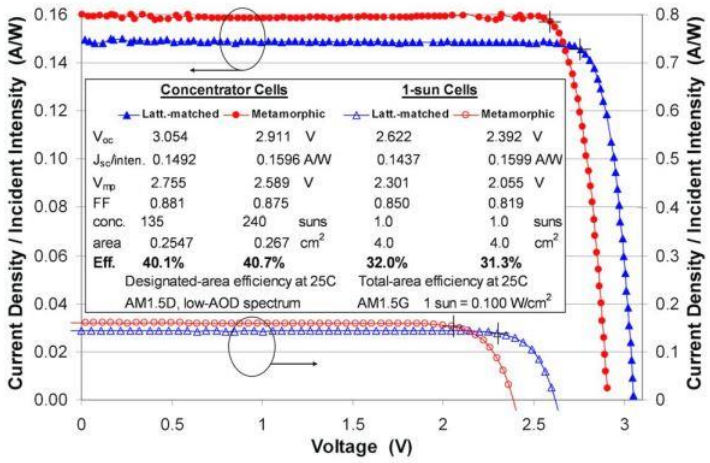

Figure 22: Efficiencies of the GaInP/GaInP/Ge MJSC. Image taken from (King et al 2007).

The image in Figure 22 was taken from (King et al. 2007) and shows the measured I-V characteristics and efficiencies for the GaInP/GaInAs/Ge MJSC, as verified by NREL in 2007. Image taken from (King et al. 2007). Each layer of the InGaP/InGaAs/Ge MJSC is closely matched in lattice constant and in bandgap energy, with a proven concentrated efficiency exceeding 40%, and a standardised 1 sun efficiency of 32%

2.13. D1 and D2 MJSC equivalent circuits

Much of the recent research models an n-junction MJSC by connecting n-number of equivalent single/double diodes in series. Papers such as (Rezk & Hasaneen 2015), (Das, Wongsodihardjo & Islam 2015) and (Hussain et al. 2016) model the conversion efficiency using a single diode multi-junction solar cell model (D1_MJSC), as shown in the left equivalent circuit of Figure 23.

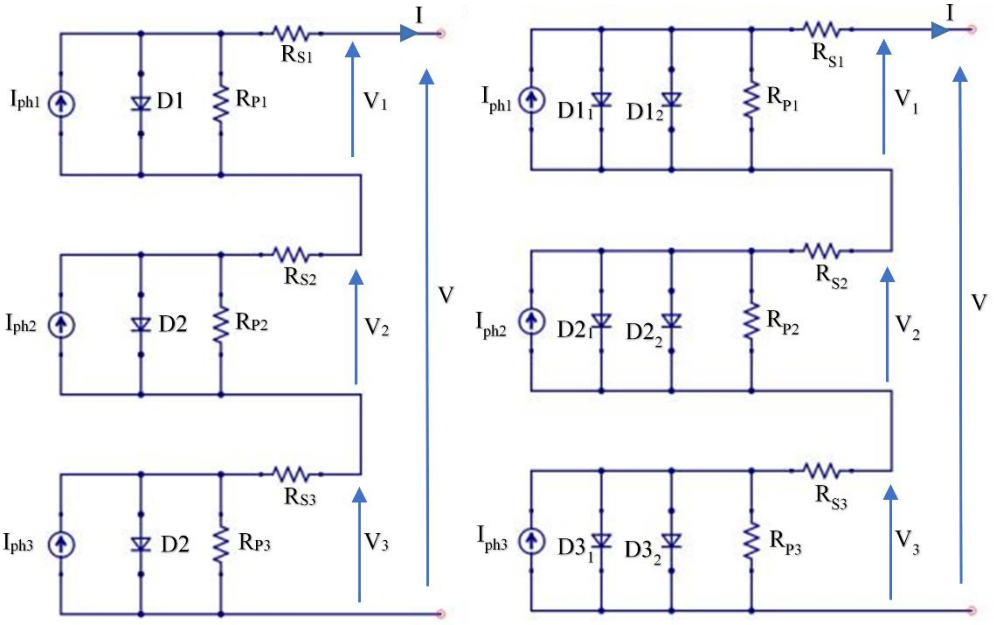

Figure 23: (Left) D1 MJSC equivalent circuit and (Right) D2 MJSC equivalent circuit.

Papers such as (Das, Al Ghadeer & Islam 2014) and (Catelani et al. 2016) model the conversion efficiency using a double diode multi-junction solar cell model (D2_MJSC), as shown in the right equivalent circuit of Figure 23.

Labelling convention applied in this paper, denotes MJSC components, parameters and constants with subscripts 1, 2 and 3 to represent the upper, middle and lower junctions respectively.

2.14. Iterative changes to SJSC design for MJSC architecture

An iterative approach design methodology has been applied to identify possible SJSC modelling practices, or suitable design benchmarks, on which to derive modelling practices for the architecture of MJSCs.Testing involved simple trial and error approach where the Eg form SJSC models, were simulated against MJSC parameters whilst observing the characteristic curves.

2.14.1. SJSC algorithm for parameter extraction in MJSCs

The first SJSC modelling technique tested was the parameter extraction algorithm used to find for the unknown resistances from the manufacturer data sheets.

Testing of the algorithm on the MJSC confirmed that it was not possible to extract the MJSC parameters using the SJSC extraction algorithm. This result was expected, as the triple junction

MJSCs have three different junctions made of materials that vary in bulk characteristic behaviour, making the SJSC algorithm incompatible for parameter extraction.

Developing a suitable MJSC extraction algorithm is not within the scope of this paper, so the resistance parameters supplied in the (Segev, Mittelman & Kribus 2012) will be used for model simulation. Note that the development of an appropriate algorithm for extracting resistance parameters from MJSC manufacturer datasheets may be a possible opportunity for future research.

2.14.2. Adapting the saturation current to the MJSC architecture

The SJSC value for silicon bandgap energy was substituted with the various MJSC values of bandgap energy. The change in bandgap energy values resulted in an inconsequential affect on the characteristic curves.

Investigation of the literature revealed that the modelling techniques used to model SJSC saturation current were not suitable for MJSC architecture. A solution was discovered in many of the papers reviewed for this project, however (Hussain et al. 2016) and (Segev, Mittelman & Kribus 2012), provided a succinct account of the design practices required to overcome the problem

The MJSC model of saturation current required the following design changes:

1. The value of the recombination current was to be determined through experimental measurement. The expression used to approximate the recombination current, Equation 18, is not applied for MJSC simulation. The constant value provided in (Segev, Mittelman & Kribus 2012) is applied in place:
    - I_{rsn} denotes the recombination current for the nth layer junction, where n denotes the upper, middle or lower junction layer.
2. The device bandgap energy is modelled as a function of temperature. Many papers discuss the merits of modelling the bandgap as a function of temperature, including (Hussain et al. 2016) and (Segev, Mittelman & Kribus 2012). This behaviour is given by Equation 25:

$$Eg_n(T_C) = Eg_n(0) - \frac{\alpha_n \cdot T_C^2}{T_C + \beta_n} \qquad \textit{Equation 25}$$

Where: Eg(0) is the given bandgap energy (ev),

T_C is the measured temperature of the cell,

α is a material energy per Kelvin fitting parameter,

β is a material temperature fitting parameters,

and n denotes the upper, middle or lower junction layer.

Modelling the bandgap is given as a function of temperature, allows the Group III-V alloy materials to be selected based on their super positional properties (Segev, Mittelman & Kribus 2012). Note that modelling the bandgap as a function of temperature correlates with the expected responses listed in Table 3. The table outlines three changes in observable characteristics as a result of an increase in temperature as:

i. A small reduction in open circuit voltage,

ii. a small increase in short circuit current,

iii. and a slight reduction in bandgap energy.

The final expression for the diode saturation currents (I_{S1n} *and* I_{S2n}) are given by Equation 26

$$I_{S1n} = I_{S2n} = I_{rsn} \cdot T_C^{\left(\frac{3+\gamma_n}{2}\right)} \cdot exp\left(\frac{-q \cdot Eg_n(T_C)}{a_n \cdot k \cdot T_C}\right) \quad \textit{Equation 26}$$

Where:

I_{rsn} is the recombination current, as a measured experimental value,

T_C is the actual measured temperature of the PV cell (°C),

γ_n is an ideality constant,

q is the charge of an electron, 1.602E-19 C,

$Eg_n(T_C)$ is the temperature dependant bandgap,

a_{1n} is the first diode ideality factor,

a_{2n} is the second diode ideality factor,

k is Boltzmann's constant, 1.381E-23,

2.14.3. Simulink adjustments

The architecture of the Simulink MJSC block model is constructed to simulate the cell, as represented by the D2 MJSC equivalent circuit in Figure 23

The blocks in are Figure 24 labelled to denote the respective order of each blue coloured blocks represent a cell junction, from top to middle to bottom.

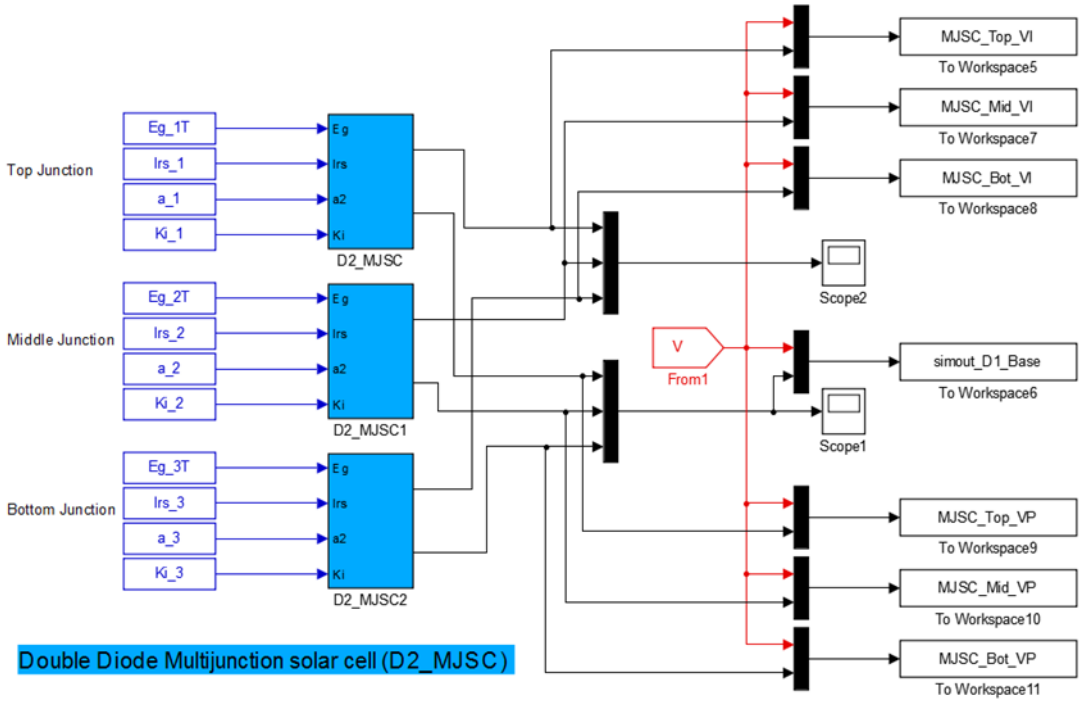

Figure 24: Simulink model of a triple junction solar cell.

Consider the D2 MJSC equivalent circuit on page 37, where the total open circuit voltage is calculated by adding the individual junction open circuit voltages. However when calculating the total current – a simplifying assumption for this paper is that each cell junction generates current of equal density, that is, the junctions are current matched (Hussain et al. 2016). Hence the individual junction current outputs are of the same value as the total cell current output, as per the MJSC series connected equivalent circuit. Consider Equation 16:

$$I_n = I_{ph} - I_{s1}\left[\exp\left(\frac{\mathrm{V+I}\cdot R_s}{a1\cdot V_t}\right) - 1\right] - I_{s2}\left[\exp\left(\frac{\mathrm{V+I}\cdot R_s}{a2\cdot V_t}\right) - 1\right] - \frac{V+I\cdot R_s}{R_p}$$

Where n denotes the top/middle/bottom junction of the cell,

The Simulink block model of the current output of each cell junction is shown in Figure 25, and the Simulink block model for the junction saturation current, given by Equation 26 on page 39, is shown in Figure 26.

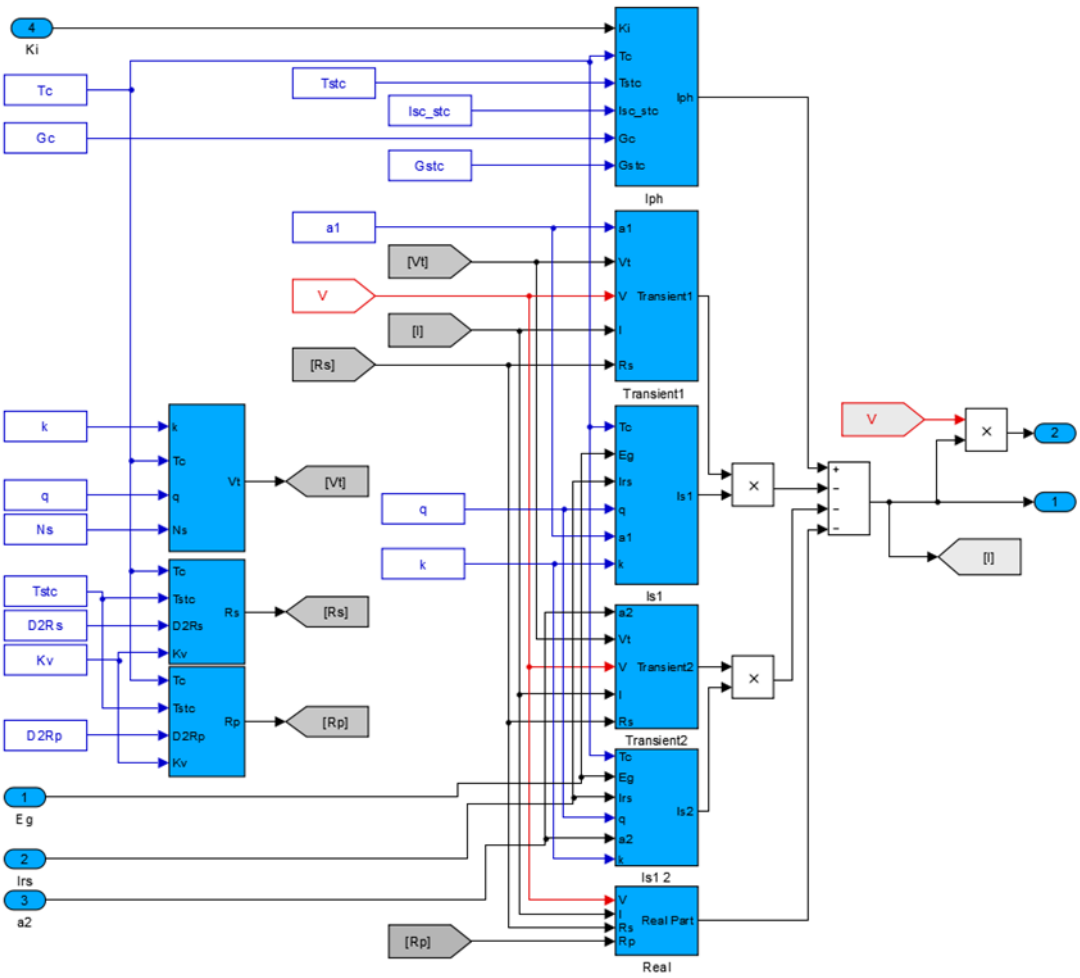

Figure 25: D2 Simulink model of a single cell junction.

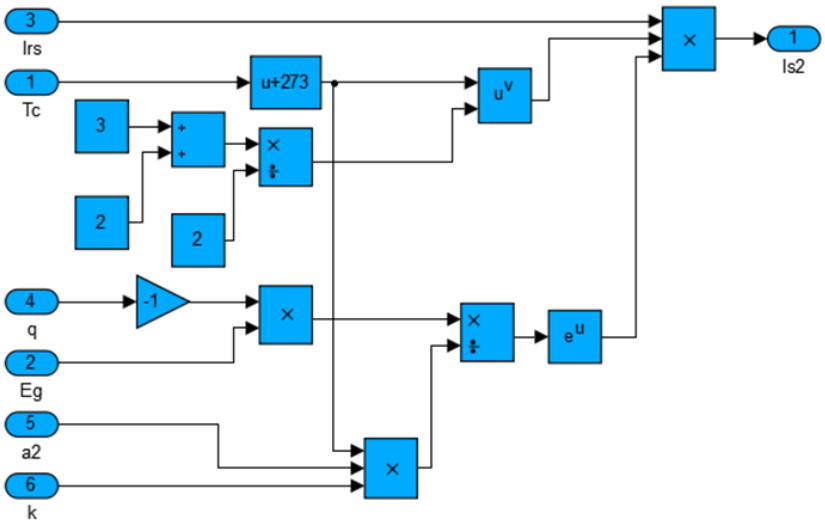

Figure 26: Simulink modelled MJSC junction saturation current.

2.14.4. Modelling conversion efficiency in MJSCs

The modelled expression for the MJSC conversion efficiency differs from the SJSC version because of the change in bulk characteristic behaviour due to the series connected junction layers. The SJSC version of cell the equation for cell efficiency is given by Equation 6:

$$Single\ junction\ cell\ efficiency = \eta_{SJSC} = \frac{P_{mpp}}{P_{in}} = \frac{V_{oc} \cdot I_{sc} \cdot FF}{\left(\frac{Area(mm^2)}{1000}\right)} \cdot 100$$

The SJSC version is the maximum power, divided by the input power for the one single cell junction and is relatively simple to model. The MJSC requires that the input power for each cell junction must be summed before being divided by the input power, as given by Equation 27:

$$MJSC\ efficiency = \eta_{MJSC} = \frac{1}{P_{in}} \sum_{junctions} (V_{oc} \cdot I_{sc} \cdot FF)_j \cdot 100 \qquad \textit{Equation 27}$$

2.14.5. Calculating total Voc

During MJSC testing , there were difficulties summing the individual junction V_{OC} values to find for the total V_{OC} of the cell – from within the Simulink block environment. The solution applied to this challenge was to export the voltage, current and power characteristic related data to the Matlab global workspace via the out-ports of the junction blocks and calculate total cell V_{OC} by:

1. Importing each junction VI and VP curve as a separate array,
2. Interpolate the individual arrays over 10e+3 sample points between V = 0 and I = 0,
3. The total V_{OC} value is then calculated by adding the individual junction array sample points according to the respective VI and VP arrays.
4. The resultant total characteristic curve were then numerically integrated and compared to the sum of the individual numerically integrated curves resulting in a percentage error of 0.00312% of area.

2.15. Summary of characteristics

Table 3 outlines many of the observable simulation/modelling characteristics, and provides as a reference chart for analysis and discussion. Device characteristics are described by measuring standardised equivalent circuit models consisting of of lumped components.

Table 3: Analysis chart summarising parameter characteristics.

Characteristic/Parameter/Behaviour.		
Open circuit voltage.	Proportional to natural log of irradiance (G) , less dependant on G than I_{SC}.	
	V_{OC} (Eg), therefore higher bandgap energy;	Higher V_{OC}
	Higher V_{OC} leads to higher FF, until optimum bandgap exceeded (I_{SC} will start to drop).	Higher *FF*
Short circuit current.	Low parasitic resistance, I_{ph} approximated by I_{SC}.	$I_{ph} \equiv I_{SC}$
	In ideal diodes, I_{SC} is proportional to G when $V_{OC} = 0$.	$I_{SC} \propto G$
	Lower Eg energy (Higher proportion of photons absorbed).	Higher I_{SC}
Bandgap energy	Lower bandgaps energy (ev).	Higher I_{SC}
	Higher bandgaps energy (ev).	Higher V_{OC}
	An optimum bandgap exists for a given spectrum.	
Fill factor	Determined by the shape of the diode VI characteristic.	
	Less rounded usually represents higher quality cell.	
	Difficult to improve FF of poor quality cell.	
	Easy to degrade FF of good quality cell	
Increase temperature	Reduces the FF	Lower Eg; Lower V_{OC}; Higher I_{SC};
Increase irradiance	As (R_P approaches ∞) and (R_S aproaches 0);	Higher FF; ↑ $V_{OC} \propto ln(G)$; ↑ $I_{SC} \propto G$;
Irradiance Mid R_P	Mid range RP and as (R_S aproaches 0);	Higher FF; ↑ $V_{OC} \propto ln(G)$; Higher I_{SC};
Irradiance High R_S	High range RS and as (R_P aproaches ∞);	Lower FF; ↑ $V_{OC} \propto ln(G)$; Higher I_{SC};

2.16. Summary of modelled expressions for MJSC simulation

Table 4: Equations required for MJSC D2 equivalent model.

Modelled expressions and equations for each solar cell junction
Each cell junction has an output given by Equation 16: $I_n = I_{ph} - I_{s1}\left[\exp\left(\frac{\mathrm{V}+\mathrm{I}\cdot R_s}{a1\cdot V_t}\right)-1\right] - I_{s2}\left[\exp\left(\frac{\mathrm{V}+\mathrm{I}\cdot R_s}{a2\cdot V_t}\right)-1\right] - \frac{V+I\cdot R_s}{R_p}$; Where n denotes the top/middle/bottom layer of the cell as 1, 2, 3 respectively;
The temperature dependant resistances are given by Equation 21 and Equation 22: $R_P(\mathrm{T}) = R_P\left(\frac{T_c}{T_{stc}}\right)^{-K_V}, \qquad R_S(\mathrm{T}) = R_S\left(\frac{T_c}{T_{stc}}\right)^{-K_V}$;
The temperature voltage dependant voltage is given by Equation 10: $\mathrm{V}_t = \frac{N_s\cdot k\cdot T_c}{q}$;
The irradiance and temperature dependant photocurrent is given by Equation 8: $I_{ph} = \left[I_{sc\_STC} + K_I\,(T_c - T_{stc})\right]\cdot\left(\frac{G_c}{G_{stc}}\right)$
The diode reverse saturation currents are given by Equation 26: $I_{S1n} = I_{S2n} = I_{rsn}\cdot T_C^{\left(\frac{3+\gamma_n}{2}\right)}\cdot exp\left(\frac{-q\cdot Eg_n(T_C)}{a_n\cdot k\cdot T_C}\right)$ Where $Eg_n(T_C)$ is the temperature dependant bandgap energy, given by Equation 25: $Eg_n(T_C) = Eg_n(0) - \frac{\alpha_n\cdot T_C^2}{T_C+\beta_n}$; and n denotes the nth layer junction. and n denotes the top/middle/bottom layer of the cell as 1, 2, 3 respectively;

Where: I_{rsn} is the recombination current, as a measured experimental value,

T_C is the actual measured temperature of the PV cell (°C),

γ_n is an ideality constant,

q is the charge of an electron, 1.602E-19 C,

a_{1n} is the first diode ideality factor,

a_{2n} is the second diode ideality factor,

k is Boltzmann's constant, 1.381E-23,

V is the total voltage generated by each cell,

I_{RS} is the voltage across the series resistances,

N_S is the number of cells in the PV cell module,

R_P represents the shunt losses within the PV cell,

V_{tc} is the Temperature dependant voltage for Ns cells (at any temperature).

α_n is a material energy per Kelvin fitting parameter,

β_n is a material temperature fitting parameters,

n denotes the respective upper, middle or lower junction layer.

Summary of literature review outcomes

This chapter contained a brief introduction to several topics including conventional SJSCs, P-N junction diodes, bandgap energy models. A literature review of SJSCs subjects included photodiode characteristics, conventional solar cell characteristics and D1 and D2 models. A literature review of MJSCs subjects included structures that influence modelling techniques, loss mechanisms related to MJSCs and provided a chart to assist analysing SJSC and MJSC characteristics.

Chapter 3: Methodology

Chapter 3 contains the project methodology. A Simulink simulation method is proposed for comparing the accuracy of D1 and D2 SJSCs with regards to conversion efficiency, and a Simulink simulation method is proposed for modelling the conversion efficiency of MJSCs

3.1. Simulation methods within Matlab/Simulink

MATLAB Simulink software (by MathWorks) will be used to perform the simulations for this dissertation. The Simulink graphical user interface (GUI) allows the user to represent a system of mathematical expressions as a block systems and subsystems.

The system blocks are connected by operators, functions, sinks and scopes to perform the necessary mathematical operations. The Simulink environment is ideal for producing data in a graphical form where the user also has the ability to export the data from Simulink environment to the Matlab environment to for further analysis.

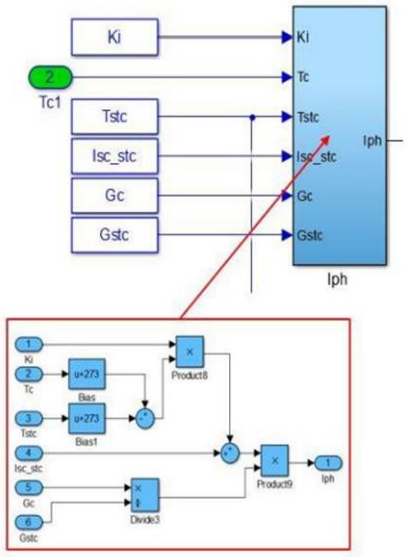

Figure 27: An example of the Simulink block environment.

The flowchart shown in Figure 28 outlines the simulation process and identifies which steps are to be run in the MATLAB script environment (blue blocks), and which steps are to be run in the Simulink block environment (green blocks).

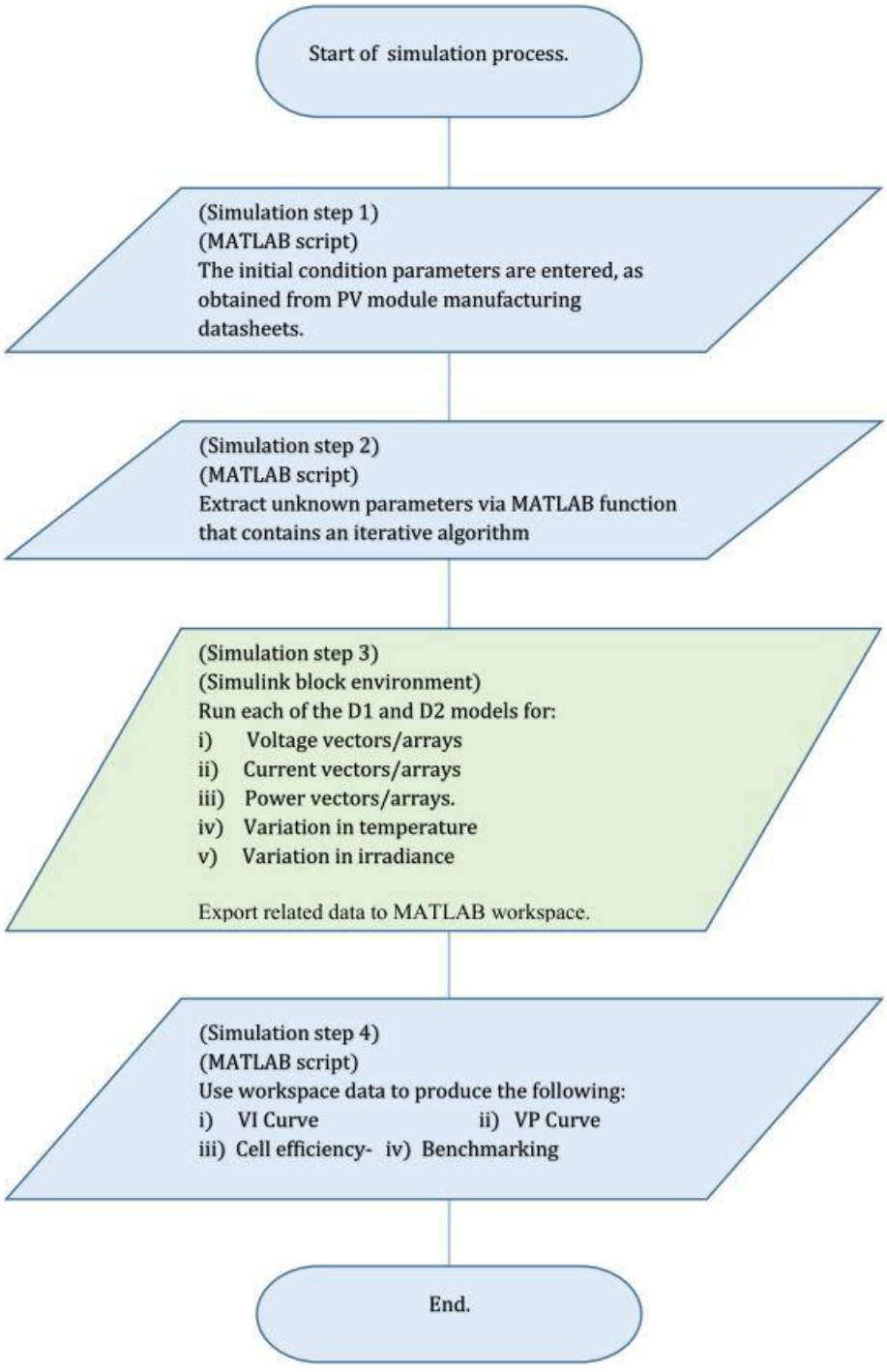

Figure 28: Flow chart outlining simulation process.

3.1.1. Loading initial conditions (Step 1)

The first step of the simulation process, as shown in the flowchart in Figure 28, is to run a MATLAB script to load all parameters required to simulate the models within the Matlab/Simulink environment, including:

- The initial conditions such as the test condition temperature and test condition irradiance,
- The model constants such as Boltzmann's constant and the electron charge value,
- Known manufacturer datasheet parameters such as module area, number of cells, module short circuit current, module open circuit voltage, bandgap energy etc.

3.1.2. Extracting unknown parameters (Step 2)

The second step, as shown in the Figure 28 flowchart, involves finding for the unknown model parameters. Datasheets provided by manufacturers do not provide information regarding cell resistances, hence, the information must be translated before being of use to most models (Chin, Salam & Ishaque 2015).

Parameter extraction is a well documented method of finding for the required resistances, where a Newton-Raphson algorithm is written to calculate the module series resistance and parallel resistance. Of the many papers reviewed regarding extraction techniques, including - (Celik & Acikgoz 2007), (Bellia, Youcef & Fatima 2014), (Aoun et al. 2014), (Chin, Salam & Ishaque 2015), (Humada et al. 2016) and (Mertens & Roth 2014), the code provided by (Vika 2014) was found to be of particular relevance to this paper.

Series resistance (R_S) and parallel resistance (R_P) are dependant parameters that can be found when three independent points are considered - namely the short circuit point, the voltage at open circuit and the maximum current at the power point.

The derivation of the single diode version of the algorithm follows, where firstly, several local initial conditions are entered into the algorithm:

i. An approximated value for the temperature dependant voltage:

$$V_{tn} = (\mathrm{k} \cdot T_{stc})/q \qquad \textit{Equation 28}$$

ii. An approximated value for the saturation current:

$$I_{sn} = \frac{I_{sc\_stc}}{exp\left(\frac{V_{oc\_stc}}{a \cdot N_S \cdot V_{tn}}\right) - 1}$$ *Equation 29*

iii. And an approximated value for the photocurrent:

$$I_{phn} = I_{sc\_stc}$$ *Equation 30*

Then consider that the first (independent) expression (the short circuit current) occurs when the current output is at maximum and the voltage potential is zero (Mertens & Roth 2014). The short circuit current is shown on the vertical axis of Figure 8 (page 9), where the shorted condition (0, Isc_stc) is given by:

$$I_{sc} = I_{ph} - I_s \left(\exp\left(\frac{I_{sc\_stc} \cdot R_s}{a \cdot V_t}\right) - 1\right) - \frac{I_{sc\_stc} \cdot R_s}{R_p}$$ *Equation 31*

The second (independent) expression is the open circuit voltage, that occurs when the voltage potential is at maximum and I_{SC} is equal to zero (Mertens & Roth 2014), as shown on the horizontal axis of Figure 8 (page 9),. The open circuit voltage is given by:

$$0 = I_{ph} - I_s \left(\exp\left(\frac{V_{oc\_stc}}{a \cdot V_t}\right) - 1\right) - \frac{V_{oc\_stc}}{R_p}$$ *Equation 32*

The third (independent) expression is the current at the maximum power point (shown on the VI curve knee point in Figure 8 (page 9), - the maximum power that the PV cell can provide. The MPP (Vmpp, Impp) is given by:

$$I_{mpp} = I_{ph} - I_s \left(\exp\left(\frac{V_{mpp} + I_{mpp} \cdot R_s}{a \cdot V_t}\right) - 1\right) - \frac{V_{mpp} + I_{mpp} \cdot R_s}{R_p}$$ *Equation 33*

The derivative of the maximum power is equal to zero, and as there is no change in current with respect to voltage at the maximum, so the extraction algorithm is provided an appropriate point to commence. The derivative of Pmpp is given by:

$$\left.\frac{dP}{dV}\right|_{mpp} = \left.\frac{d(VI)}{dV}\right|_{mpp} = I_{mpp} + V_{mpp}\left.\frac{dI}{dV}\right|_{mpp} = 0 \qquad \textit{Equation 34}$$

Therefore, the expression can be solved for the series resistance as follows:

$$0 = I_{mpp} + V_{mpp}\left.\frac{dI}{dV}\right|_{mpp}$$

$$Rs = \frac{V_{mpp\_stc}}{I_{mpp\_stc}} - \frac{R_p a N_s V_{tn}}{R_p \cdot q \cdot I_s \cdot exp\left(\frac{q(V_{mpp\_stc}+I_{mpp\_stc}\cdot Rs)}{aN_s \cdot V_{tn}}\right)+aN_s V_{tn}} \qquad \textit{Equation 35}$$

The expression for the series resistance can then serve as the first error in the extraction algorithm:

$$\therefore \; ErrRs = \frac{V_{mpp\_stc}}{I_{mpp\_stc}} - \frac{R_p a N_c V_{tn}}{R_p \cdot q \cdot I_s \cdot exp\left(\frac{q(V_{mpp\_stc}+I_{mpp\_stc}\cdot Rs)}{aN_s \cdot V_{tn}}\right)+aN_s V_{tn}} - R_s \qquad \textit{Equation 36}$$

The shunt resistance is found by evaluating the current at the maximum power point, equation (Equation 33), and solving for the shunt resistance:

$$\frac{P_{mpp\_stc}}{V_{mpp\_stc}} = I_{mpp} = I_{ph} - I_s\left(\exp\left(\frac{V_{mpp+}I_{mpp}\cdot R_S}{a\cdot V_t}\right)-1\right) - \frac{V_{mpp+}I_{mpp}\cdot R_S}{R_p}$$

$$\frac{V_{mpp+}I_{mpp}\cdot R_S}{R_p} = I_{ph} - I_s\left(\exp\left(\frac{V_{mpp+}I_{mpp}\cdot R_S}{a\cdot V_t}\right)-1\right) - I_{mpp\_stc}$$

$$R_p = \frac{V_{mpp+}I_{mpp}\cdot R_S}{I_{ph} - I_s\left(\exp\left(\frac{V_{mpp+}I_{mpp}\cdot R_S}{a\cdot V_t}\right)-1\right) - I_{mpp\_stc}} \qquad \textit{Equation 37}$$

Again, the expression for the shunt resistance can then serve as the second error in the extraction algorithm:

$$\therefore \quad RpErr = \frac{V_{mpp+}\, I_{mpp} \cdot R_S}{I_{ph} - I_s\left(\exp\left(\frac{V_{mpp+}\, I_{mpp} \cdot R_S}{a \cdot V_t}\right) - 1\right) - I_{mpp\_stc}} - R_p$$ *Equation 38*

The photocurrent is the third and final error that will be required to form the boundaries for the extraction algorithm, and is given by:

$I_{ph} = I_{sc\_stc}\left(\frac{R_p + R_s}{R_p}\right)$ ...to give the third error as:

$$IphErr = I_{sc\_stc}\left(\frac{R_p + R_s}{R_p}\right) - I_{ph}$$ *Equation 39*

Finally, the minimum error chosen can be compared to the total of all errors, take the square of each error and sum them for:

$$TotalErr = RsErr^2 + RpErr^2 + IphErr^2$$ *Equation 40*

A flowchart of the single diode algorithm is provided in Figure 29. The double diode version of the extraction algorithm largely follows on from the D1 model, excepting:

i. The extra diode dark saturation current multiplier is to be included in the initial conditions, resulting in saturation currents Is1n and Is2n;

ii. The second diode ideality factor is also to be included in the initial conditions, resulting in ideality factors a1 and a2;

iii. The errors must be solved for double exponential expressions, rather than the single exponential expression shown in the D1 extraction algorithm.

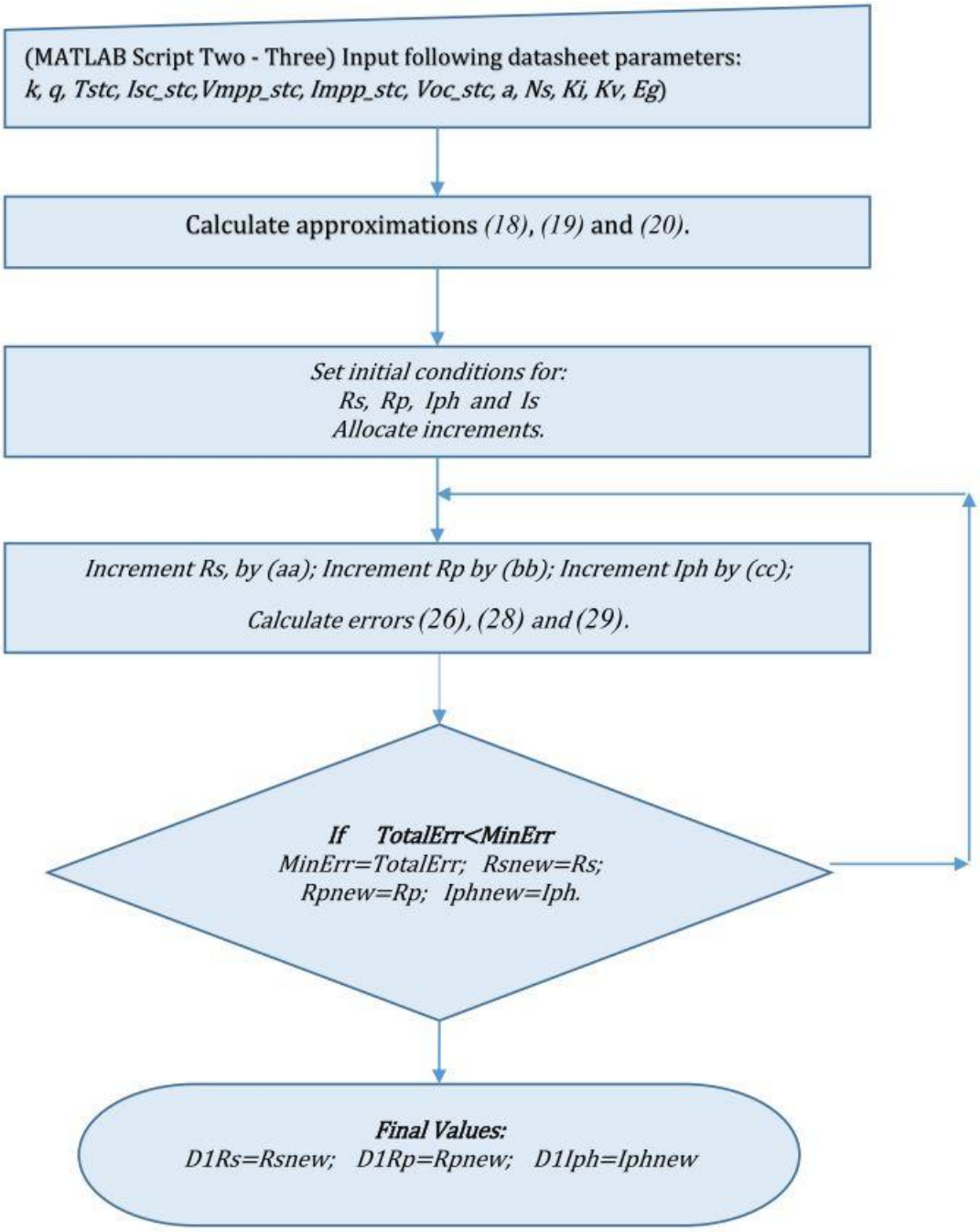

Figure 29: MATLAB script 2 and 3 extraction algorithm flowchart.

3.1.3. Simulated Model forms (Step 3)

The third step of the simulation process, as shown in the Figure 28 flowchart, is to run the built models in the Simulink environment. The parameter detail of the four SJSC models to be built, are as follows:

1. ***D1_Kv model (Single diode model, with Kv form saturation current)***

   The single diode version of the Kv-form model does NOT contain the bandgap energy within the saturation current. The behaviour of D1_Kv form model is to be simulated using the following seven expressions, with equations as numbered in Table 5:

   i. The output current : Equation 13
   ii. The photocurrent: Equation 8
   iii. Voltage (Temperature): Equation 10
   iv. The reverse saturation current: Equation 19
   v. The recombination current: *Cancelled within saturation current*
   vi. Series resistance (Temperature): Equation 24
   vii. Shunt resistance (Temperature): Equation 23

Table 5: Summary of equations within D1_Kv and D2_Kv models.

Modelled expressions and equations	***(#)***	***D1_Kv***	***D2_Kv***
$I = I_{ph} - I_s\left[\exp\left(\frac{q(\mathrm{V}+\mathrm{I}\cdot R_S)}{a\cdot N_S\cdot \mathrm{k}\cdot T_c}\right)-1\right] - \frac{V+I\cdot R_S}{R_p}$	*(13)*	✓	
$I = I_{ph} - I_{s1}\left[\exp\left(\frac{\mathrm{V}+\mathrm{I}\cdot R_s}{a1\cdot V_t}\right)-1\right] - I_{s2}\left[\exp\left(\frac{\mathrm{V}+\mathrm{I}\cdot R_s}{a2\cdot V_t}\right)-1\right] - \frac{V+I\cdot R_s}{R_p}$	*(16)*		✓
$R_P(\mathrm{T}) = R_P\left(\frac{T_c}{T_{stc}}\right)^0$ $R_S(\mathrm{T}) = R_S\left(\frac{T_c}{T_{stc}}\right)^0$	*(24)* *(23)*	✓	✓
$\mathrm{V}_t = \frac{N_S\cdot k\cdot T_c}{q}$	*(10)*	✓	✓
$I_{ph} = \left[I_{sc\_STC} + K_I\,(T_c - T_{stc})\right]\cdot\left(\frac{G_c}{G_{stc}}\right)$	*(8)*	✓	✓
$I_s = \frac{I_{sc\_stc}+K_I\cdot(T_c-T_{stc})}{\left[\exp\left(\frac{V_{oc\_stc}+K_V\cdot(T_c-T_{stc})}{a\cdot V_t}\right)-1\right]}$	*(19)*	✓	
$I_{s1} = I_{s2} = \frac{I_{sc\_stc}+K_I\cdot(T_c-T_{stc})}{\left[\exp\left(\frac{V_{oc\_stc}+K_V\cdot(T_c-T_{stc})}{\left(\frac{a1+a2}{P_e}\right)\cdot V_{tc}}\right)-1\right]}$	*(20)*		✓

2. ***D2_Kv model (Double diode model, with Kv form saturation current)***

The double diode version of the Kv-form model does NOT contain the bandgap energy within the saturation current. The behaviour of D2_Kv form model is to be simulated using the following seven expressions, with equations as numbered in Table 5:

i. The output current : Equation 16
ii. The photocurrent: Equation 8
iii. Voltage (Temperature): Equation 10
iv. The diode saturation current: Equation 20
v. The recombination current: *Cancelled within saturation current*
vi. Series resistance (Temperature): Equation 24
vii. Shunt resistance (Temperature): Equation 23

3. ***D1_Eg model (Single diode model, with Eg form saturation current)***

The single diode version of the Eg-form model includes the bandgap energy within the saturation current. The behaviour of D1_Eg form model is to be simulated using the following seven expressions, with equations as numbered in Table 6:

i. The output current : Equation 13
ii. The photocurrent: Equation 8
iii. Voltage (Temperature): Equation 10
iv. The diode saturation current: Equation 11
v. The recombination current : Equation 12
vi. Series resistance (Temperature): Equation 22
vii. Shunt resistance (Temperature): Equation 21

4. D2_Eg model (Double diode model, with Eg form saturation current)

The double diode version of the Eg-form model also includes the bandgap energy within the saturation current. The behaviour of D2_Eg form model is to be simulated using the following seven expressions, with equations as numbered in Table 6

i. The output current : Equation 16
ii. The photocurrent: Equation 8
iii. Voltage (Temperature): Equation 10
iv. The diode saturation current: Equation 17
v. The recombination current: Equation 18
vi. Series resistance (Temperature): Equation 22
vii. Shunt resistance (Temperature): Equation 21

Table 6: Summary of equations within D1_Eg and D2_Eg models.

Summary of Eg form expressions and equations	***(#)***	***D1_Eg***	***D2_Eg***
$I = I_{ph} - I_s\left[\exp\left(\frac{q(\mathrm{V}+\mathrm{I}\cdot R_S)}{a\cdot N_S\cdot \mathrm{k}\cdot T_c}\right) - 1\right] - \frac{V+I\cdot R_s}{R_p}$	*(13)*	✔	
$I = I_{ph} - I_{s1}\left[\exp\left(\frac{\mathrm{V}+\mathrm{I}\cdot R_s}{a1\cdot V_t}\right) - 1\right] - I_{s2}\left[\exp\left(\frac{\mathrm{V}+\mathrm{I}\cdot R_s}{a2\cdot V_t}\right) - 1\right] - \frac{V+I\cdot R_s}{R_p}$	*(16)*		✔
$R_P(\mathrm{T}) = R_P\left(\frac{T_c}{T_{stc}}\right)^{-K_V}$ $R_S(\mathrm{T}) = R_S\left(\frac{T_c}{T_{stc}}\right)^{-K_V}$	*(24)* *(23)*	✔	✔
$\mathrm{V}_t = \frac{N_S\cdot k\cdot T_c}{q}$	*(10)*	✔	✔
$I_{ph} = \left[I_{sc\_STC} + K_I\,(T_c - T_{stc})\right]\cdot\left(\frac{G_c}{G_{stc}}\right)$	*(8)*	✔	✔
$I_s = I_{rs}\left(\frac{T_c}{T_{stc}}\right)^3\cdot exp\left(\left(\frac{q\cdot E_g}{a\cdot k}\right)\left(\frac{1}{T_{stc}} - \frac{1}{T_c}\right)\right)$ where... $I_{rs} = \frac{I_{ph\_stc}}{exp\left(\frac{V_{oc\_stc}}{a\cdot V_{tstc}}\right)-1} = \frac{I_{sc\_stc}}{exp\left(\frac{V_{oc\_stc}}{a\cdot V_{tstc}}\right)-1}$	*(11)* *(12)*	✔	
$I_{s1} = I_{s2} = I_{rs2}\left(\frac{T_c}{T_{stc}}\right)^3\cdot exp\left(\left(\frac{q\cdot E_g}{a2\cdot k}\right)\left(\frac{1}{T_{stc}} - \frac{1}{T_c}\right)\right)$ where ... $I_{rs_1} = I_{rs_2} = \frac{I_{ph\_stc}}{\exp\left(\frac{V_{oc\_stc}}{a_2\cdot V_t}\right)-1} = \frac{I_{sc\_stc}}{\exp\left(\frac{V_{oc\_stc}}{a_2\cdot\frac{Ns\cdot k\cdot T_c}{q}}\right)-1}$	*(17)* *(18)*		✔

3.1.4. Collating simulation results for discussion (Step 4)

The fourth and final step of the simulation process, as shown in the Figure 28 flowchart, is to write a Matlab script that collects the data from the Simulink environment, loads it into the Matlab environment and prints the various characteristic curves for analysis.

The first set of data will be collated to analyse the Kv form simulated models and:

i. Compare the conversion efficiency of the D1_Kv model to the conversion efficiency of the D2_Kv form model, with respect to accuracy;

ii. Compare the conversion efficiency of the D1_Kv model to the conversion efficiency of the D2_Kv form model, with respect to irradiance;

iii. Compare the conversion efficiency of the D1_Kv model to the conversion efficiency of the D2_Kv form model, with respect to temperature.

The second set of data will be collated to analyse the Eg form simulated models and:

i. Compare the conversion efficiency of the D1_Eg model to the conversion efficiency of the D2_Eg form model, with respect to accuracy;

ii. Compare the conversion efficiency of the D1_Eg model to the conversion efficiency of the D2_Eg form model, with respect to irradiance;

iii. Compare the conversion efficiency of the D1_Eg model to the conversion efficiency of the D2_Eg form model, with respect to temperature.

3.1.5. Validation and relative error percentage

The data used for validation is limited to material reviewed within the literature. The results of the single junction simulations are validated against the data results published in (Ishaque, Salam & Taheri 2011), referred to as the 'Validation Data'. The (Ishaque, Salam & Taheri 2011) paper by provides data regarding the single and double diode modelling of Siemens SP70 PV modules with respect to:

i. Resolved initial extraction values for photocurrent, ideality factors; series resistances and parallel resistances for a single diode model;

ii. Resolved initial extraction values for photocurrent, ideality factors; series resistances and parallel resistances for a double diode model;

iii. Measured values of *Pmpp* and *Vmpp* at various values of temperature and corresponding expected values for the percentage error of each value;

Data will be accepted as validated if the percentage relative error for the simulated measurement is within a predetermined percentage value relative to the Validation data, where the error percentage is given by:

$$Error(\%) = \frac{Modelled\ measurement - Theoretical\ measurement}{Theoretical\ measurement} \times 100 \qquad \textit{Equation 41}$$

A maximum relative error of +/- 5% will be applied in this paper and will be deemed acceptable if the Error (%) for the simulated measurement is within +/-5% of the Validation data.

Values of error for Pmpp and Vmpp are designated as primary Error (%) values. All other values of error are designated as secondary Error (%) values. There may be instances where a secondary error percentage is outside of the 5% relative range and deemed acceptable. These instances will be deemed 'Acceptable' provided that simulation can prove that the secondary error does not push the primary Error (%) outside of the 5% relative range.

3.2. Simulated single junction solar cells

Chapter 3.2 provides a discussion on the results of the comparative simulation between D1 and D2 SJSCs with regards to conversion efficiency.

3.2.1. Results of parameter extraction

Extraction of the unknown parameters is completed first and validated before including in the initial conditions. The extracted parameters listed in table Table 7 is relavent to the respective D1 and D2 models, irrespective of their form.

The results of the extraction codes, were analysed to ensure that the initial values were acceptable compared to the validation data. There were several percentage errors greater than the 5% range, including the ideality factors (an), the shunt resistances and the series resistances. The ideality factor is largely used as a curve-fitting tool and is commonly used to fine-tune the models to a lower error and the Eg form models performed more accurately with an ideality factor of 1.4. This change in ideality had a knock on effect that changes the expected values of the resistances. All values of expected and resultant parameters were simulated within the environment and the parameters listed below produced the most accurate results.

Table 7: Validation of D1 and D2 extracted parameters.

Published data taken from (Ishaque, Salam & Taheri 2011)			
Extracted data taken from the Mono-crystalline SP-70 PV cell module datasheet included in the appendices.			
Single Diode Extracted parameters			
	Published	***D1 models***	***Error (%)***
I_{ph} *(A) =*	*4.72*	*4.7*	*0.42%*
a =	*1.3*	*1.3*	*0.00%*
R_p *(ohm) =*	*122.1*	*149*	*22.03%*
R_s *(ohm) =*	*0.4*	*0.409*	*2.25%*

Double Diode Extracted parameters			
	Published	***D2 models***	***Error (%)***
Iph (A) =	*4.7*	*4.73*	*0.64%*
a1 =	*1*	*1*	*0.00%*
a2 =	*2*	*2*	*0.00%*
Rs (ohm) =	*91*	*85*	*6.59%*
Rp (ohm) =	*0.51*	*0.527*	*3.33%*

Simulation of these particular parameters demonstrated that the discrepancies will be of little consequence to the final simulation results.

Although the the extracted data was not within the 5%Error, repeated simulation confirmed that the relative secondary errors in the extraction values do not adversely affect the primary error percentage range for the Pmpp and Vmpp values.

3.3. Simulated multijunction solar cell

3.3.1. GaInP/GaInAs/Ge (D2) simulation

The same validation principles apply as discussed on page 56. The results of the GaInP/GaInAs/Ge (D2) triple MJSC simulations are validated against the data results published in (Hussain et al. 2016). The paper provides data related to experimental results of testing a D2 MJSC simulated model against a Sharp GaInP/GaInAs/Ge solar cell.

The (Hussain et al. 2016) paper provides comparative results results for I_{mpp}, V_{mpp}, V_{OC}, I_{SC} and FF at full and half sun irradiance values. The data will be accepted as validated if the results fall within the maximum relative error of +/- 5%.

3.3.2. GaInP/GaInAs/Ge (D2) triple MJSC initial conditions

The initial conditions for the GaInP/GaInAs/Ge (D2) triple MJSC is provided in Table 8.

Table 8: GaInP/GaInAs/Ge (Hussain et al. 2016) (D2) triple MJSC initial parameters

Initial Parameters: GaInP/GaInAs/Ge (Hussain et al. 2016) (D2) triple MJSC.			
Parameter:	**Value**	**Parameter:**	**Value**
Voc_stc (V)	5.178	a1 (top junct.)	1.37

Isc_stc (A)	0.206	a2 (mid junct.)	1.15
Vmpp_stc (V)	4.544	a3 (lower junct.)	1.36
Impp_stc (A)	0.196	Irs_1 (A) (top junct.)	1.86E-09
Pmpp_stc (W)	0.89	Irs_2 (A) (mid junct.)	1.28E-08
Irradiance (W/m2)	500	Irs_3 (A) (lower junct.)	0.0000105
Temperature (‘C)	40	KI1 (A) (top junct.)	0.00075
Cell Area (m^2)	0.000049	KI2 (A) (middle junct.)	0.000558
Number of cells	1	KI3 (A) (lower junct.)	0.0004774
RS (Ω)	0.219	β1 (K) (top junct.)	372
RP (Ω)	-	β2 (K) (mid junct.)	204
a1 (top junct.)	1.37	β3 (K) (lower junct.)	235
Junction:	**Material**	**Bandgap (ev)**	**Wavelength (nm)**
Upper/top (Eg1)	GaInP	2.637	470
Middle (Eg2)	GaInAs	1.874	662
Lower/bottom (Eg3)	Ge	0.6583	1883

Chapter 4: Results and Analysis

Chapter 4 provides a discussion on the results of the comparative simulation between D1 and D2 SJSCs with regards to conversion efficiency and contains a discussion on the results of the MJSC conversion efficiency simulations.

Single junction solar cell results

4.1. Results of Kv form simulations

A copy of the Matlab script used to load the initial conditions into the simulation environment is provided in Appendix 6 and the initial conditions for the Kv form of simulated models is summarised in Table 9.

Table 9: Initial conditions for the Kv form D1 and D2 models.

Single Diode Kv Form (D1_Kv) and Double Diode Kv Form (D2_Kv) model parameters.							
Initial Parameters:	***Eg parameter not included.***						
Type of Cell:	Mono-crystalline Siemens SP70 PV Module						
P_{mpp_stc} (W) =	*70*	N_s =	*36*	*Area* (m^2) =	*0.5625*	*D1Rs* =	*0.371*
I_{mpp_stc} (A) =	*4.24*	K_I (A/K) =	*0.002*	*a* =	*1.3*	*D1Rp* =	*158*
V_{mpp_stc} (V) =	*16.5*	K_v (V/K) =	*-0.076*	*a1* =	*1*	*D2Rs* =	*0.527*
V_{oc_stc} (V) =	*21.4*	T_c (‘C) =	*25*	*a2* =	*1.3*	*D2Rp* =	*89*
I_{sc_stc} (A) =	*4.7*	G_c (W/m^2) =	*1000*	P_e =	*2.3*		

The complete build of the each of the Simulink models, as seen from GUI perspective, is included in the appendices as follows:

- Appendix 11 contains the D1_Kv model , and can be identified by yellow coloured Simulink blocks, as shown in Figure 30;
- Appendix 12 contains the D2_Kv model and can be identified by cyan coloured Simulink blocks, as shown in Figure 31;

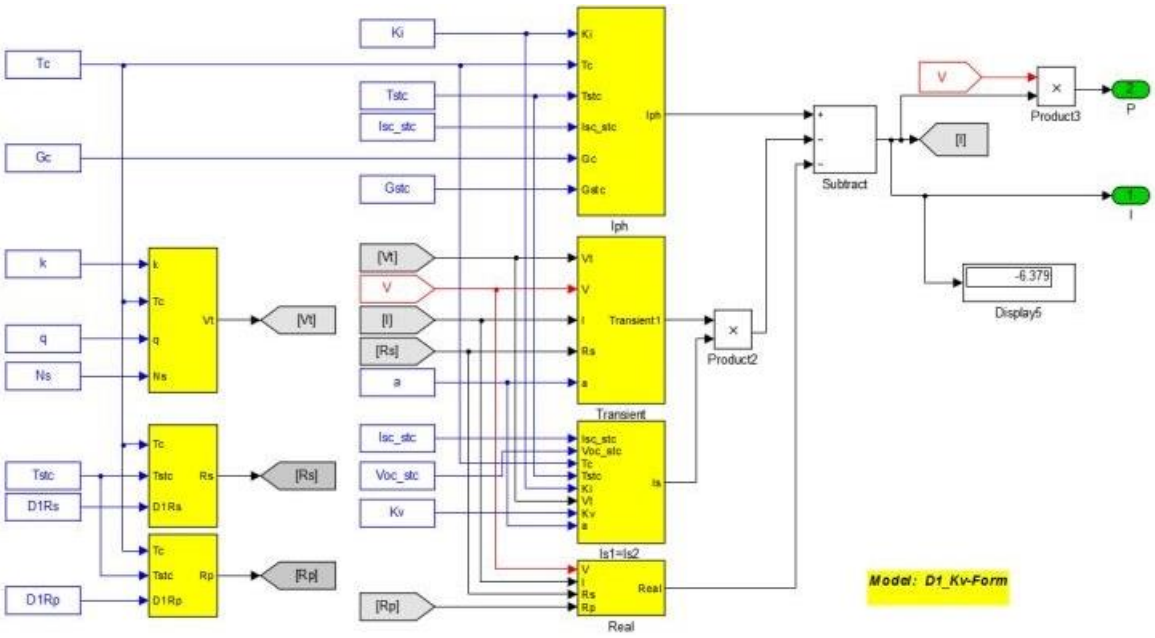

Figure 30: The D1_Kv output current (I) block build, as seen within the Simulink GUI.

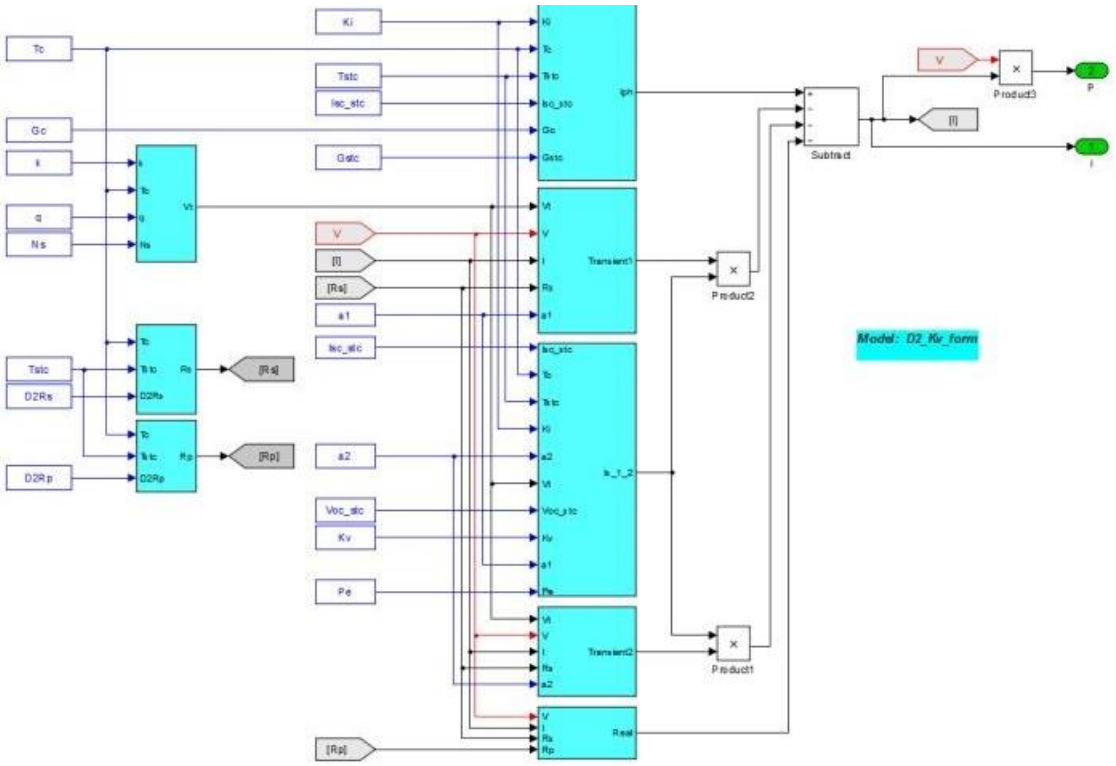

Figure 31: The D2_Kv output current (I) block build, as seen within the Simulink GUI.

4.1.1. Kv form efficiency with respect to model accuracy

The second step was to validate that the voltage and current outputs, were within the acceptable error percentage range of 5%. The Validation Data provided a maximum power point and a maximum voltage point for each of the variations in temperature, and as Table 10 shows:

i. The expected errors of the individual validation data points are listed in column 5, and the averaged relative error is shown in the final row of column 5;

ii. Each of the individual D1_Kv data points are well within the 5% range, with an averaged relative error of 0.38%;

iii. Likewise, the individual D2_Kv data points are well within the 5% range, with an averaged relative error of 0.35%;

Table 10: Relative MPP errors for D1_Kv and D2_Kv form models.

Relative errors on the maximum power point for D1 and D2 models against varying temperatures for a SP-70 mono-crystalline module.

Temp (˚C)	*Measured data*	*D1_Kv-Form*	*D2_Kv-Form*	*Expected Error (%)*	*Error D1 (%)*	*Error D2 (%)*
50	$P_{mpp} = 62.13$	$P_{mpp} = 61.37$	$P_{mpp} = 61.68$	*0.612*	*1.22*	*0.73*
	$V_{mpp} = 14.60$	$V_{mpp} = 14.61$	$V_{mpp} = 14.59$	*0.000*	*0.07*	*0.07*
25	$P_{mpp} = 70.00$	$P_{mpp} = 69.56$	$P_{mpp} = 69.73$	*0.014*	*0.63*	*0.38*
	$V_{mpp} = 16.50$	$V_{mpp} = 16.50$	$V_{mpp} = 16.50$	*0.000*	*0.00*	*0.00*
0	$P_{mpp} = 77.80$	$P_{mpp} = 77.71$	$P_{mpp} = 77.66$	*0.393*	*0.11*	*0.18*
	$V_{mpp} = 18.40$	$V_{mpp} = 18.45$	$V_{mpp} = 18.46$	*0.543*	*0.27*	*0.33*
-25	$P_{mpp} = 85.75$	$P_{mpp} = 85.79$	$P_{mpp} = 85.43$	*0.665*	*0.05*	*0.37*
	$V_{mpp} = 20.30$	$V_{mpp} = 20.44$	$V_{mpp} = 20.45$	*0.985*	*0.69*	*0.74*
				0.40	*0.38*	*0.35*

4.1.2. Kv form efficiency with respect to irradiance

Both the single and double PV cells are modelled with respect to the environmental changes in temperature and irradiance (Weidong, Dunford & Capel 2004). As the irradiance of a cell increases, the PV cell produces more power, but only to a point, because - as the temperature of cell approaches the maximum power point - the voltage of the cell drops.

The VP curves, Figure 33, are the simulated characteristics of the D1_Kv model and the D2_Kv model, and as expected, an increase in irradiance results in an increase in output power. The power increase then results in a increase in efficiency, Figure 33, due to the fact that the cell/module is producing more power per unit of area.

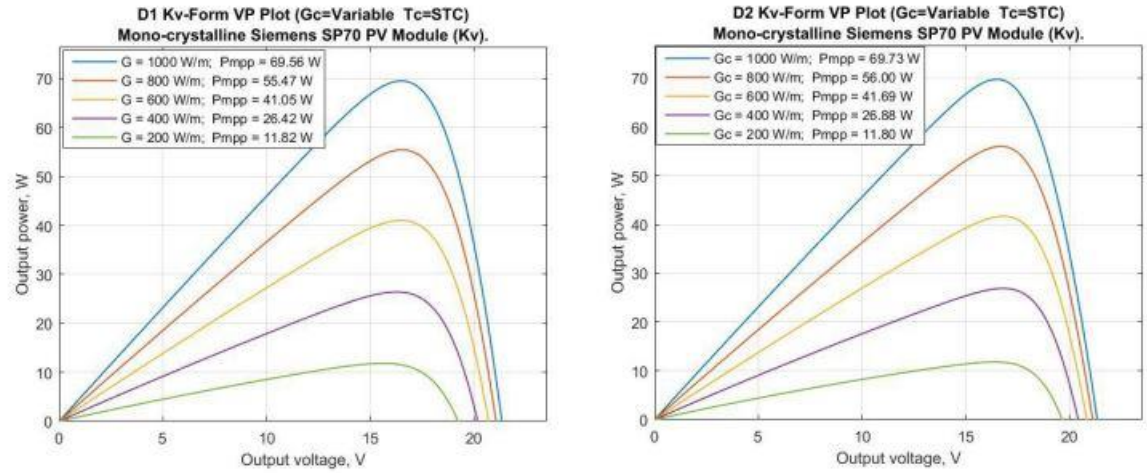

Figure 33: Comparison of D1_Kv and D2_Kv VP curves with respect to irradiance.

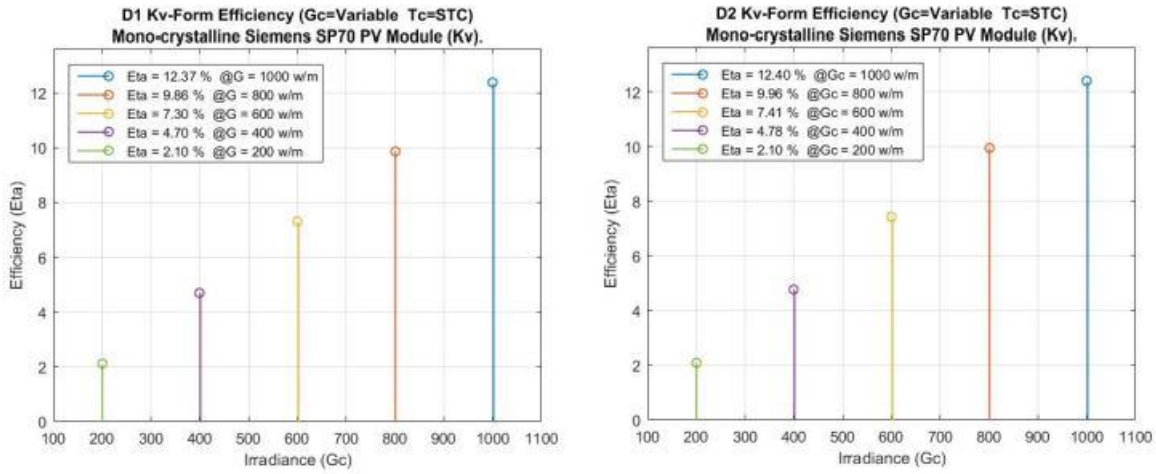

Figure 33: Comparison of D1_Kv and D2_Kv efficiency, with respect to irradiance.

The data extracted from the D1_Kv and D2_Kv simulation for the power and efficiency at various levels of irradiance is summarised in Table 11 and Table 12.

Consider the following observations:

i. An increase in irradiance does result in an expected increase in power for both D1_Kv and D2_Kv models.

ii. An increase in irradiance does result in an expected increase in efficiency for both D1_Kv and D2_Kv models.

iii. When the D2_Kv model, is compared to the D1_Kv model, it is expected that the D1_Kv model would have an equal or higher rate of efficiency with respect to irradiance in the D2_Kv model. The results show an unexpected averaged efficiency of 0.04% in the D2_Kv model, however this is well within the accepted 5% error range.

Table 11: D1_Kv form model data for efficiency with respect to irradiance.

D1_Kv-Form (Efficiency at varying irradiances) (Temperature: Tc = Tstc = 25(˚C))							
Gc (W/m^2)	*P_{mpp} (W)*	*V_{mpp} (V)*	*I_{mpp} (A)*	*I_{sc} (A)*	*V_{oc} (V)*	*FF*	*Efficiency (%)*
1000	*69.56*	*16.50*	*4.22*	*4.68*	*21.35*	*0.70*	*12.37*
800	*55.47*	*16.54*	*3.35*	*3.75*	*21.07*	*0.70*	*9.86*
600	*41.05*	*16.49*	*2.49*	*2.81*	*20.71*	*0.71*	*7.30*
400	*26.42*	*16.28*	*1.62*	*1.87*	*20.19*	*0.70*	*4.70*
200	*11.82*	*15.62*	*0.76*	*0.94*	*19.24*	*0.66*	*2.10*
							4.54

Table 12: D2_Kv form model data for efficiency with respect to irradiance.

D2_Kv-Form (Efficiency at varying irradiances) (Temperature: Tc = Tstc = 25(˚C))							
Gc (W/m^2)	*P_{mpp} (W)*	*V_{mpp} (V)*	*I_{mpp} (A)*	*I_{sc} (A)*	*V_{oc} (V)*	*FF*	*Efficiency (%)*
1000	*69.73*	*16.50*	*4.23*	*4.67*	*21.35*	*0.70*	*12.40*
800	*56.00*	*16.69*	*3.36*	*3.74*	*21.13*	*0.71*	*9.96*
600	*41.69*	*16.82*	*2.48*	*2.80*	*20.84*	*0.71*	*7.41*
400	*26.88*	*16.81*	*1.60*	*1.87*	*20.43*	*0.70*	*4.78*
200	*11.80*	*16.37*	*0.72*	*0.93*	*19.66*	*0.64*	*2.10*
							4.58

4.1.3. Kv form efficiency with respect to temperature

Both the D1 and D2 model PV cells are modelled with respect to the environmental changes in temperature and irradiance (Weidong, Dunford & Capel 2004). All semiconductor devices are sensitive to the effects temperature (Kelvin), including photovoltaic cells, as an increase in temperature will effectively reduce the bandgap and increase the ability of a bounded electron to break free from its valence (Liu & Dougal 2002).

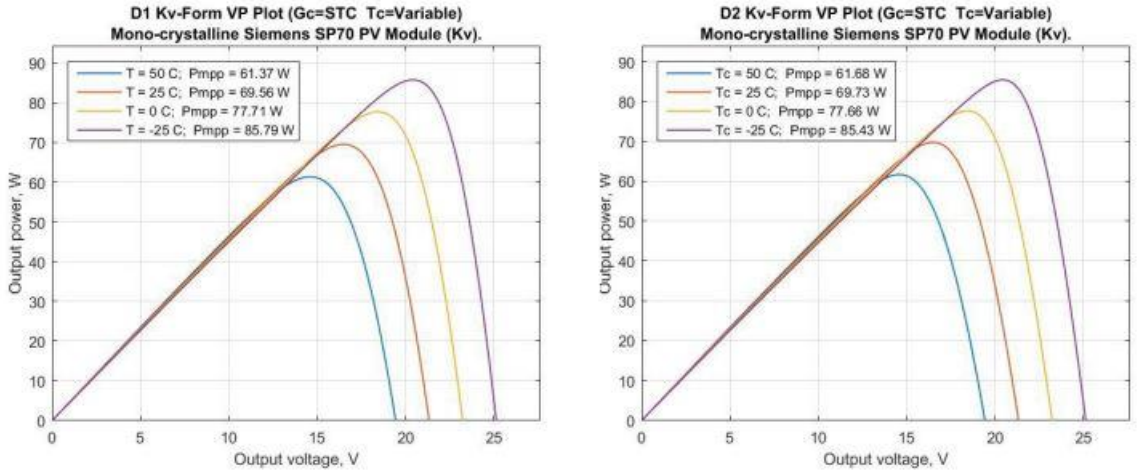

Figure 34: Comparison of D1_Kv and D2_Kv VP plots with respect to temperature.

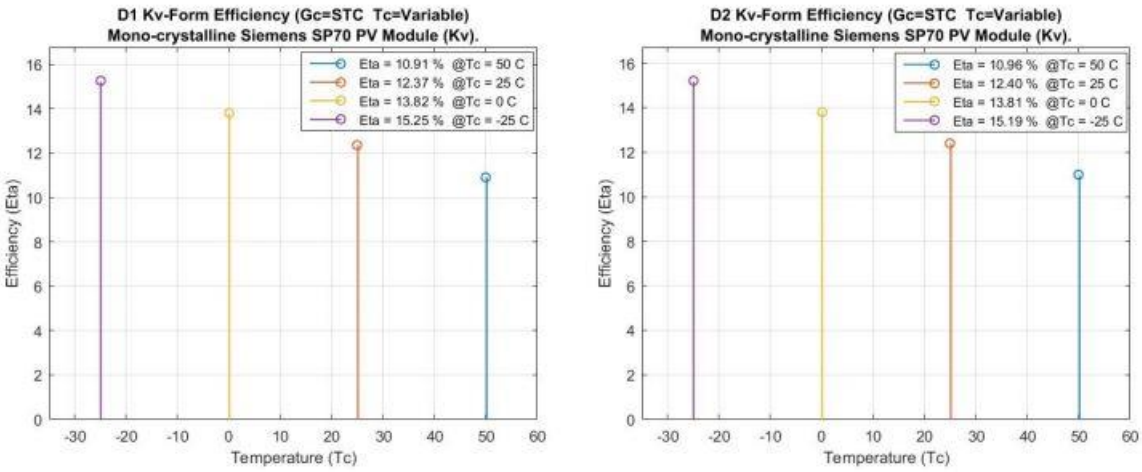

Figure 35: Comparison of D1_Kv and D2_Kv efficiency, with respect to temperature.

The VP curves shown in Figure 34 are the simulated characteristics of the D1_Kv model and the D2_Kv model, and as expected, an increase in temperature results in a drop in output power. The power drop then results in a drop in efficiency, Figure 35, due to the fact that the cell/module is producing less power per unit of area.

The data extracted from the D1_Kv and D2_Kv simulation for the power and efficiency with respect to temperature is summarised in Table 13 and Table 14.

Consider the following observations:

i. An increase in temperature results in an expected drop in power for both D1_Kv and D2_Kv models.

ii. An increase in temperature results in an expected drop in efficiency for both D1_Kv and D2_Kv models.

iii. When the D2_Kv model, is compared to the D1_Kv model, it is expected that the D1_Kv model would have an equal or higher rate of efficiency with respect to irradiance in the D2_Kv model. The results show an equal averaged efficiency, with individual errors well less than the accepted 5% error range.

Table 13: D1_Kv form model data of efficiency with respect to temperature.

D1_Kv-Form (Efficiency at varying temperatures.) (Irradiance: Gc = Gstc = 1000w/m^2)							
Tc (˚C)	*P_{mpp} (W)*	*V_{mpp} (V)*	*I_{mpp} (A)*	*I_{sc} (A)*	*V_{oc} (V)*	*FF*	*Efficiency (%)*
50	*61.37*	*14.61*	*4.20*	*4.73*	*19.45*	*0.67*	*10.91*
25	*69.56*	*16.50*	*4.22*	*4.68*	*21.35*	*0.70*	*12.37*
0	*77.71*	*18.45*	*4.21*	*4.63*	*23.25*	*0.72*	*13.82*
-25	*85.79*	*20.44*	*4.20*	*4.58*	*25.15*	*0.74*	*15.25*
							6.54

Table 14: D2_Kv form model data of efficiency with respect to temperature.

D2_Kv-Form (Efficiency at varying temperatures.) (Irradiance: Gc = Gstc = 1000w/m ^{2})							
Tc (˚C)	*P_{mpp} (W)*	*V_{mpp} (V)*	*I_{mpp} (A)*	*I_{sc} (A)*	*V_{oc} (V)*	*FF*	*Efficiency (%)*
50	*61.68*	*14.59*	*4.23*	*4.72*	*19.44*	*0.67*	*10.96*
25	*69.73*	*16.50*	*4.23*	*4.67*	*21.35*	*0.70*	*12.40*
0	*77.66*	*18.46*	*4.21*	*4.62*	*23.25*	*0.72*	*13.81*
-25	*85.43*	*20.45*	*4.18*	*4.57*	*25.15*	*0.74*	*15.19*
							6.54

4.2. Results of Eg form simulations

A copy of the Matlab script used to load the initial conditions into the simulation environment is provided in Appendix 6, and the initial conditions for the Eg form of simulated models is summarised in Table 15.

Table 15: Initial conditions for the Eg form of D1 and D2 models.

Single Diode Eg Form (D1_Eg) and Double Diode Eg Form (D2_Eg) model parameters.							
Initial Parameters:	***Eg included.***						
Type of Cell:	Mono-crystalline Siemens SP70 PV Module						
P_{mpp_stc} (W) =	*70*	*N_s =*	*36*	*Area (m^2) =*	*0.5625*	*D1Rs =*	*0.371*
I_{mpp_stc} (A) =	*4.24*	*K_I (A/K) =*	*0.002*	*a =*	*1.3*	*D1Rp =*	*158*
V_{mpp_stc} (V) =	*16.5*	*K_v (V/K) =*	*-0.076*	*a1 =*	*1*	*D2Rs =*	*0.527*
V_{oc_stc} (V) =	*21.4*	*T_c (‘C) =*	*25*	*a2 =*	*1.3*	*D2Rp =*	*89*
I_{sc_stc} (A) =	*4.7*	*G_c (W/m^2) =*	*1000*	*P_e =*	*2.3*	***Eg =***	***N/A***
Irs (A) =	*3.1E-7*	*Irs1=Irs2 (A) =*	*4.1E-10*	*Eg =*	*1.12*		

The complete build of the each of the Simulink models, as seen from GUI perspective, is included in been included in the appendices as follows:

- Appendix 9 contains the D1_Eg model , and can be identified by lime coloured Simulink blocks, as shown in Figure 36;

- Appendix 10 contains the D2_Eg model and can be identified by violet coloured Simulink blocks, as shown in Figure 37;

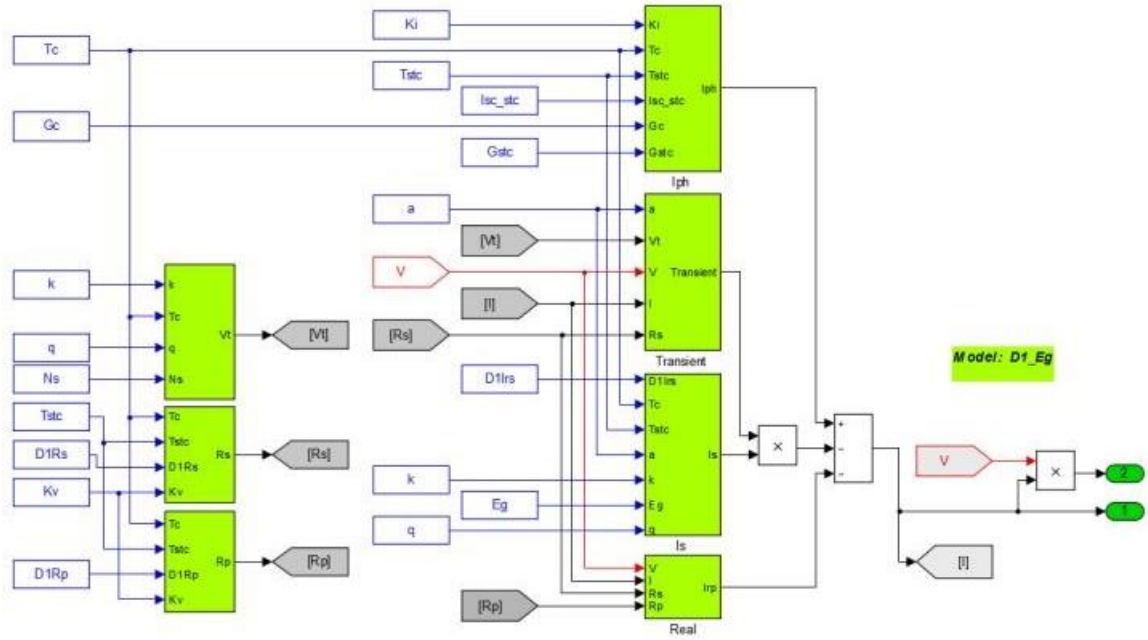

Figure 36: The D1_Eg output current (I) block build, as seen within the Simulink GUI.

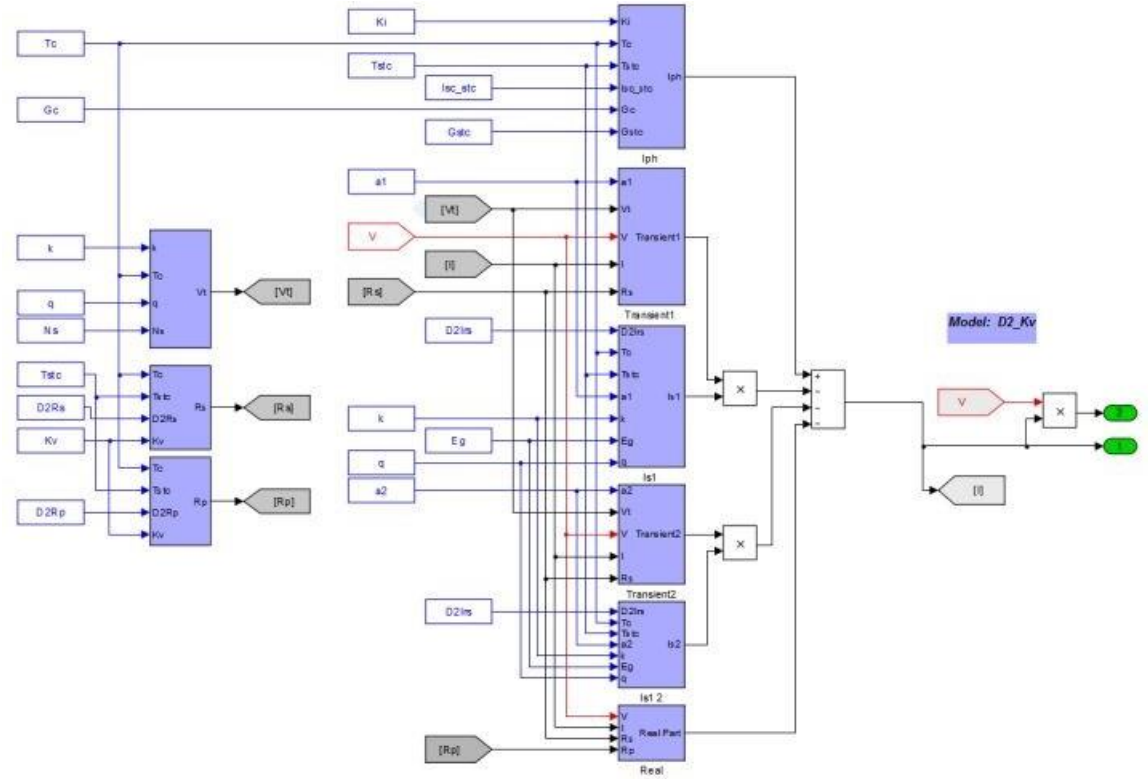

Figure 37: The D2_Eg output current (I) block build, as seen within the Simulink GUI.

4.2.1. Eg form efficiency with respect to model accuracy

The second step was to validate that the voltage and current outputs, were within the acceptable error percentage range of 5%. The validation data provided a maximum power point and a maximum voltage point for each of the variations in temperature, and as Table 16 shows:

i. The expected errors of the individual validation data points are listed in column 5, with the averaged relative error shown in the final row of column five;

ii. Each of the individual D1_Eg data points are well within the 5% error range, with an averaged relative error of 0.39%;

iii. Likewise, the individual D2_Eg data points are well within the 5% range, with an averaged relative error of 0.31%;

Table 16: Relative MPP errors for D1_Eg and D2_Eg form models.

Relative errors on the maximum power point for D1_Eg and D2-Eg models against varying temperatures for a SP-70 mono-crystalline module.

Temp (˚C)	*Measured data*	*D1_Eg Model*	*D2_Eg Model*	*Expected Error (%)*	*Error D1 (%)*	*Error D2 (%)*
50	$P_{mpp} = 62.13$	$P_{mpp} = 61.54$	$P_{mpp} = 62.27$	*0.612*	*0.95*	*0.23*
	$V_{mpp} = 14.60$	$V_{mpp} = 14.59$	$V_{mpp} = 14.66$	*0.000*	*0.07*	*0.41*
25	$P_{mpp} = 70.00$	$P_{mpp} = 69.96$	$P_{mpp} = 69.98$	*0.014*	*0.06*	*0.03*
	$V_{mpp} = 16.50$	$V_{mpp} = 16.50$	$V_{mpp} = 16.50$	*0.000*	*0.00*	*0.00*
0	$P_{mpp} = 77.80$	$P_{mpp} = 78.27$	$P_{mpp} = 77.50$	*0.393*	*0.60*	*0.39*
	$V_{mpp} = 18.40$	$V_{mpp} = 18.43$	$V_{mpp} = 18.37$	*0.543*	*0.16*	*0.16*
-25	$P_{mpp} = 85.70$	$P_{mpp} = 86.42$	$P_{mpp} = 84.80$	*0.665*	*0.84*	*1.06*
	$V_{mpp} = 20.30$	$V_{mpp} = 20.39$	$V_{mpp} = 20.26$	*0.985*	*0.44*	*0.20*
				0.40	*0.39*	*0.31*

4.2.2. Eg form efficiency with respect to irradiance

The VP curves shown in Figure 38 are the simulated characteristics of the D1_Eg model and the D2_Eg model, and as expected, an increase in irradiance results in an increase in output power. The

power increase then results in a increase in efficiency, Figure 39, due to the fact that the cell/module is producing more power per unit of area.

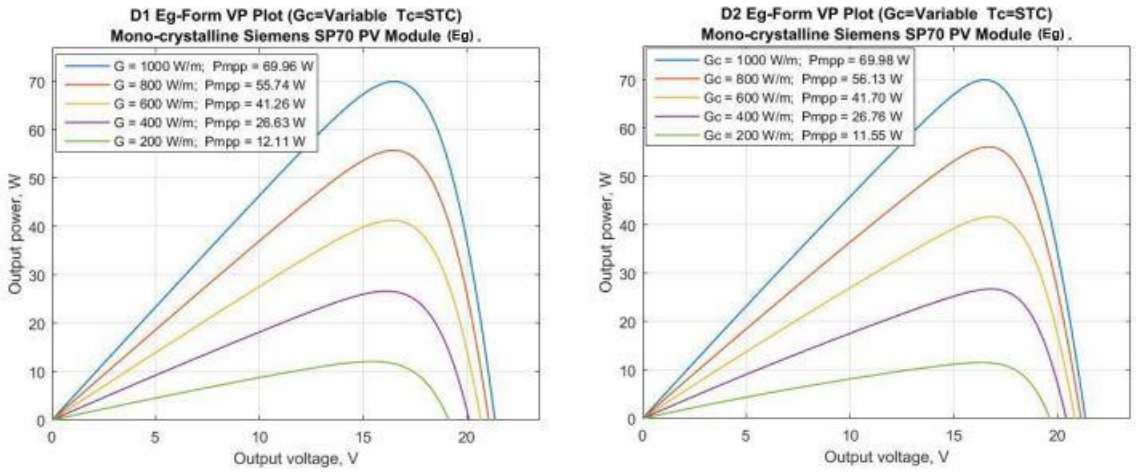

Figure 38: Comparison of D1_Eg and D2_Eg VP curves with respect to irradiance.

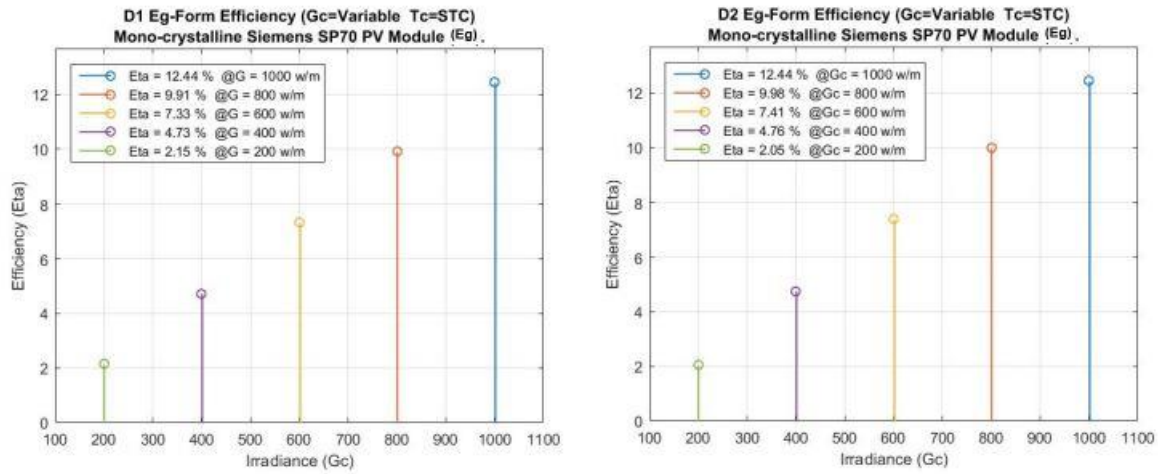

Figure 39: Comparison of D1_Eg and D2_Eg efficiency, with respect to irradiance.

The data extracted from the D1_Eg and D2_Eg simulation for the power and efficiency at various levels of irradiance is summarised in Table 17 and Table 18.

Consider the following observations:

i. An increase in irradiance does result in an expected increase in power for both D1_Eg and D2_Eg models.

ii. An increase in irradiance does result in an expected increase in efficiency for both D1_Eg and D2_Eg models.

iii. When the D2_Eg model, is compared to the D1_Eg model, it is expected that the D1 model would have an equal or higher rate of efficiency with respect to irradiance than the D2 model. The results show an unexpected higher averaged efficiency in the D2 model, however, the result falls well within the accepted 5% error range.

Table 17: D1_Eg form efficiency with respect to irradiance.

D1_Eg (Efficiency at varying irradiances) (Temperature: Tc = Tstc = 25(°C))							
$Gc\ (W/m^2)$	$P_{mpp}\ (W)$	$V_{mpp}\ (V)$	$I_{mpp}\ (A)$	$I_{sc}\ (A)$	$V_{oc}\ (V)$	*FF*	*Efficiency (%)*
1000	*69.96*	*16.50*	*4.24*	*4.70*	*21.37*	*0.70*	*12.44*
800	*55.74*	*16.49*	*3.38*	*3.76*	*21.07*	*0.70*	*9.91*
600	*41.26*	*16.40*	*2.52*	*2.82*	*20.68*	*0.71*	*7.33*
400	*26.63*	*16.14*	*1.65*	*1.88*	*20.13*	*0.70*	*4.73*
200	*12.11*	*15.44*	*0.78*	*0.94*	*19.14*	*0.67*	*2.15*
							4.57

Table 18: D2_Eg form efficiency with respect to irradiance.

D2_Eg (Efficiency at varying irradiances) (Temperature: Tc = Tstc = 25(°C))							
$Gc\ (W/m^2)$	$P_{mpp}\ (W)$	$V_{mpp}\ (V)$	$I_{mpp}\ (A)$	$I_{sc}\ (A)$	$V_{oc}\ (V)$	*FF*	*Efficiency (%)*
1000	*69.98*	*16.50*	*4.24*	*4.71*	*21.36*	*0.70*	*12.44*
800	*56.13*	*16.70*	*3.36*	*3.77*	*21.14*	*0.70*	*9.98*
600	*41.70*	*16.82*	*2.48*	*2.83*	*20.85*	*0.71*	*7.41*
400	*26.76*	*16.80*	*1.59*	*1.88*	*20.43*	*0.70*	*4.76*
200	*11.55*	*16.33*	*0.71*	*0.94*	*19.64*	*0.62*	*2.05*
							4.58

4.2.3. Eg form efficiency with respect to temperature

The VP curves shown in Figure 40 are the simulated characteristics of the D1_Eg model and the D2_Eg model, and as expected, an increase in temperature results in a drop in output power. The power drop then results in a drop in efficiency, Figure 41, due to the fact that the cell/module is producing less power per unit of area.

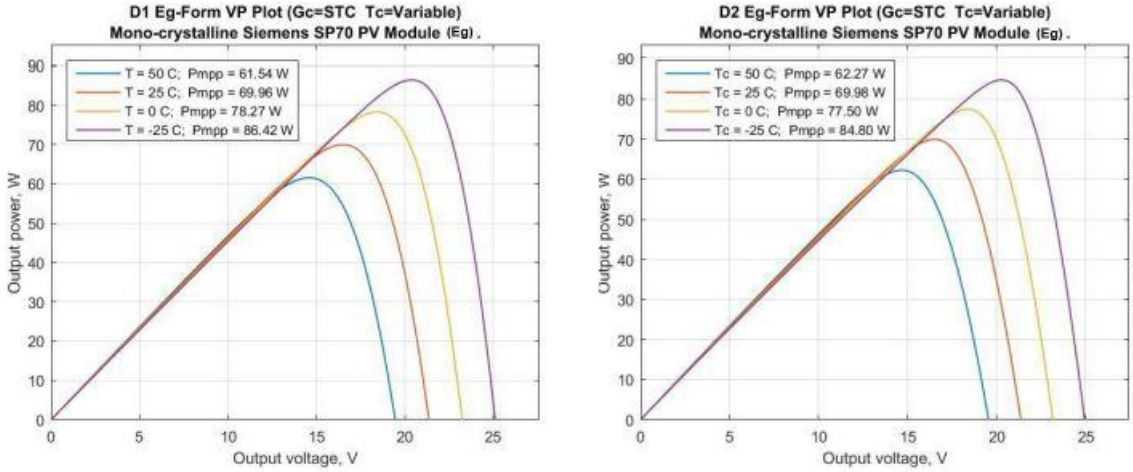

Figure 40: Comparison of D1_Eg and D2_Eg VP curves, with respect to temperature.

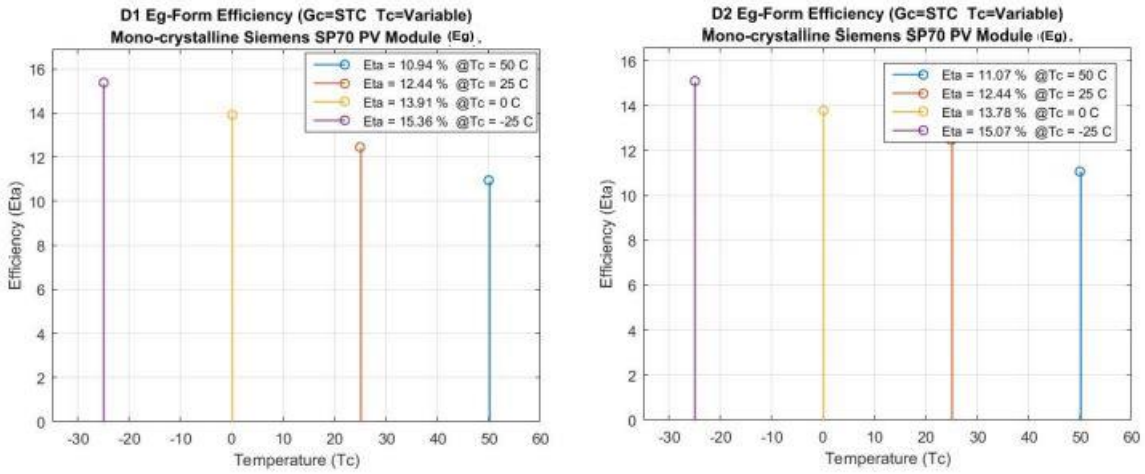

Figure 41: Comparison of D1_Eg and D2_Eg efficiency with respect to temperature.

The data extracted from the D1_Eg and D2_Eg simulation for the power and efficiency with respect to temperature is summarised in Table 19 and Table 20.

Consider the following observations:

i. An increase in temperature results in an expected drop in power for both D1_Eg and D2_Eg models.

ii. An increase in temperature results in an expected drop in efficiency for both D1_Eg and D2_Eg models.

iii. When the D2_Eg model is compared to the D1_Eg model, the results confirm that the D1_Eg model has an an equal or higher rate of efficiency with respect to temperature than the D2_Eg model – as expected.

Table 19: D1_Eg form efficiency with respect to temperature.

D1_Eg (Efficiency at varying temperatures.) (Irradiance: Gc = Gstc = 1000w/m^2)							
Tc (˚C)	*P_{mpp} (W)*	*V_{mpp} (V)*	*I_{mpp} (A)*	*I_{sc} (A)*	*V_{oc} (V)*	*FF*	*Efficiency (%)*
50	*61.54*	*14.59*	*4.22*	*4.75*	*19.46*	*0.67*	*10.94*
25	*69.96*	*16.50*	*4.24*	*4.70*	*21.37*	*0.70*	*12.44*
0	*78.27*	*18.43*	*4.25*	*4.65*	*23.25*	*0.72*	*13.91*
-25	*86.42*	*20.39*	*4.24*	*4.60*	*25.11*	*0.75*	*15.36*
							6.58

Table 20: D2_Eg form efficiency with respect to temperature.

D2_Eg (Efficiency at varying temperatures.) (Irradiance: Gc = Gstc = 1000w/m^2)							
Tc (˚C)	*P_{mpp} (W)*	*V_{mpp} (V)*	*I_{mpp} (A)*	*I_{sc} (A)*	*V_{oc} (V)*	*FF*	*Efficiency (%)*
50	*62.27*	*14.66*	*4.25*	*4.76*	*19.54*	*0.67*	*11.07*
25	*69.98*	*16.50*	*4.24*	*4.71*	*21.36*	*0.70*	*12.44*
0	*77.50*	*18.37*	*4.22*	*4.66*	*23.16*	*0.72*	*13.78*
-25	*84.80*	*20.26*	*4.19*	*4.61*	*24.94*	*0.74*	*15.07*
							6.55

Multijunction solar cell results

4.3. GaInP/GaInAs/Ge simulation results

The GaInP/GaInAs/Ge simulation results are shown in Table 21, where the percentage error for each simulation benchmark is listed in the final row of the table. The validation data is given for the 500 W/m2 condition, was tested using an irradiance lamp at 500W. The efficiency is based on the standard test condition (1000W/m^2 25˚C). It is assumed that the temperature in the cell is uniform and that the shunt resistances approaching infinity and can be ignored.

Table 21: GaInP/GaInAs/Ge simulation results at 0.5 suns, 40˚C. .

Simulation Results: GaInP/GaInAs/Ge (Hussain et al. 2016) (D2) triple MJSC. *(500 W/m^2, 40˚C)*								
	Pmpp (W)	Impp (A)	Vmpp (V)	Voc (V)	Isc (A)	Pin (W/m^2)	FF (%)	η (%)
(Hussain et al 2016) Results	0.487	0.101	4.821	5.144	0.103	0.0245	0.92	18.28
Simulation (0.5 sun)	0.480	0.100	4.795	5.077	0.103	0.0245	0.916	17.94
% Error	1.478	0.941	0.541	1.302	0.00	-	00.33	1.851

When the simulation results are compared to the results published in (Hussain et al. 2016), each of the benchmarks are within the +/- 5% tolerance for percentage error. The results correlate with the data in (Hussain et al. 2016), and efficiency approximately 18 % at 0.5 suns and 40˚C. The simulation was run at standard test conditions of 1,000 W/m2 25˚C, and as expected - the efficiency increases two-fold to approximately 35% (Table 22).

Table 22: GaInP/GaInAs/Ge simulation results at 1 suns, 25˚C.

Simulation Results: GaInP/GaInAs/Ge (Hussain et al. 2016) (D2) triple MJSC. *(1,000 W/m2, 25˚C)*								
	Pmpp (W)	Impp (A)	Vmpp (V)	Voc (V)	Isc (A)	Pin (W/m^2)	FF (%)	η (%)
Simulation (1-Sun)	0.959	0.199	4.831	5.233	0.206	0.0245	0.904	34.99

The record efficiency for the GaInP/GaInAs/Ge cell at STC exceeds 32%, so the 35% efficiency indicates that this cell is of a very high quality.

GaInP/GaInAs/Ge cells are lattice matched to reduce recombination due to dislocation at the layer interface (cracking or deformation). The distribution of the spectrum region over more than one band gap is a challenge when matching the current of each series connected layer.

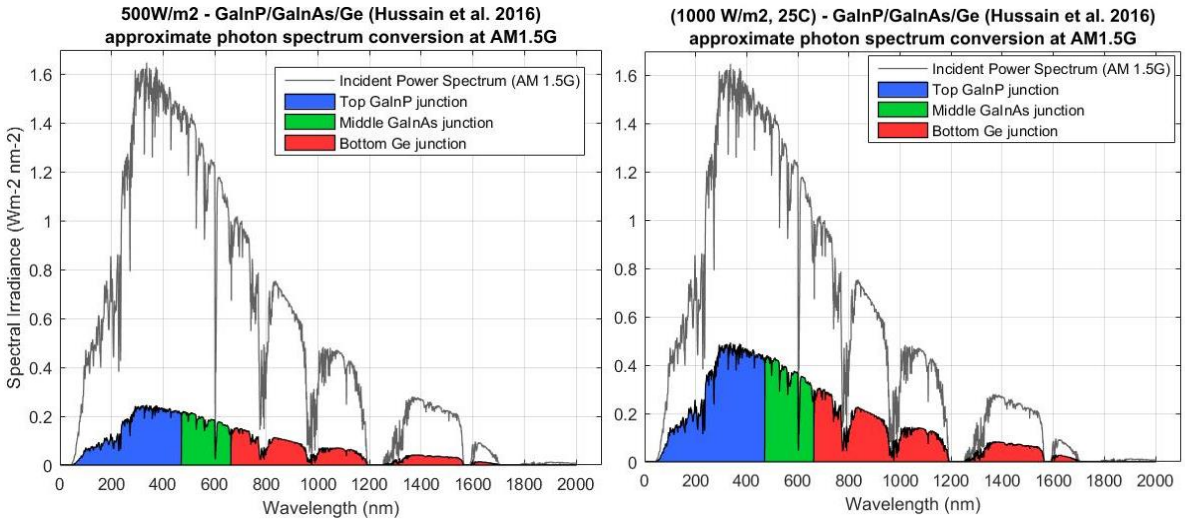

Figure 42: Approximation of spectral absorption at (500 & 1000)W/m2

Even though the lattice match is very good, the less than optimal current match between the second and third layers restricts the total cell potential efficiency. The 36 % simulation result, as validated by the (Hussain et al. 2016) paper, coupled with the FF exceeding 90% indicates that this is a very good quality cell.

Note that a copy of the characteristic curves for the VI, VP for the GaInP/GaInAs/Ge cell 0.5 suns and 1 suns, is included in Appendix 19.

4.3.1. GaInP/GaInAs/Ge open circuit voltage characteristics

The MJSC open circuit voltage is a function of the bandgap, therefore, it is expected that the open circuit voltage should increase or decrease – as the bandgap energy increases or decreases.

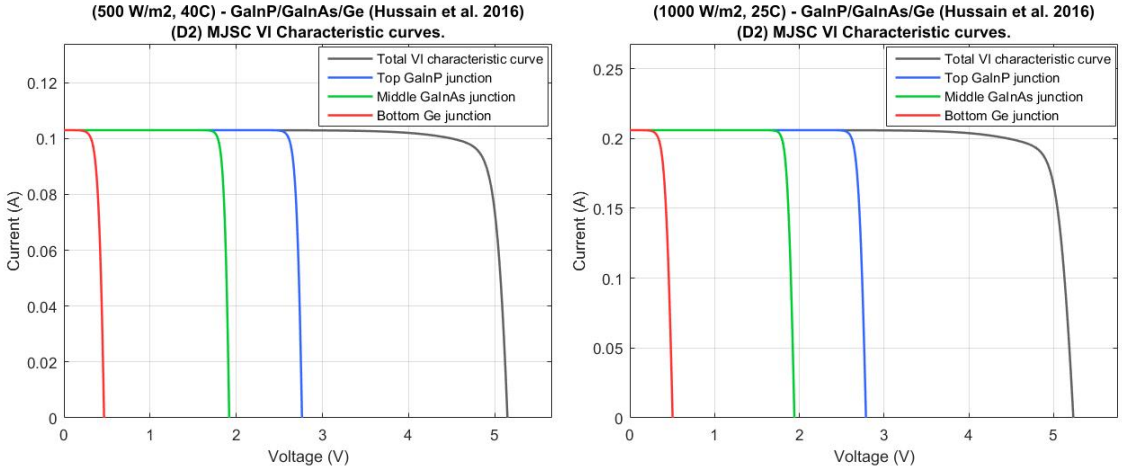

Figure 43: GaInP/GaInAs/Ge VI characteristics at 500W/m2 and at 1000 W/m2

Consider the open circuit voltage characteristics in Figure 43:

1. The 500W/m2 VI characteristic plots (left) show the GaInP/GaInAs/Ge open circuit voltages as:
    a. The Ge junction Eg = 0.6583 ev, V_{OC} = 0.4655 V,
    b. the GaInAs junction Eg =1.874 ev, V_{OC} = 1.918 V,
    c. the GaInP junction Eg = 2.637 ev. V_{OC} o= 2.762 V,
    d. resulting in a total cell V_{OC} of 5.146 V.
2. The 1000W/m2 VI characteristic plots (right) show the GaInP/GaInAs/Ge open circuit voltages as:
    a. The Ge junction Eg = 0.6583 ev, V_{OC} = 0.5048 V,
    b. the GaInAs junction Eg = 1.874 ev, V_{OC} = 1.942 V,
    c. the GaInP junction Eg = 2.637 ev. V_{OC} = 2.786 V,
    d. resulting in a total cell V_{OC} of 5.233 V.

Note also that - as expected – each of the individual junction values of V_{OC} have increased in magnitude , with respect to the plotted increase in simulated irradiance.

The GaInP/GaInAs/Ge open circuit voltage characteristics behave as expected, where V_{OC} is behaves as a function of bandgap energy and responds to changes in bandgap energy accordingly.

4.3.2. GaInP/GaInAs/Ge recombination characteristics

The output of Voc depends on the photo current *(I_{ph})* minus the dark condition characteristic current, ie saturation current (I_s). As discussed on page 10, a cell such as this GaInP/GaInAs/Ge cell has very little parasitic resistances - and as such - I_{ph} is assumed to be the same value as *Isc*.

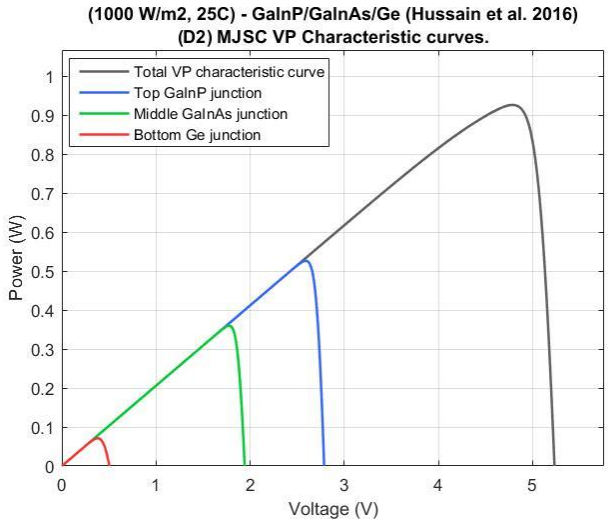

Figure 44: The VP characteristics of the GaInP/GaInAs/Ge (500 W)

The magnitude of I_s depends on the recombination in a cell, and the MJSC model used in this paper models recombination for each junction as a constant experimentally tested value of I_{rs} - or the recombination current (Table 8). Hence V_{OC} should behave as a function of I_{rs}, and respond inversely to the recombination current.

Figure 44 confirms that Ge, GaInAs and GaInP junction values of V_{OC} decrease as the recombination current increases in value:

a. The bottom layer Ge junction V_{OC} = 0.5048 V, I_{rs} = 10.5E-6 A;

b. The middle layer GaInAs junction V_{OC} = 1.942 V, I_{rs} = 1.288E-8 A,

c. The top layer GaInP junction V_{OC} = 2.786 V I_{rs} = 1.86E-9 A

4.3.3. GaInP/GaInAs/Ge efficiency with respect to irradiance and temp.

The cell total characteristic curves at varying irradiances are shown below. The VP curves (Figure 46) of the GaInP/GaInAs/Ge cell, provide the following insight:

An increase in irradiance results in an increase in output power. A high shunt resistance value and middle to low series resistance ensures that the fill factor remains relatively unchanged. This results in a relatively linear increase in efficiency with respect to irradiance (Figure 45).

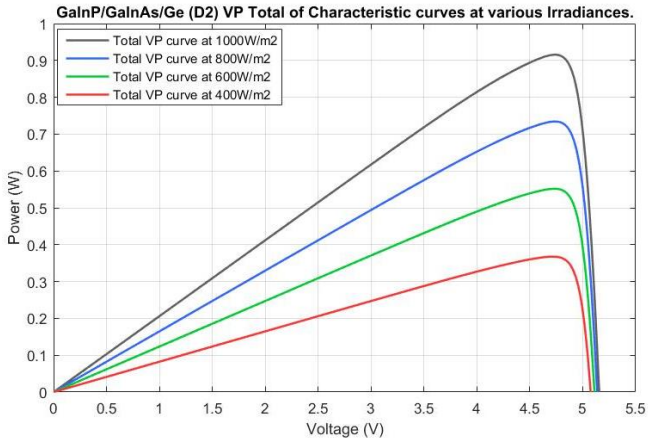

Figure 45: GaInP/GaInAs/Ge total cell VP characteristics with respect to irradiance.

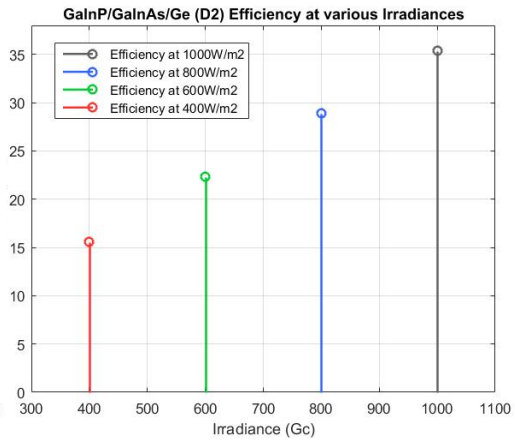

Figure 46: GaInP/GaInAs/Ge total conversion efficiency with respect to irradiance

Figure 47 shows that, as expected, the increase in irradiance provides an increase in cell/junction I_{SC} and an increase in total V_{OC}.

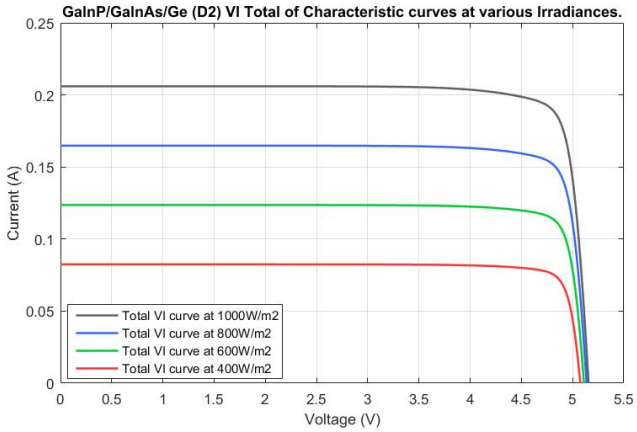

Figure 47: GaInP/GaInAs/Ge total VI curves with respect to irradiance.

The cell total efficiency with respect to varying temperatures are shown below in Figure 48, and as expected - an increase in the temperature of the GaInP/GaInAs/Ge cell results a drop in overall conversion efficiency.

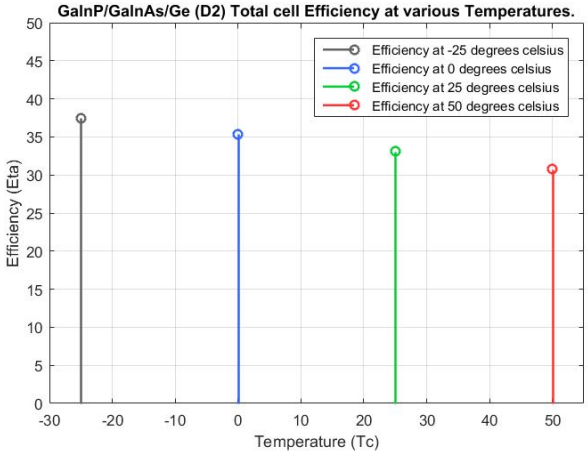

Figure 48: GaInP/GaInAs/Ge cell total efficiency at various Temperatures (˚C).

However, on closer inspection, it appears as though there is an error in the results in terms of efficiency with respect to temperature.

It is expected that V_{OC} should reduce as the temperature increases, however, as shown in Figure 49 – the V_{OC} actually increases as the temperature increases. – therefore, it is highly likely that the model is not correctly designed with respect to temperature.

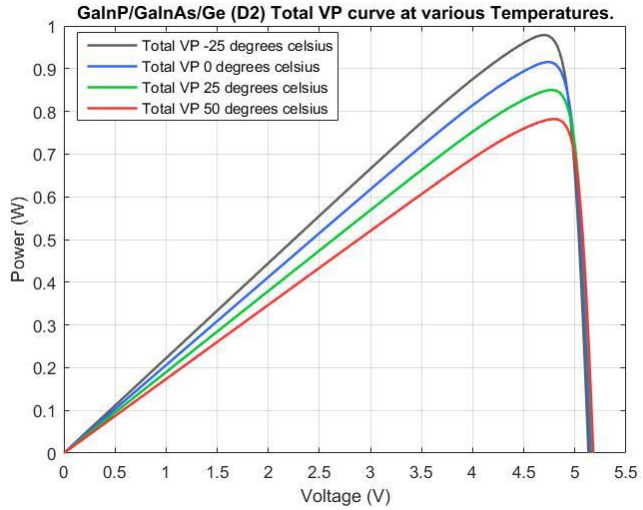

Figure 49: GaInP/GaInAs/Ge cell VP characteristics at various Temperatures (˚C).

Summary of SJSC and MJSC performance

Note that a copy of the Project specification is available in Appendix 1.

Table 23: Summary of results for the Kv form models with respect to accuracy.

	Kv form of modelling with respect to accuracy:	*Results*
1	Both of the D1 and D2 models contain extraction results that fall outside the 5% range for error. However, the relative errors in the extraction values do not adversely affect the primary error percentage range for the Pmpp and Vmpp values;	Acceptable
2	The simulated values for Pmpp and Vmpp fall well within the 5% range for relative error, and for each of the varying values of temperature;	Acceptable
3	The D1 version model has a larger averaged error (%) than the D2 version. Therefore the D2 version model is more accurate than the D1 version model.	Acceptable

Therefore Project specification 1.4 has been achieved with respect to the Kv form of PV modelling. That is, as expected, the double diode Kv form of model is closer to reality even though the efficiency is equal to or less than that of the single diode form of model.

Table 24: Summary of results for the Eg form models with respect to accuracy.

	Eg form of modelling with respect to accuracy:	*Results*
1	Both of the D1 and D2 models contain extraction results that fall outside the 5% range for error. However, the relative errors in the extraction values do not adversely affect the primary error percentage range for the Pmpp and Vmpp values;	Acceptable
2	Both of the D1 and D2 models contain extraction results that fall outside the 5% range for error. However, the relative errors in the extraction values do not adversely affect the primary error percentage range for the Pmpp and Vmpp values;	Acceptable
3	The simulated values for Pmpp and Vmpp fall well within the 5% range for relative error, and for each of the varying values of temperature;	Acceptable
4	The D1 version model has a larger averaged error (%) than the D2 version. Therefore the D2 version model is more accurate than the D1 version model;	Acceptable

Therefore Project specification 1.3 has been achieved with respect to the Eg form of PV modelling. That is, as expected, the single diode Eg form model requires further improvements in accuracy when compared to the double diode Eg form model.

Table 25: Summary of results for the Kv form of modelling with respect to efficiency.

	Kv form of modelling with respect to efficiency:	*Results*
1	As expected, an increase in irradiance does result in a power increase in the D1 version model and the D2 version model;	Acceptable
2	As expected, an increase in irradiance does result in an increase in efficiency in the D1 version model and the D2 version model;	Acceptable
3	The D2 version model has a 0.04% higher averaged efficiency than the D1 version model. This result is unexpected, however, it is acceptable as it is well within the 5% error tolerance range;	Acceptable
4	As expected, an increase in temperature results in an drop in power in the D1 version model and the D2 version model;	Acceptable
5	As expected, the drop in power results in a drop in efficiency for the D1 version model and the D2 version model;	Acceptable
6	The D1 version model has an averaged efficiency that matches the D2 version model. It is expected that the D1 version would we equal to or greater, however, it is acceptable as it is well within the 5% error tolerance range;	Acceptable

*Therefore Project specification 1.4 has been achieved with respect to the Kv form of PV modelling. That is, error tolerances not withstanding, the **double diode** Kv form of model is closer to reality even though the efficiency is equal to or less than that of the **single diode** Kv form of model.*

Table 26: Summary of results for the Eg form of modelling with respect to efficiency.

	Eg form of modelling with respect to efficiency:	*Results*
1	As expected, an increase in irradiance does result in a power increase in the D1 version model and the D2 version model;	Acceptable
2	An increase in irradiance does result in an increase in efficiency in the D1 version model and the D2 version model;	Acceptable
3	As expected, the D1 version model has a higher averaged efficiency than the D2 version model;	Acceptable
4	As expected, an increase in temperature results in an drop in power in the D1 version model and the D2 version model;	Acceptable
5	As expected, the drop in power results in a drop in efficiency for the D1 version model and the D2 version model;	Acceptable
6	As expected, the D1 version model has a higher averaged efficiency than the D2 version model.	Acceptable

*Therefore Project specification 1.4 has been achieved with respect to the Eg form of PV modelling. That is, as expected, the **double diode** Eg form of model is closer to reality even though the efficiency is equal to or less than that of the **single diode** Eg form of model.*

Table 27: Summary of GaInP/GaInAs/Ge simulation results

	Summary of GaInP/GaInAs/Ge MJSC simulation results	*Results*
1	Validation against the published results (shown in Table 21 and Table 22) provided a %Error ranging from 0.33% to 1.85% for values of total cell P_{mpp}, I_{mpp}, V_{mpp}, V_{OC}, *FF* and *cell efficiency*. Given that the data points less than 5% - they are considered acceptable.	Acceptable
2	V_{OC} characteristics with respect to bandgap energy behaves as expected. V_{OC} behaves as a function of bandgap energy and responds to changes in bandgap energy – where an increase in bandgap energy results in an increase in V_{OC} (Results listed on page 76).	Acceptable
3	V_{OC} characteristics with respect to recombination current behave as expected. V_{OC} increases in value as I_{rs} decreases in value. (Results listed on page 77).	Acceptable
4	Characteristics related to changes in irradiance behave as expected. An increase in irradiance provides an increase in cell output power, and a steady fill factor ensures an almost linear increase in cell efficiency (Results page 78).	Acceptable
5	Characteristics related to changes in temperature do not behave as expected. Results show that, as expected, cell efficiency decreases with an increase in temperature. However, total cell V_{OC} decreases with an increase in temperature. This behaviour is not correct – the response should be inverse. This could most likely be attributed to an incorrect mathematical relationship between the temperature dependency of the bandgap energy and the bandgap dependency of the saturation current (Results page 79).	Unacceptable
Therefore Project specification 2.4 has not been fully achieved. 2.4. *The conversion efficiency of the identified MJSC was correctly simulated with respect to a change in irradiance. However, the conversion efficiency of the identified MJSC was NOT correctly simulated with respect to a change in Temperature.*		

Chapter 5: Project conclusion

Chapter 5 contains the project conclusions and outlines the project outcomes, provides a discussion on how the project findings can benefit research, reflections on the project and identifies areas of further research.

5.1. Summary of outcomes

In chapters 4 and 5, the implemented Simulink/Matlab regimes were reported to model the VP and VI characteristics of single junction silicon solar cells (SJSCs). The remaining regime of simulations tested the accuracy of a single diode (D1) model and compared this to the accuracy of a double diode (D2) model by simulating the conversion efficiency of each model with respect to changes in irradiation and temperature.

Two forms of D1 and D2 modelling were undertaken. The first form of modelling (the 'Kv' form) ignores the cell bandgap energy, and the outcome was that the D2_Kv model is more accurate than the D1_Kv model. The second form of modelling (the 'Eg' form) includes the cell bandgap energy, and outcome was that the D2_Eg model is more accurate than the D1_Eg model.

As part of this investigation, a multijunction solar cell (MJSC) D2 model is proposed. The proposed model is an iterative design based on the SJSC D2_Eg model tested for the single junction solar cell.

The modelling in Simulink was implemented to test the accuracy of the proposed MJSC D2 model by simulating the conversion efficiency with respect to changes in irradiation and temperature. The first outcome was that the conversion efficiency of the MJSC D2 model is correct with respect to irradiance. The second outcome was that the conversion efficiency of the MJSC D2 model not correct with respect to temperature.

5.2. Project research contribution

This thesis provides a total of five separate standardised solar cell models, two D1 models used to characterise SJSCs, two D2 models used to characterise SJSCs and one D2 model used to characterise MJSCs.

All of the models are compact in type, where the device characteristics are described by measuring equivalent circuit models consisting of of lumped components. In the equivalent circuit model for the D1 versions, the photons are represented by a DC current source, a single diode represents the bulk behaviour of the device and the parasitic losses are represented by a diode-parallel shunt

resistor and a series resistor. The D2 versions have an additional diode to represent recombination losses in the depletion region.

Simulations were conducted under standardised test conditions and considered valid, within the scope of this report, when simulation results are within a (percentage error) of 5%, when compared to the published data values for V_{mpp} and P_{mpp}.

This research project contributes to broader research into the efficiency of solar cells by providing insight into the complexities and nuances of MJSC modelling, and providing a platform for subsequent researchers to build upon. It provides guidance in relation to specific pitfalls including reliance on incomplete datasets, limitations of SJSC extraction algorithms and the challenge associated with establishing accurate mathematical relationships between the temperature dependency of the bandgap energy and the bandgap dependency of the saturation current.

5.3. Project reflection and future research

The main aim of this dissertation was to provide a standardised D2 equivalent circuit model to the conversion efficiency in MJSCs. This was to be achieved through review of the literature to:

- seek an understanding of how SJSCs work and how their functionality could be extended to model MJSCs, and
- identify a range of existing SJSC modelling practices that are more/less adaptable for simulating the conversion efficiency of MJSCs within the Simulink environment.

Through simulation, it was confirmed that the D2 model is more accurate than D1 when modelling conversion efficiency. It was also determined that given that open circuit voltage, short circuit current and solar cell fill factor are functions of bandgap energy, bandgap energy is a critical component for inclusion in the modelling for MJSCs.

Research of the standardised equivalent MJSC circuits used in MJSC modelling informed the development of a MJSC model architecture comprising of series connected SJSC D2 equivalent circuits. This model was within the 5% percentage error of the published results for standard test conditions. The following characteristics behaved as expected:

- V_{OC} characteristics with respect to bandgap energy and recombination current
- *VI* and *VP* characteristics with respect to irradiation.

However, the *VI* and *VP* characteristics with respect to temperature do not behave as expected. This could most likely be attributed to an incorrect mathematical relationship between the temperature dependency of the bandgap energy and the bandgap dependency of the saturation current.

This project resulted in key learnings in relation to modelling and solar cell efficiency. In developing a compact type lumped component equivalent circuit model it is critical to understand the expected characteristics of the model. This allows for easier identification of inconsistencies rather than relying upon benchmarks and error percentages.

There are three important characteristics to understand regards to cell conversion efficiency. These are:

i. Short circuit current decreases as the energy of the bandgap increases,
ii. Open circuit voltage increases as bandgap energy increases,
iii. Fill factor is determined by the quality of a cell, however, parasitic losses will diminish the fill factor no matter the quality of the cell.

A key challenge and limitation in this project was the reliance upon datasets within the literature which were often incomplete. This necessitated the inclusion of modelling assumptions otherwise unnecessary-had complete datasets been available. In view of this limitation, future research in this area could benefit from experimentally measured data.

Another area of focus for future research is development of an appropriate algorithm for extracting resistance parameters from MJSC manufacturer datasheets. The standardised equivalent circuit SJSC models included an extraction algorithm to identify the parasitic losses unable to be determined from manufacturer datasheets. Testing of the algorithm on the MJSC confirmed that it was not possible to extract the MJSC parameters using the SJSC extraction algorithm.

List of references

Algora, C, Rey-Stolle, I, García, I, Galiana, B, Baudrit, M & González, JR 2007, 'Lattice-matched III–V dual-junction solar cells for concentrations around 1000 suns', *Journal of Solar Energy Engineering*, vol. 129, no. 3, pp. 336-9. Retrieved from <http://solarenergyengineering.asmedigitalcollection.asme.org/article.aspx?articleid=1457935>.

Alharbi, Fahhad H. & Kais, Sabre 2015, 'Theoretical limits of photovoltaics efficiency and possible improvements by intuitive approaches learned from photosynthesis and quantum coherence', *Renewable and Sustainable Energy Reviews*, vol. 43, pp. 1073-89. Retrieved from <http://www.sciencedirect.com/science/article/pii/S136403211401048X>.

Aoun, Nouar, Chenni, Rachid, Nahman, Boukheit & Bouchouicha, Kada 2014, 'Evaluation and Validation of Equivalent Five-Parameter Model Performance for Photovoltaic Panels Using Only Reference Data', *Energy and Power Engineering*, vol. Vol.06No.09, p. 11. Retrieved from <http://www.scirp.org/journal/PaperInformation.aspx?PaperID=49560>.

Bedair, SM & Samberg, Joshua P 2013, 'Current matching for high efficiency multi-junction solar cells', *Journal of Electrical & Electronics*, vol. 2012, Retrieved from.

Bellia, Habbati, Youcef, Ramdani & Fatima, Moulay 2014, 'A detailed modeling of photovoltaic module using MATLAB', *NRIAG Journal of Astronomy and Geophysics*, vol. 3, no. 1, p. 60. Retrieved from <http://www.sciencedirect.com/science/article/pii/S2090997714000182>.

Bett, Andreas W, Philipps, Simon P, Essig, Stephanie, Heckelmann, Stefan, Kellenbenz, René, Klinger, Vera, Niemeyer, Markus, Lackner, David & Dimroth, Frank 2013, 'Overview about technology perspectives for high efficiency solar cells for space and terrestrial applications', in *28th European Photovoltaic Solar Energy Conference and Exhibition*: *proceedings of the28th European Photovoltaic Solar Energy Conference and Exhibition* pp. 1-6, viewed <https://www.ise.fraunhofer.de/de/veroeffentlichungen/konferenzbeitraege/konferenzbeitraege-2013/28th-eupvsec/bett.pdf>.

Bhattacharya, I. & Foo, S. Y. 2010, 'Effects of Gallium-Phosphide and Indium-Gallium-Antimonide semiconductor materials on photon absorption of multijunction solar cells', in *IEEE SoutheastCon 2010 (SoutheastCon), Proceedings of the*: *proceedings of theIEEE SoutheastCon 2010 (SoutheastCon), Proceedings of the* pp. 316-9, viewed <http://ieeexplore.ieee.org.ezproxy.usq.edu.au/stamp/stamp.jsp?tp=&arnumber=5453863>.

Buonassisi, Tonio 2013, *2.627 Fundamentals of Photovoltaics*, Massachusetts Institute of Technology: MIT OpenCourseWare Fall, 2013, viewed 12 Feb, 2016, <http://ocw.mit.edu >.

Catelani, Marcantonio, Ciani, Lorenzo, Kazimierczuk, Marian K. & Reatti, Alberto 2016, 'Matlab PV solar concentrator performance prediction based on triple junction solar cell model', *Measurement*, vol. 88, pp. 310-7. Retrieved from <http://www.sciencedirect.com/science/article/pii/S0263224116300148>.

Celik, Ali Naci & Acikgoz, Nasır 2007, 'Modelling and experimental verification of the operating current of mono-crystalline photovoltaic modules using four- and five-parameter models', *Applied*

Energy, vol. 84, no. 1, pp. 1-15. Retrieved from <http://www.sciencedirect.com/science/article/pii/S0306261906000511>.

Chin, Vun Jack, Salam, Zainal & Ishaque, Kashif 2015, 'Cell modelling and model parameters estimation techniques for photovoltaic simulator application: A review', *Applied Energy*, vol. 154, p. 502. Retrieved from <http://www.sciencedirect.com/science/article/pii/S0306261915006455>.

Cotal, Hector, Fetzer, Chris, Boisvert, Joseph, Kinsey, Geoffrey, King, Richard, Hebert, Peter, Yoon, Hojun & Karam, Nasser 2009, 'III-V multijunction solar cells for concentrating photovoltaics', *Energy & Environmental Science*, vol. 2, pp. 174-92. Retrieved from <http://dx.doi.org/10.1039/B809257E>.

Das, N., Wongsodihardjo, H. & Islam, S. 2013, 'Photovoltaic cell modeling for maximum power point tracking using MATLAB/Simulink to improve the conversion efficiency', in *Power and Energy Society General Meeting (PES), 2013 IEEE*: *proceedings of thePower and Energy Society General Meeting (PES), 2013 IEEE* pp. 1-5, viewed <http://ieeexplore.ieee.org.ezproxy.usq.edu.au/stamp/stamp.jsp?tp=&arnumber=6672819>.

Das, N., Al Ghadeer, A. & Islam, S. 2014, 'Modelling and analysis of multi-junction solar cells to improve the conversion efficiency of photovoltaic systems', in *Power Engineering Conference (AUPEC), 2014 Australasian Universities*: *proceedings of thePower Engineering Conference (AUPEC), 2014 Australasian Universities* pp. 1-5, viewed <http://ieeexplore.ieee.org.ezproxy.usq.edu.au/stamp/stamp.jsp?tp=&arnumber=6966482>.

Das, Narottam, Wongsodihardjo, Hendy & Islam, Syed 2015, 'Modeling of multi-junction photovoltaic cell using MATLAB/Simulink to improve the conversion efficiency', *Renewable Energy*, vol. 74, pp. 917-24. Retrieved from <http://www.sciencedirect.com/science/article/pii/S0960148114005813>.

Foozieh Sohrabi, Arash Nikniazi and Hossein Movla 2013, 'Optimization of Third Generation Nanostructured Silicon- Based Solar Cells', *InTech*, vol. Solar Cells - Research and Application Perspectives, Retrieved from <http://www.intechopen.com/books/solar-cells-research-and-application-perspectives/optimization-of-third-generation-nanostructured-silicon-based-solar-cells>.

Friedman, D. J. 2010, *Progress and challenges for next-generation high-efficiency multijunction solar cells*, 12//, <http://www.sciencedirect.com/science/article/pii/S135902861000032X>.

Friedman, D.J., Olson, J.M. and Kurtz, S. 2011, 'IC-6. High Efficiency III-V Multijunction Solar Cells', *Handbook of Photovoltaic Science and Engineering*, vol. Second Edition, pp. 314-64. Retrieved from <http://app.knovel.com/hotlink/pdf/id:kt00BIPDW2/solar-cells-materials/ic-6-high-efficiency>.

González-Longatt, Francisco M 2005, 'Model of photovoltaic module in Matlab', *II CIBELEC*, vol. 2005, pp. 1-5. Retrieved from <http://matlabproject.ir/forms/files/618671.pdf>.

Green, Martin A. 1982, *Solar cells : operating principles, technology, and system applications*, Prentice Hall, Englewood Cliffs NJ.

Humada, Ali M., Hojabri, Mojgan, Mekhilef, Saad & Hamada, Hussein M. 2016, 'Solar cell parameters extraction based on single and double-diode models: A review', *Renewable and Sustainable Energy Reviews*, vol. 56, pp. 494-509. Retrieved from <http://www.sciencedirect.com/science/article/pii/S1364032115013180>.

Hussain, Abdulrahman Babiker, Abdalla, Abdelrahman S, Mukhtar, Abdellahi Sidi, Elamin, M, Alammari, R & Iqbal, A 2016, 'Modelling and simulation of single-and triple-junction solar cells using MATLAB/SIMULINK', *International Journal of Ambient Energy*, pp. 1-9. Retrieved from <http://www.tandfonline.com/doi/abs/10.1080/01430750.2016.1181567?journalCode=taen20>.

Hyvarinen, Jaakko & Karila, J. 2003, 'New analysis method for crystalline silicon cells', in *Photovoltaic Energy Conversion, 2003. Proceedings of 3rd World Conference on*: *proceedings of thePhotovoltaic Energy Conversion, 2003. Proceedings of 3rd World Conference on* pp. 1521-4 Vol.2, viewed <http://ieeexplore.ieee.org.ezproxy.usq.edu.au/stamp/stamp.jsp?tp=&arnumber=1306216>.

Ishaque, K., Salam, Z. and Taheri, H. 2011, 'Accurate MATLAB Simulink PV System Simulator Based on a Two-Diode Model', *Journal of Power Electronics*, vol. 11, pp. 179-87. Retrieved from <http://dx.doi.org/10.6113/JPE.2011.11.2.179 >.

Ishaque, Kashif, Salam, Zainal & Syafaruddin 2011, 'A comprehensive MATLAB Simulink PV system simulator with partial shading capability based on two-diode model', *Solar Energy*, vol. 85, no. 9, pp. 2217-27. Retrieved from <http://www.sciencedirect.com/science/article/pii/S0038092X11002118>.

Ishaque, Kashif, Salam, Zainal & Taheri, Hamed 2011, 'Simple, fast and accurate two-diode model for photovoltaic modules', *Solar Energy Materials and Solar Cells*, vol. 95, no. 2, pp. 586-94. Retrieved from <http://www.sciencedirect.com/science/article/pii/S0927024810005477>.

Jain, Nikhil & Hudait, Mantu K 2012, 'Design of metamorphic dual-junction InGaP/GaAs solar cell on Si with efficiency greater than 29% using finite element analysis', in *Photovoltaic Specialists Conference (PVSC), 2012 38th IEEE*: *proceedings of thePhotovoltaic Specialists Conference (PVSC), 2012 38th IEEE* IEEE, pp. 002056-60, viewed <http://ieeexplore.ieee.org.ezproxy.usq.edu.au/stamp/stamp.jsp?tp=&arnumber=6318003>.

Jena, Debashisha & Ramana, Vanjari Venkata 2015, 'Modeling of photovoltaic system for uniform and non-uniform irradiance: A critical review', *Renewable and Sustainable Energy Reviews*, vol. 52, pp. 400-17. Retrieved from <http://www.sciencedirect.com/science/article/pii/S1364032115007261>.

Jha, A.R. 2009, *Solar Cell Technology and Applications*, CRC Press.

Kayes, B. M., Zhang, L., Twist, R., Ding, I. K. & Higashi, G. S. 2014, 'Flexible Thin-Film Tandem Solar Cells With >30% Efficienc', *IEEE Journal of Photovoltaics*, vol. 4, no. 2, pp. 729-33. Retrieved from <http://ieeexplore.ieee.org.ezproxy.usq.edu.au/stamp/stamp.jsp?tp=&arnumber=6729050>.

King, RR, Law, DC, Edmondson, KM, Fetzer, CM, Kinsey, GS, Yoon, H, Sherif, RA & Karam, NH 2007, '40% efficient metamorphic GaInP/GaInAs/Ge multijunction solar cells', *Applied Physics Letters*, vol. 90, no. 18, pp. 183516-900. Retrieved from

<http://www.spectrolab.com/pv/support/R.%20King%20et%20al.,%20Appl.%20Phys.%20Lett.%202007,%2040%20percent%20efficient%20MM%20solar%20cells.pdf>.

Lineykin, Simon, Averbukh, Moshe & Kuperman, Alon 2014, 'An improved approach to extract the single-diode equivalent circuit parameters of a photovoltaic cell/panel', *Renewable and Sustainable Energy Reviews*, vol. 30, pp. 282-9. Retrieved from <http://www.sciencedirect.com/science/article/pii/S1364032113007144>.

Liu, Shengyi & Dougal, R. A. 2002, 'Dynamic multiphysics model for solar array', *Energy Conversion, IEEE Transactions on*, vol. 17, no. 2, pp. 285-94. Retrieved from <http://ieeexplore.ieee.org.ezproxy.usq.edu.au/stamp/stamp.jsp?tp=&arnumber=1009482>.

Mahmoud, Soliman A., Alsari, M. M., Reda, E. I. & Alhammadi, R. M. 2012, 'MATLAB modeling and simulation of photovoltaic modules', in *Circuits and Systems (MWSCAS), 2012 IEEE 55th International Midwest Symposium on*: *proceedings of theCircuits and Systems (MWSCAS), 2012 IEEE 55th International Midwest Symposium on* pp. 786-9, viewed <http://ieeexplore.ieee.org.ezproxy.usq.edu.au/stamp/stamp.jsp?tp=&arnumber=6292138>.

Markvart, Tom & Castañer, Luis 2012, 'Chapter IA-1 - Principles of Solar Cell Operation', in *Practical Handbook of Photovoltaics (Second Edition)*, Academic Press, Boston, pp. 7-31.

MathWorks, Inc 2015, *MATLAB Documentation, Solar Cell, Solar Cell Model*, <http://au.mathworks.com/help/physmod/elec/ref/solarcell.html?searchHighlight=solar%20cell>.

McEvoy, Augustin, Castaner, Luis & Markvart, Tom 2012, 'IA-3. Ideal Efficiencies', in *Solar Cells - Materials, Manufacture and Operation (2nd Edition)*, Elsevier.

Mertens, K. & Roth, G. 2014, *Photovoltaics: Fundamentals, Technology and Practice*, Wiley.

Rezk, Hegazy & Hasaneen, El-Sayed 2015, 'A new MATLAB/Simulink model of triple-junction solar cell and MPPT based on artificial neural networks for photovoltaic energy systems', *Ain Shams Engineering Journal*, vol. 6, no. 3, pp. 873-81. Retrieved from <http://www.sciencedirect.com/science/article/pii/S2090447915000404>.

Sah, C. t., Noyce, R. N. & Shockley, W. 1957, 'Carrier Generation and Recombination in P-N Junctions and P-N Junction Characteristics', *Proceedings of the IRE*, vol. 45, no. 9, pp. 1228-43. Retrieved from <http://ieeexplore.ieee.org.ezproxy.usq.edu.au/stamp/stamp.jsp?tp=&arnumber=4056679>.

Segev, Gideon, Mittelman, Gur & Kribus, Abraham 2012, 'Equivalent circuit models for triple-junction concentrator solar cells', *Solar Energy Materials and Solar Cells*, vol. 98, pp. 57-65. Retrieved from <http://www.sciencedirect.com/science/article/pii/S0927024811005782>.

Takamoto, Tatsuya, Ikeda, Eiji, Kurita, Hiroshi & Ohmori, Masamichi 1997, 'Over 30% efficient InGaP/GaAs tandem solar cells', *Applied Physics Letters*, vol. 70, no. 3, pp. 381-3. Retrieved from <http://scitation.aip.org/content/aip/journal/apl/70/3/10.1063/1.118419>.

Tanabe, Katsuaki 2009, 'A review of ultrahigh efficiency III-V semiconductor compound solar cells: multijunction tandem, lower dimensional, photonic up/down conversion and plasmonic

nanometallic structures', *Energies*, vol. 2, no. 3, pp. 504-30. Retrieved from <www.mdpi.com/1996-1073/2/3/504/pdf>.

Tanvir Ahmad*, Sharmin Sobhan, Md. Faysal Nayan March 2016, 'Comparative Analysis between Single Diode and Double Diode Model of PV Cell: Concentrate Different Parameters Effect on Its Efficiency', Retrieved from <www.scirp.org/journal/PaperDownload.aspx?paperID=65220>.

Vika, Håvard Breisnes 2014, 'Modelling of Photovoltaic Modules with Battery Energy Storage in Simulink/Matlab: With in-situ measurement comparisons', Institutt for elkraftteknikk, viewed Retrieved from https://brage.bibsys.no/xmlui/handle/11250/257839?show=full.

Villalva, M. G., Gazoli, J. R. & Filho, E. R. 2009, 'Comprehensive Approach to Modeling and Simulation of Photovoltaic Arrays', *Power Electronics, IEEE Transactions on*, vol. 24, no. 5, pp. 1198-208. Retrieved from <http://ieeexplore.ieee.org.ezproxy.usq.edu.au/stamp/stamp.jsp?tp=&arnumber=4806084>.

W. Shockley, and H. J. Queisser 1961, 'Detailed Balance Limit of Efficiency of p-n Junction Solar Cells', *J. Appl. Phys.*, vol. 32, no. 510, Retrieved from <http://dx.doi.org/10.1063/1.1736034>.

Weidong, Xiao, Dunford, W. G. & Capel, A. 2004, 'A novel modeling method for photovoltaic cells', in *Power Electronics Specialists Conference, 2004. PESC 04. 2004 IEEE 35th Annual*: *proceedings of thePower Electronics Specialists Conference, 2004. PESC 04. 2004 IEEE 35th Annual* pp. 1950-6 Vol.3, viewed <http://ieeexplore.ieee.org.ezproxy.usq.edu.au/stamp/stamp.jsp?tp=&arnumber=1355416>.

Appendices

Appendix 1 Project Specification

ENG4111/4112 Research Project

Project Specification

For:	Anthony Laurent
Title:	Modelling and analysis of multi-junction photovoltaic cells using MATLAB/ Simulink for the improvement of conversion efficiency.
Major:	Power engineering
Supervisors:	Dr Narottam Das and Andreas Helwig
Enrolment:	ENG4111 – Ext S1, 2016; ENG4112 – Ext S2, 2016.
Project Aim:	To improve the conversion efficiency of multijunction photovoltaic (PV) cells by comparing different modelling methods when simulated within the Matlab/Simulink environment.

Programme: (Issue C) (26th September 2016)

1. *(Part A)*

1.1. Research the literature and compare the single diode (D1) model photovoltaic (PV) cell design to double-diode (D2) model PV cell design.

1.2. Research the literature to determine how the D1 and D2 models are simulated within the Matlab/Simulink environment.

1.3. Use Matlab/Simulink simulation to determine if the theoretical D1 model requires further improvements in accuracy when compared to the D2 model.

1.4. Use Matlab/Simulink simulation to determine if the D2 model offers a result closer to the reality even though the efficiency is less than the D1 model.

2. *(Part B)*

2.1. Research the literature and identify how SJSC models can be adapted to multi-junction solar cell (MJSC) characteristics.

2.2. Research the literature and identify proven MJSCs.

2.3. Propose a an iterative Matlab/Simulink design that will simulate the conversion efficiency of identified MJSCs.

If time permits:

2.4. Simulate the conversion efficiency of the identified MJSCs using the proposed Matlab/Simulink model.

Appendix 2 Project Plan Risk Assessment

This project is confined to an office environment and will not require any occupational health and safety measures, with regards to site visits or laboratory safety protocol. However, there are significant risks to plan for with regards to the project objectives, deliverables and milestones.

The table below defines the labels that have been applied to a project associated risk and each level of risk has been allocated an appropriate contingency action that needs to be acted upon.

Table: Legend defining the degrees of risk.

Risk Label	Effects	Appropriate contingency
Minimum Risk	Requires little or no pre-emptive action; Cause minor inconvenience; Will not affect the project deliverables;	Be aware of the potential.
Moderate Risk	Requires pre-emptive action; Cause for concern; May cause considerable delay in project deliverables if not addressed;	Requires some form protocol/pre-emptive action.
High Risk	Requires pre-emptive action and involvement of other stakeholders; Major cause for concern; May fail project objectives if not addressed;	Requires some form protocol/pre-emptive action that includes communication/reporting to other stakeholders

Appendix 3 Project Plan Communication

Table: Risks associated with project objectives, deliverables and milestones.

Associated Risk	Risk Level	Contingency	Resultant Risk
Access to literature. Some particular paper is not available on a data base available to the university	Minimum	In order: Contact the USQ Toowoomba library Contact project supervisor Contact project co-supervisor Find alternative literature	Acceptable
Inability to complete the work due to lack expertise/knowledge	High	Ensure that reporting protocol is adhered to; Be direct in communications to stakeholders; See the communication protocol	Dependant
Project data. Files damaged/corrupted, soft records lost or work not backed up correctly.	Moderate	All files to be saved onto Google Drive. The files are to be stored in a synchronised folder so that they are backed up automatically and live.	Acceptable
Project Software. Laptop and/or software corrupted/damaged/lost (MATLAB Simulink) (MS Office) (ENDNOTE) (MATHCAD)	Moderate	Ensure that the following links for each of the listed software packages are saved onto Google Drive: On-line licences/proof of purchase Help desk Operation manuals	Acceptable
Requirement for external expertise	Minimum	Communicate with the supervisors as the need arises; Do not engage external assistance unless the supervisors approve.	

Appendix 4 Project Plan Resources

The several objectives of the communication plan is to provide the following:

- A defined line of communication between the stakeholders (the student, the supervisors and the course administrator) as shown below;
- Provide a record of communications;
- Provide a log of next actions for each stakeholder to refer to;

The lines of communication, as shown below, are co-ordinated by the student so that the supervisors will have a clear record of communication in the form of an on-line log where they can refer to see the student's project progress, or past discussions/decisions with the student.

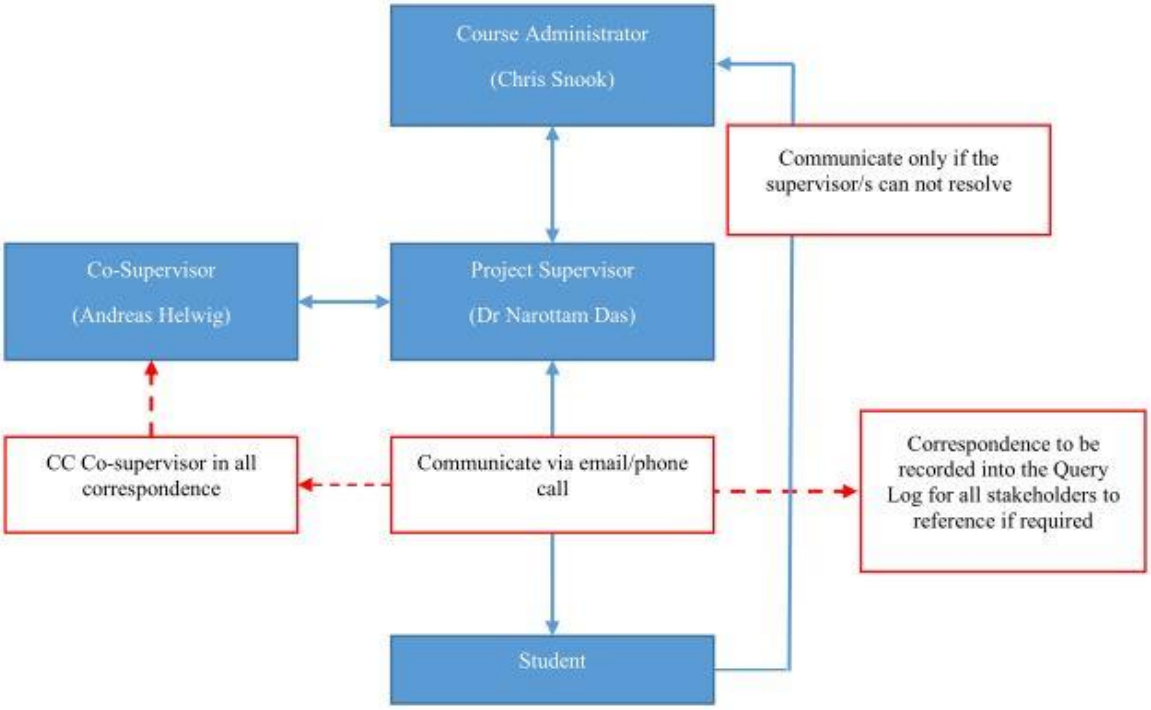

Query Log

The Query Log is a live document that is used to record correspondence between the student an the project supervisors. It is a summary of queries / responses / next-actions regarding the students dissertation and is kept up to date by the student to provide immediate access to an up-to-date and centralised log of all correspondence between the project stakeholders. The supervisors have been provided with a link to the log.

Appendix 5 Project Plan Timeline

General costs

It appears that the only cost to be incurred for this project is the annual fees for the MATLAB/Simulink licence and service renewals.

Item	Quantity	Cost each	Total
Microsoft Office	1	-	-
EndNote X7	1	-	-
PTC Mathcad	1	-	-
MATLAB and Simulink Student Suite	1	$115.00	
SimDriveline	1	NA	
SimElectronics	1	$12.00	
SimHydraulics	1	NA	
SimMechanics	1	NA	
SimPowerSystems	1	$12.00	
SimPowerSystems	1	$12.00	
			$151.00
Unless told otherwise, it is assumed that the costs listed are to be met by the student.			

Data

The proposed project should not incur any costs for project data. The paper will focus on software simulation of mathematical relationships and a selection of manufactured multijunction and single junction photovoltaic cells will be discussed, as a means to verify the simulations.

Each part of the research paper will require some form of validation and it is expected that the parameters measured in the Matlab/Simulink simulations can be compared to experimental data extracted from manufacturer's data sheets.

Furthermore, the paper will include some amount of research on validation methodology. There is discussion of validation methodology in the field literature, hence a large quantity of data contained within the literature is available through the online bibliographic databases available through the USQ Library.

USQ Facilities

There should not be a need to access the USQ facilities. There may be a need to speak by phone/Skype to the Supervisors or their faculty staff regarding Matlab/Simulink expertise, however this can be negotiated via email if the need arises.

Appendix 6 MATLAB script - Initial conditions

```
%_____________________________________________________________________
% Datasheet_SP70

% Written: 26.04.16
% Author : Anthony Laurent
% Input parameters for Datasheet Initial conditions

% Datasheet taken from:
% Siemens, Solar module SP70, 2012, Siemens AG and Bayernwerk AG, Germany,
% Retrieved from  <http://www.solardirect.com/PDF/SolarElectric/sp70.pdf>.

% Note:
% D1 = Single diode model
% D2 = Double diode model

Model = 'Mono-crystalline Siemens SP70 PV Module.';%Model name to input to
Sim_Results = 'Sim_Results_SP70';  %Write to xcell sheet

Pmpp_stc = 70;  %(W) Maximum power point under STC

L = 1.125;      %(m) Length of the module
W = 0.500;      %(m) Width of the module
Area = L*W;     %Total module area (m^2)

Voc_stc = 21.4;     %(V) Open circuit voltage at STC
Isc_stc = 4.7;      %(A) Short circuit current at STC
Impp_stc = 4.25;    %(A) Maximum power point current at STC
Vmpp_stc = 16.5;    %(V) Maximum power point voltage at STC

Ns = 36;            %Number of series connected cells
Ki = 0.00206;       %(A /'C) Temperature coefficient of Isc
Kv = -0.077;        %(V /'C) Temperature coefficient of Voc
Tc = 25;            %(Celcius) Initial measured temperature
Gc = 1000;          %(W/m^2) Initial Measured Irradiance

%Estimated Values for Parameter extraction:
a = 1.3;            %Diode ideality factor (D1 only)
a1 = 1.0;           %Diode 1 ideality factor (D2 only)
a2 = 2.0;           %Diode 2 ideality factor (D2 only)
Pe = a1 + a2;       %Ideal fact denominator (D2 rev. sat. I)

%Constants:
k = 1.38065e-23;    %Boltsmans constant
q = 1.602e-19;      %Electron charge
Gstc = 1000;        %Irradiance at STC
Tstc = 25;          %Temperature at STC
Eg = 1.12;          %Silicon bandgap energy

%Export the following values for parameter extraction:
[D1Rs,D1Rp,D1Iph] = Extraction_D1(Vmpp_stc,Isc_stc,Impp_stc,a,Ns,Voc_stc);

[D2Rs,D2Rp,D2Iph] =
Extraction_D2(Vmpp_stc,Isc_stc,Impp_stc,a1,a2,Ns,Voc_stc);
```

Appendix 7 MATLAB script - D1 extraction

```
function [D1Rs,D1Rp,D1Iph] = Extraction_D1(Vmpp_stc,Isc_stc,Impp_stc,a,Ns,Voc_stc)
% Date:     25.03.16
% Author:   Anthony Laurent, based on code by:
% Vika, Håvard Breisnes 2014, 'Modelling of Photovoltaic Modules with
% Battery Energy Storage in Simulink/Matlab: With in-situ measurement
% comparisons', Institutt for elkraftteknikk, viewed
% Retrieved from https://brage.bibsys.no/xmlui/handle/11250/257839?show=full.

k = 1.38065e-23;                    % Boltzman constant (J/oK)
q = 1.602e-19;                      % Elementary charge on an electron (oC)
T_stc = (25+273);                   % STC cell temp
Vt = (k*T_stc)/q;                   % Thermal voltage
Isn = Isc_stc/(exp(Voc_stc/(a*Ns*Vt))-1);  % Aproximate value for Is

Rs_0 = 0.15;            % Initial condition for Rs
Rs_increment = 0.001;   % Step size for Rs
Rp_0 = 10;              % Starting value of Rp
Rp_increment = 1;       % Step size for Rp
Iphn = Isc_stc;         % Starting value of Iph/Ipv
Iph_increment = 0.001;  % Step size for Iph/Ipv
MinErr = inf;           % Minimum = infinity


for aa=1:1000           % Counter for Rs
    for bb=1:1000       % Counter for Rp
        for cc=1:100    % Counter for Iph

            Rs = Rs_0 + Rs_increment * aa;  %Increment Rs the 'aa'th time
            Rp = Rp_0 + Rp_increment * bb;  %Increment Rp the 'bb'th time
            Iph = Iphn+Iph_increment* cc;   %Increment Iph the 'cc'th time

            RsErr=(Vmpp_stc/Impp_stc)-
            ((a*Ns*Vt*Rp)/((Is*Rp*exp((Vmpp_stc+(Impp_stc*Rs))/(a*Ns*Vt)))+(a*Ns*Vt
            )))-Rs;
                %Series equivalent resistance solved for zero.
                %(Sangsawang & Chaitusaney 2012)

             RpErr=(Vmpp_stc+(Impp_stc*Rs))/(Iph-Impp_stc-
             Is*(exp((Vmpp_stc+(Impp_stc*Rs))/(a*Ns*Vt))-1))-Rp;
                %Parallel equivalent resistance solved for zero.
                %(Sangsawang & Chaitusaney 2012)

            IphErr=(((Rp+Rs)/Rp)*Isc_stc)-Iph;  %Iph solved for zero.

            TotalErr=RsErr^2+RpErr^2+IphErr^2;  %Solve for the total error

            if TotalErr<MinErr  %If the total error is less than infinity
                MinErr=TotalErr;%Replace MinErr with TotalErr
                Rsnew=Rs;       %The new best value for Rs
                Rpnew=Rp;       %The new best value for Rp
                Iphnew=Iph;     %The new best value for Iph
            end
        end
    end
end
D1Rp=Rpnew;      % Pass the D1 value for Rp value back to the main script
D1Rs=Rsnew;      % Pass the D1 value for Rs value back to the main script
D1Iph=Iphnew;    % Pass the D1 value for Ipv value back to the main script
end
%_____________________END of code_____________________________________
```

Appendix 8 MATLAB script - D2 extraction

```
function [D2Rs,D2Rp,D2Iph] =
Extraction_D2(Vmpp_stc,Isc_stc,Impp_stc,a1,a2,Pe,Ns,Voc_stc)
% Date:     25.03.16
% Author:   Anthony Laurent, based on code by:
% Vika, Håvard Breisnes 2014, 'Modelling of Photovoltaic Modules with
% Battery Energy Storage in Simulink/Matlab: With in-situ measurement
% comparisons', Institutt for elkraftteknikk, viewed
% Retrieved from https://brage.bibsys.no/xmlui/handle/11250/257839?show=full.
k=1.38065e-23;                          % Boltzman constant (J/oK)
q=1.602e-19;                            % Elementary charge on an electron (oC)
T_stc = (25+273);                       % STC cell temp
Vtn = (k*T_stc)/q;                      % Thermal voltage

% (Sangsawang & Chaitusaney 2012)D2 model Is1 and Is2
Is1n =Isc_stc/(exp(Voc_stc/(a1*Ns*Vtn))-1);
Is2n =Isc_stc/(exp(Voc_stc/(((a1+a2)/Pe)*Ns*Vtn))-1);

Rs_0=0.15;              % Initial condition for Rs
Rs_increment=0.001;     % Increment for Rs
Rp_0=10;                % Initial condition for Rp
Rp_increment=1;         % Increment for Rp
Iphn=Isc_stc;           % Initial condition Iphn
Iph_increment=0.001;    % Increment for Iphn
MinErr=inf;             % Minimum = infinity

for aa=1:1000           % Counter for Rs
    for bb=1:1000       % Counter for Rp
        for cc=1:100    % Counter for Iph
            Rs=Rs_0+Rs_increment*aa;     %Increment Rs the 'aa'th time
            Rp=Rp_0+Rp_increment*bb;     %Increment Rp the 'bb'th time
            Iph=Iphn+Iph_increment*cc;   %Increment Iph the 'cc'th time

             RsErr=(Vmpp_stc/Impp_stc)-
             (1/(((Is1*exp((Vmpp_stc+Impp_stc*Rs)/(a1*Ns*Vtn)))/(a1*Ns*Vtn)) +
             ((Is2*exp((Vmpp_stc+Impp_stc*Rs)/(a2*Ns*Vtn)))/(a2*Ns*Vtn))+(1/Rp)))-
             Rs;
             %Series equivalent resistance solved for zero.
             %(Sangsawang & Chaitusaney 2012)

             RpErr=(Vmpp_stc+(Impp_stc*Rs))/(Iph-
             Is1*(exp((Vmpp_stc+(Impp_stc*Rs))/(a1*Ns*Vtn))-1)-
             Is2*(exp((Vmpp_stc+(Impp_stc*Rs))/(a2*Ns*Vtn))-1)-Impp_stc)-Rp;
             %Parallel equivalent resistance solved for zero.
             %(Sangsawang & Chaitusaney 2012)

             IphErr=(((Rp+Rs)/Rp)*Isc_stc)-Iph;  %Iph solved for zero.

             TotalErr=RsErr^2+RpErr^2+IphErr^2;  %Solve for the total error

            if TotalErr<MinErr   %If the total error is less than infinity

                MinErr=TotalErr;%Replace MinErr with TotalErr
                Rsnew=Rs;       %The new best value for Rs
                Rpnew=Rp;       %The new best value for Rp
                Iphnew=Iph;     %The new best value for Iph

            end
        end
    end
end
%% Output Values
D2Rp=Rpnew;      % Pass the Rp value back to the main script
D2Rs=Rsnew;      % Pass the Rs value back to the main script
D2Iph=Iphnew;    % Pass the Ipv value back to the main script
%_____________________END of code_____________________________________
```

Appendix 9 Simulink block model - D1_Eg

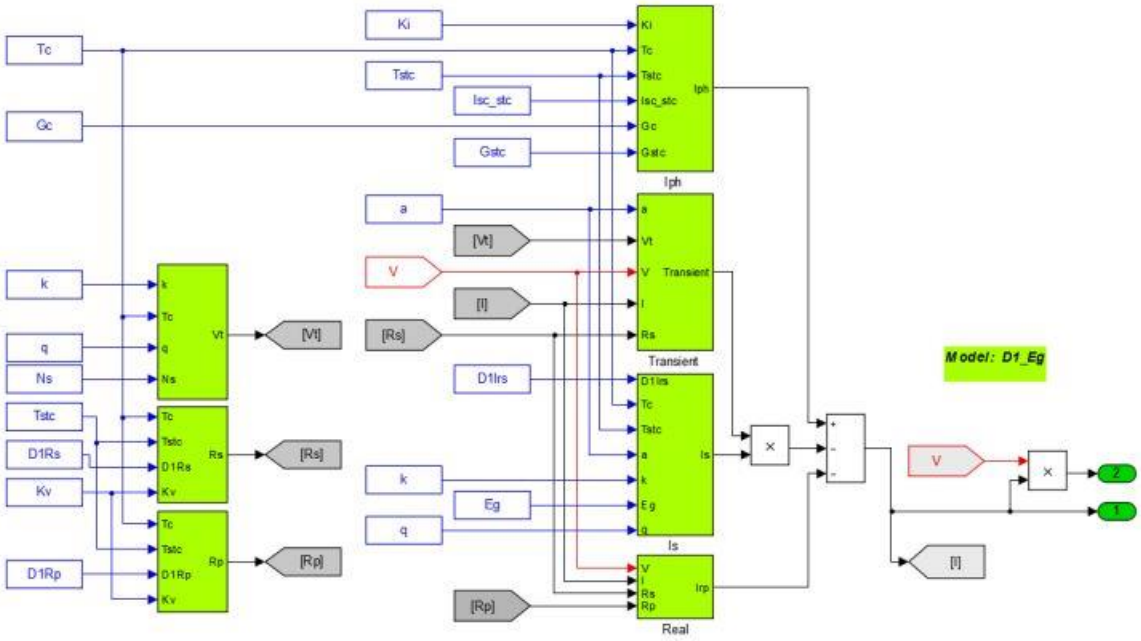

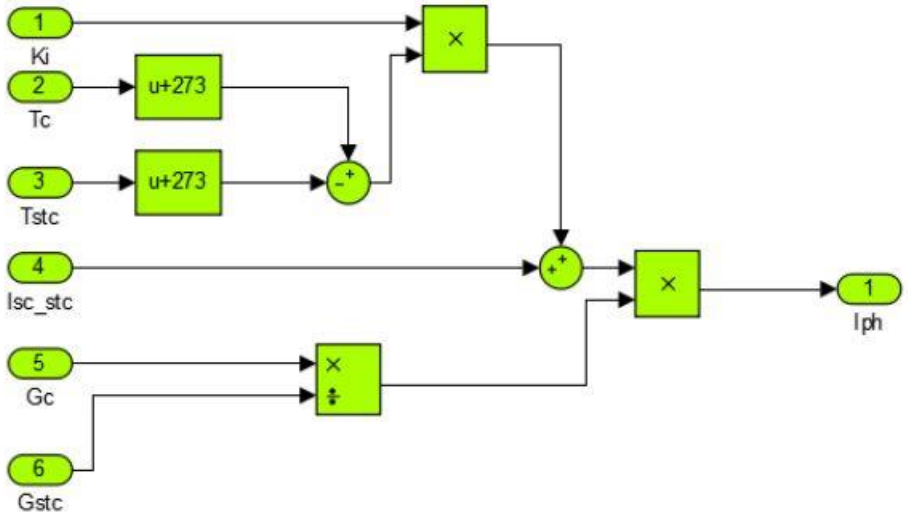

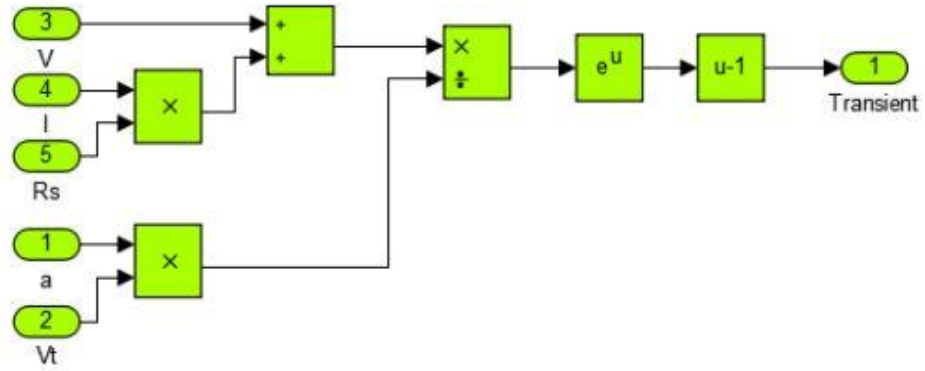
3
V
4
I
5
Rs
1
a
2
Vt
e^u
u-1
1
Transient

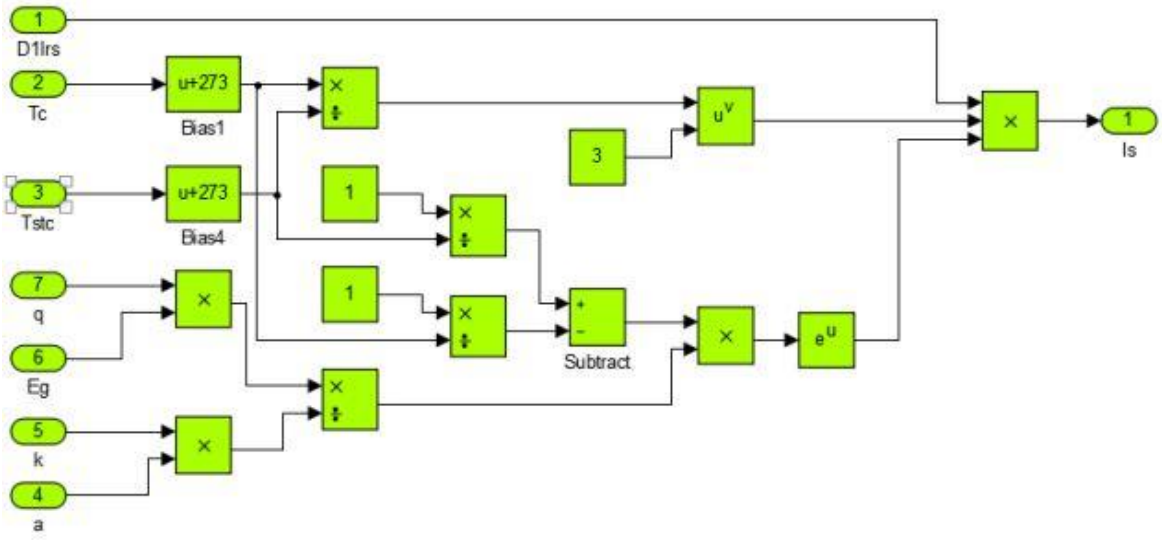
1
D1Irs
2
Tc
u+273
Bias1
3
Tstc
u+273
Bias4
7
q
6
Eg
5
k
4
a
1
1
3
u^v
Subtract
e^u
1
Is

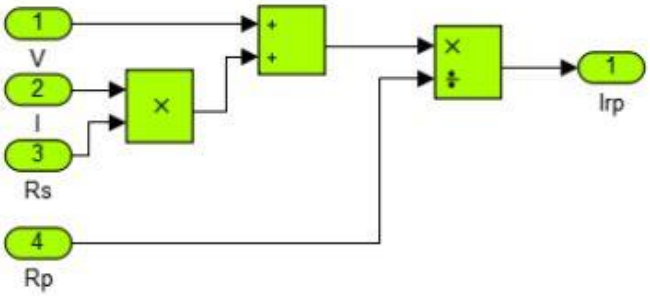
1
V
2
I
3
Rs
4
Rp
1
Irp

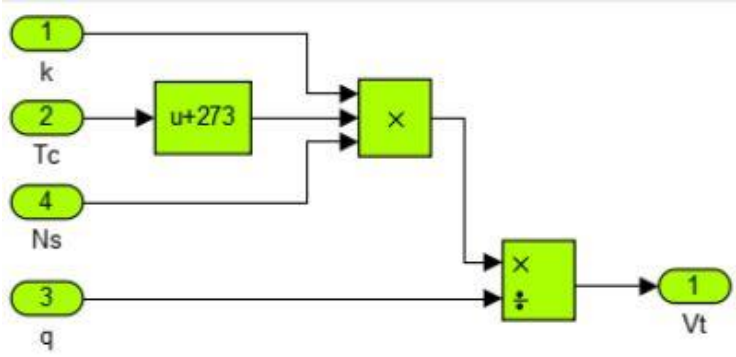
1
k
2
Tc
u+273
4
Ns
3
q
×
×
÷
1
Vt

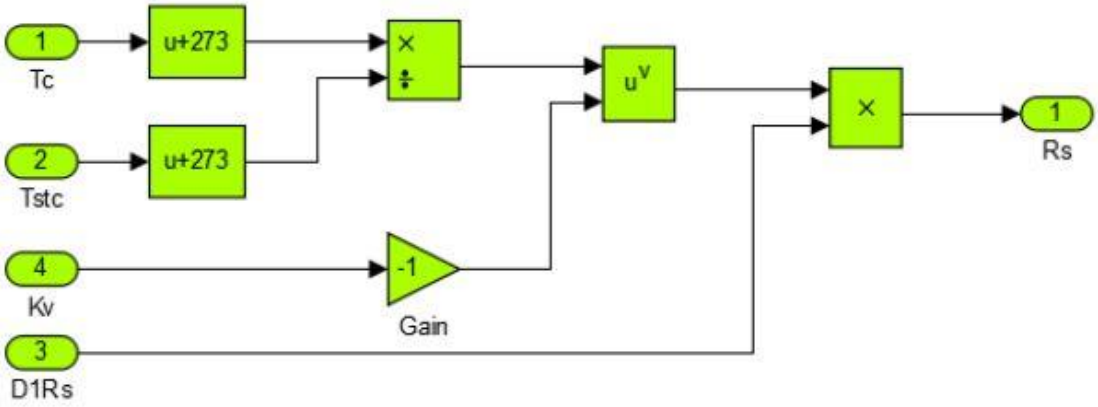
1
Tc
u+273
2
Tstc
u+273
4
Kv
-1
Gain
3
D1Rs
×
÷
u^v
×
1
Rs

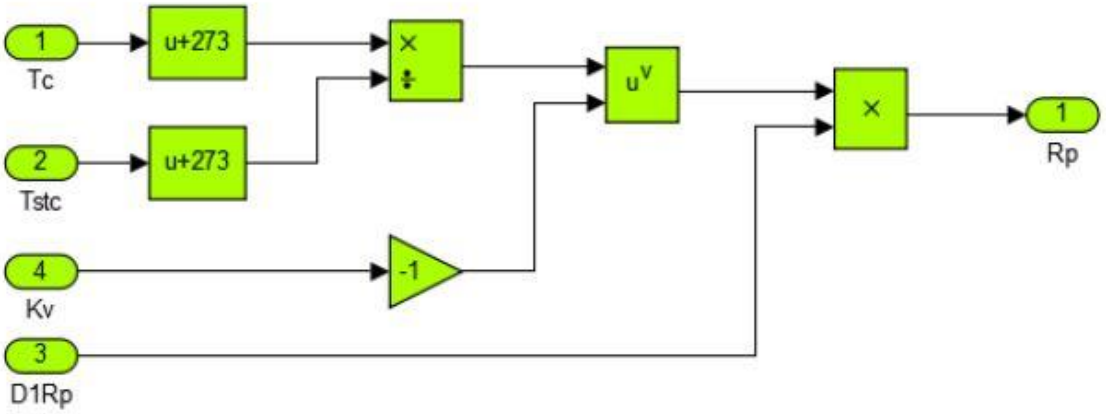
1
Tc
u+273
2
Tstc
u+273
4
Kv
-1
3
D1Rp
×
÷
u^v
×
1
Rp

Appendix 10 Simulink D2_Eg block model

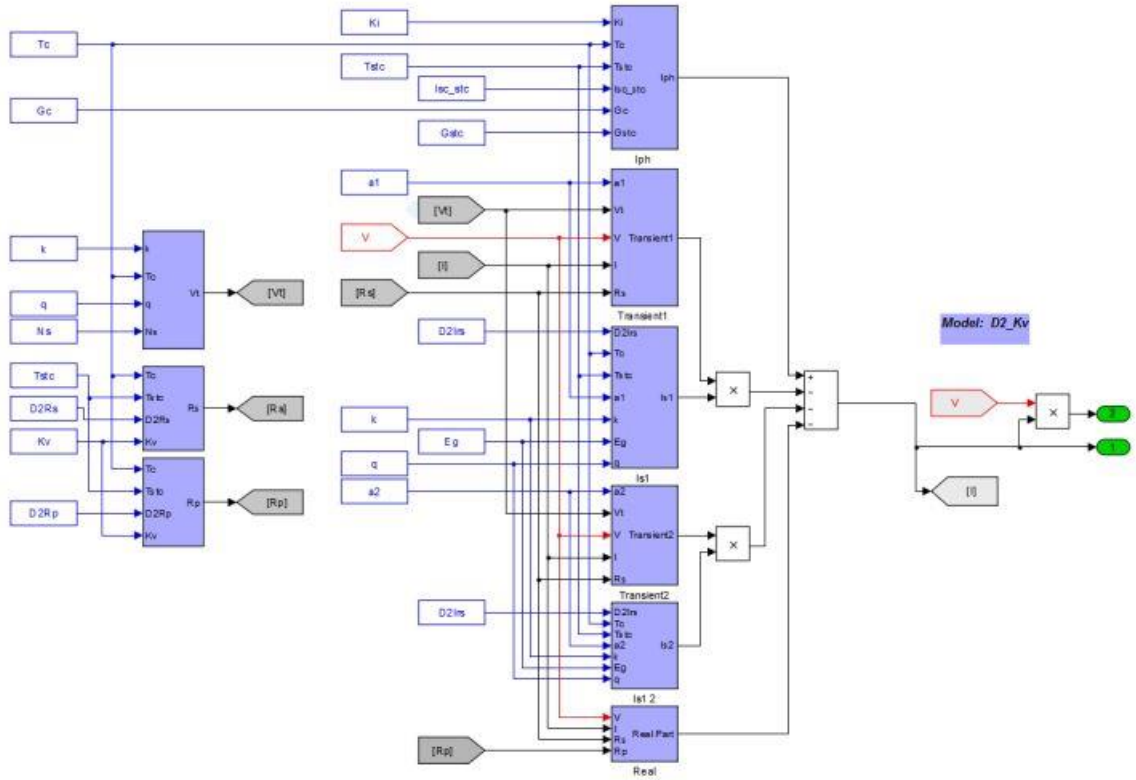

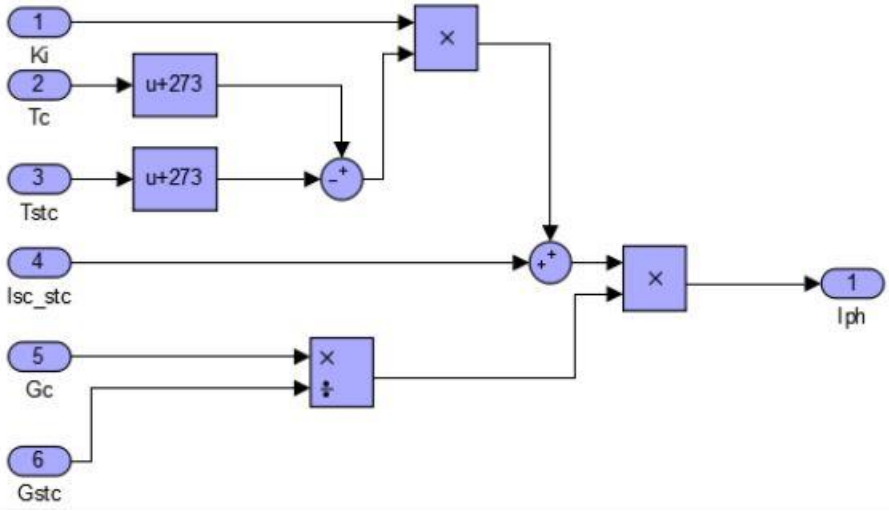

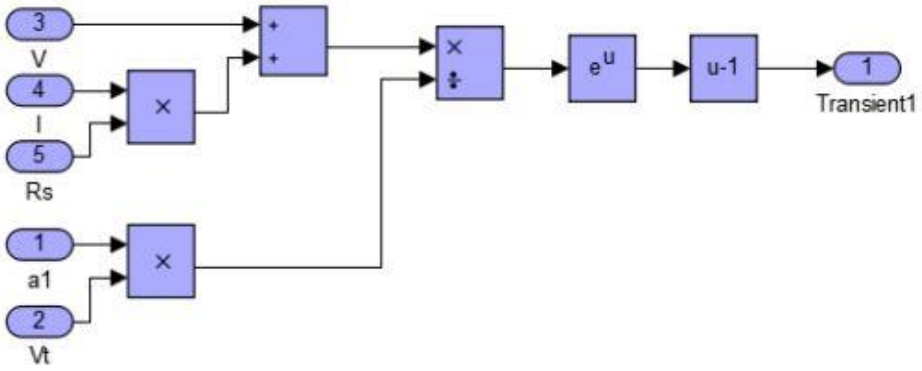
3
V
4
I
5
Rs
1
a1
2
Vt
e^u
u-1
1
Transient1

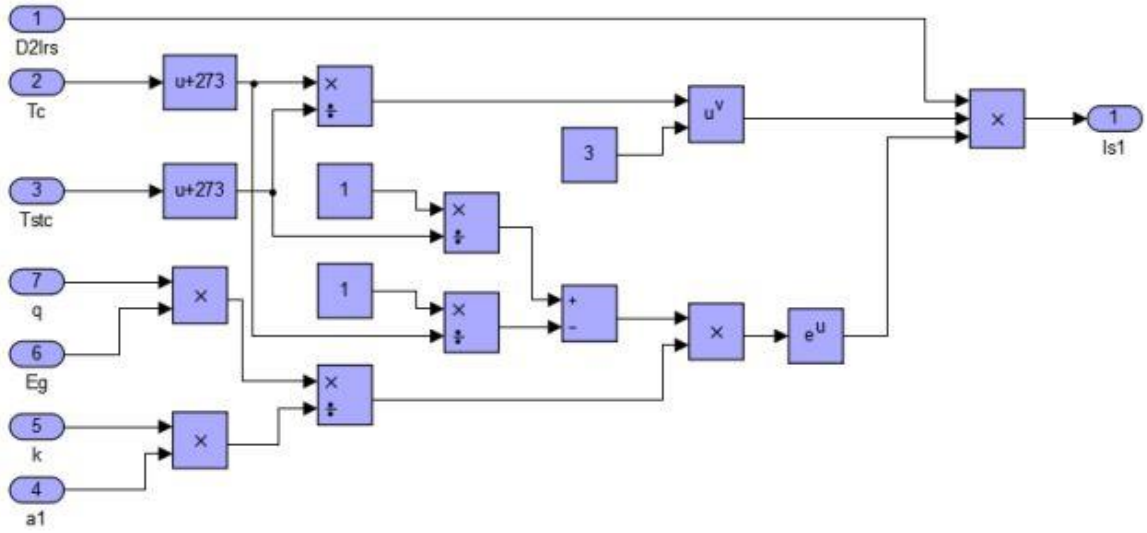
1
D2Irs
2
Tc
3
Tstc
7
q
6
Eg
5
k
4
a1
u+273
u+273
1
1
3
u^v
e^u
1
Is1

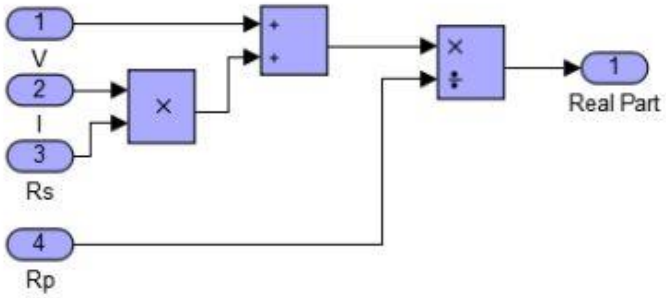
1
V
2
I
3
Rs
4
Rp
1
Real Part

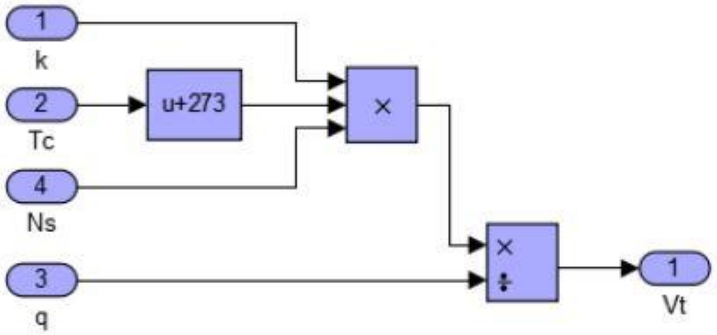
1
k
2
Tc
u+273
4
Ns
3
q
×
×
÷
1
Vt

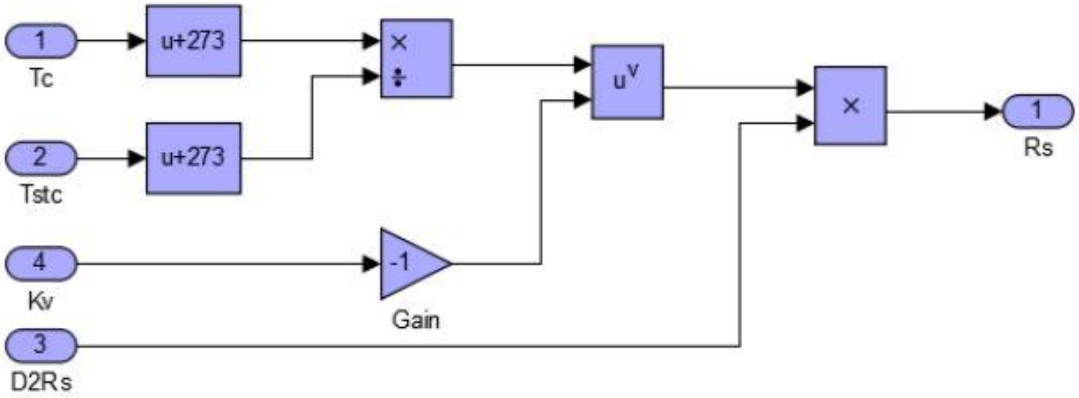
1
Tc
u+273
2
Tstc
u+273
4
Kv
-1
Gain
3
D2Rs
×
÷
u^v
×
1
Rs

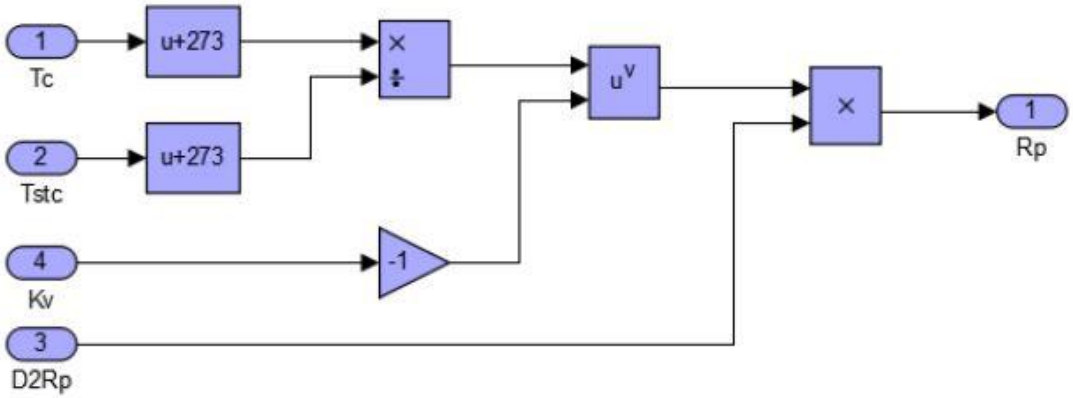
1
Tc
u+273
2
Tstc
u+273
4
Kv
-1
3
D2Rp
×
÷
u^v
×
1
Rp

Appendix 11 Simulink D1_Kv block model

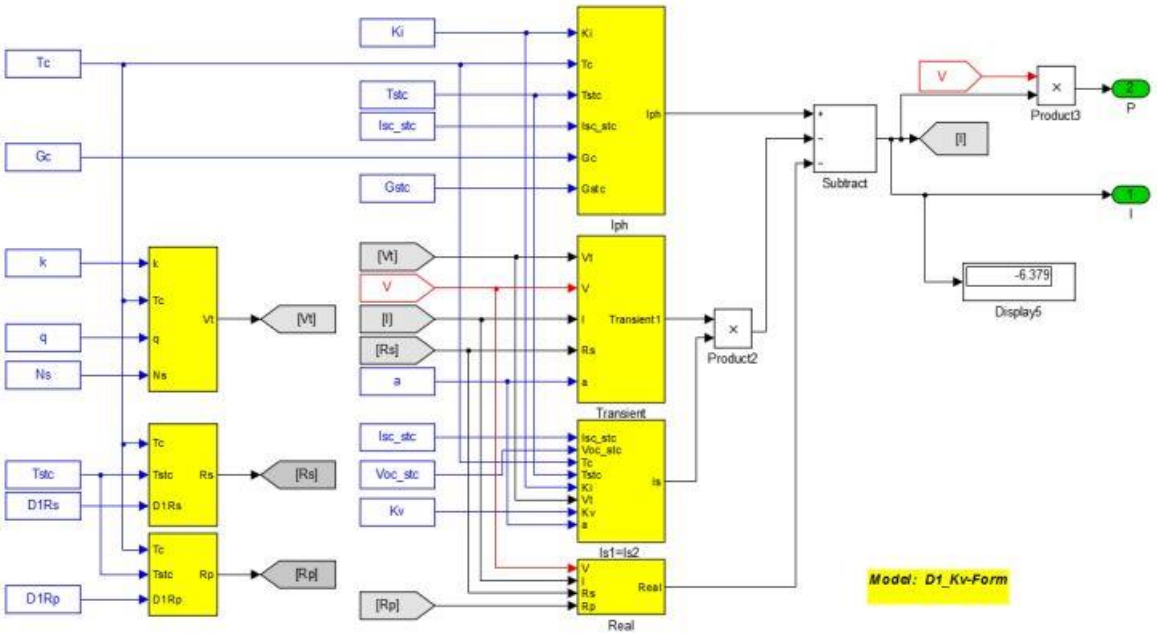

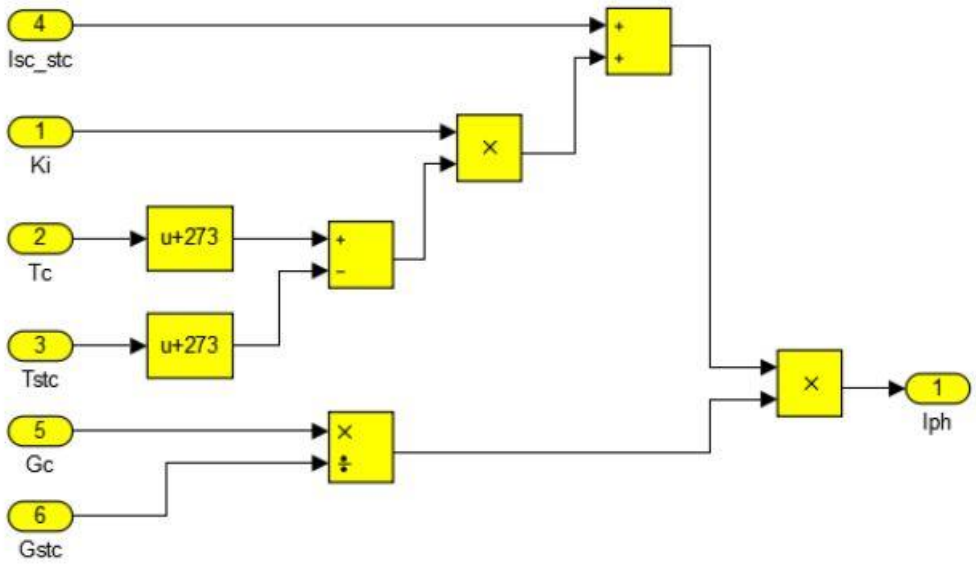

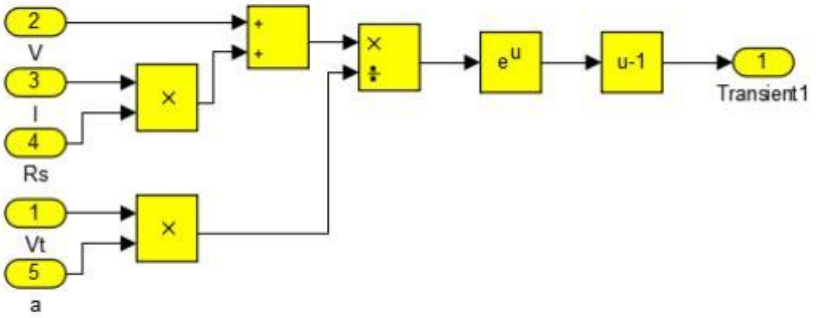
2
V
3
I
4
Rs
1
Vt
5
a
e^u
u-1
1
Transient1

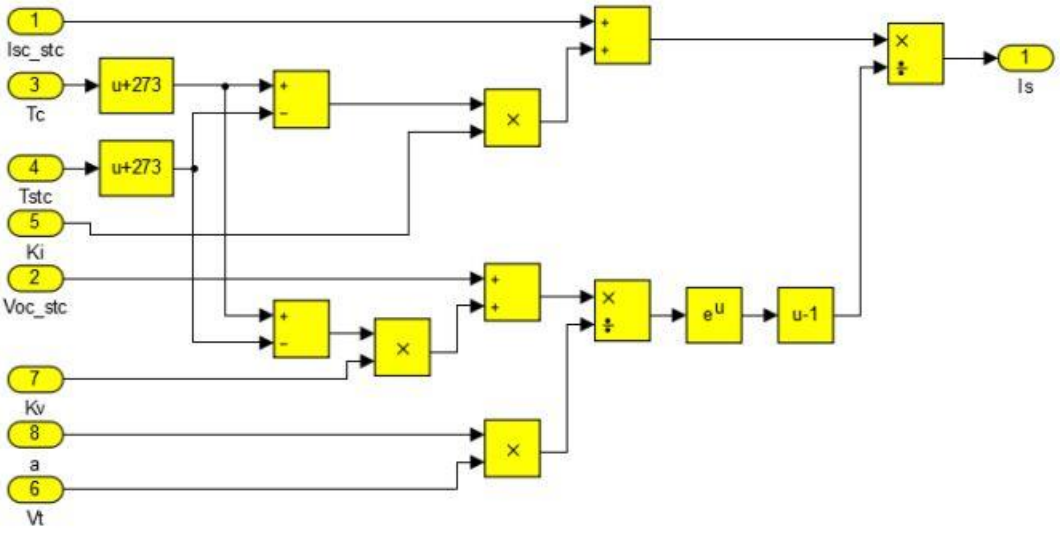
1
Isc_stc
3
Tc
u+273
4
Tstc
u+273
5
Ki
2
Voc_stc
7
Kv
8
a
6
Vt
e^u
u-1
1
Is

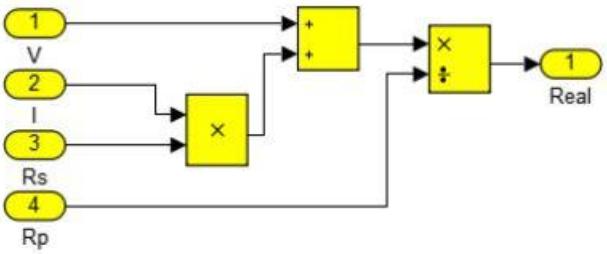
1
V
2
I
3
Rs
4
Rp
1
Real

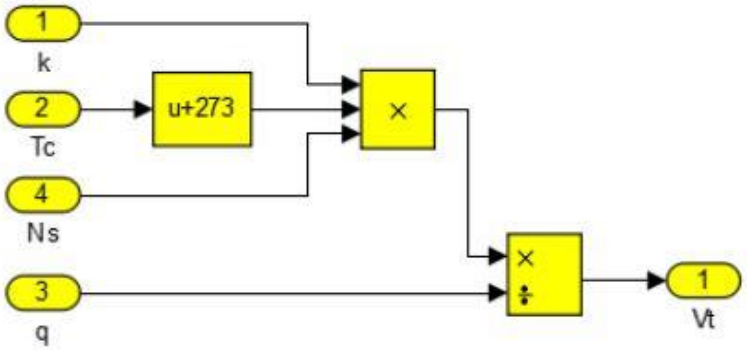
1
k
2
Tc
u+273
4
Ns
3
q
×
×
1
Vt

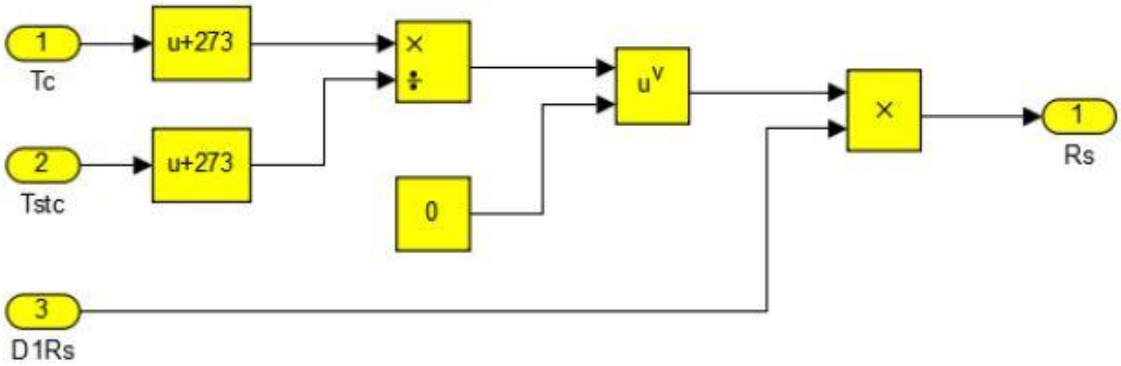
1
Tc
u+273
2
Tstc
u+273
0
×
u^v
×
1
Rs
3
D1Rs

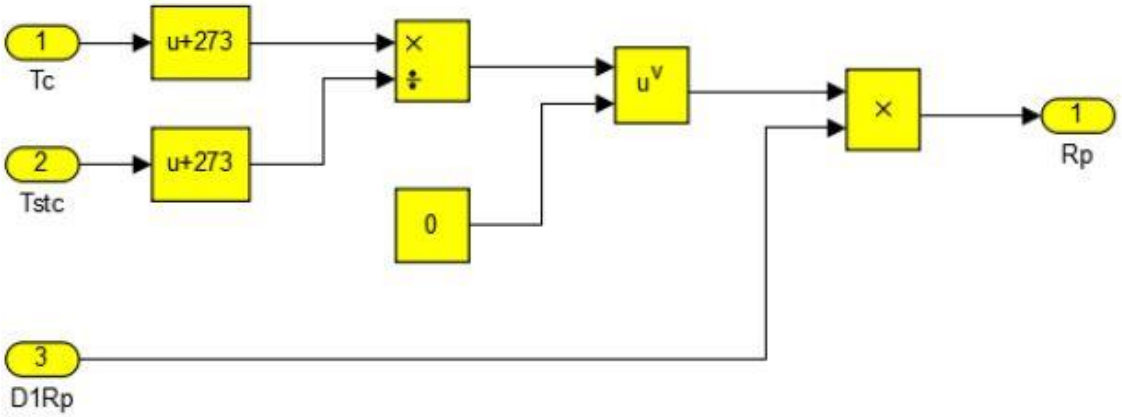
1
Tc
u+273
2
Tstc
u+273
0
×
u^v
×
1
Rp
3
D1Rp

Appendix 12 Simulink D2_Kv block model

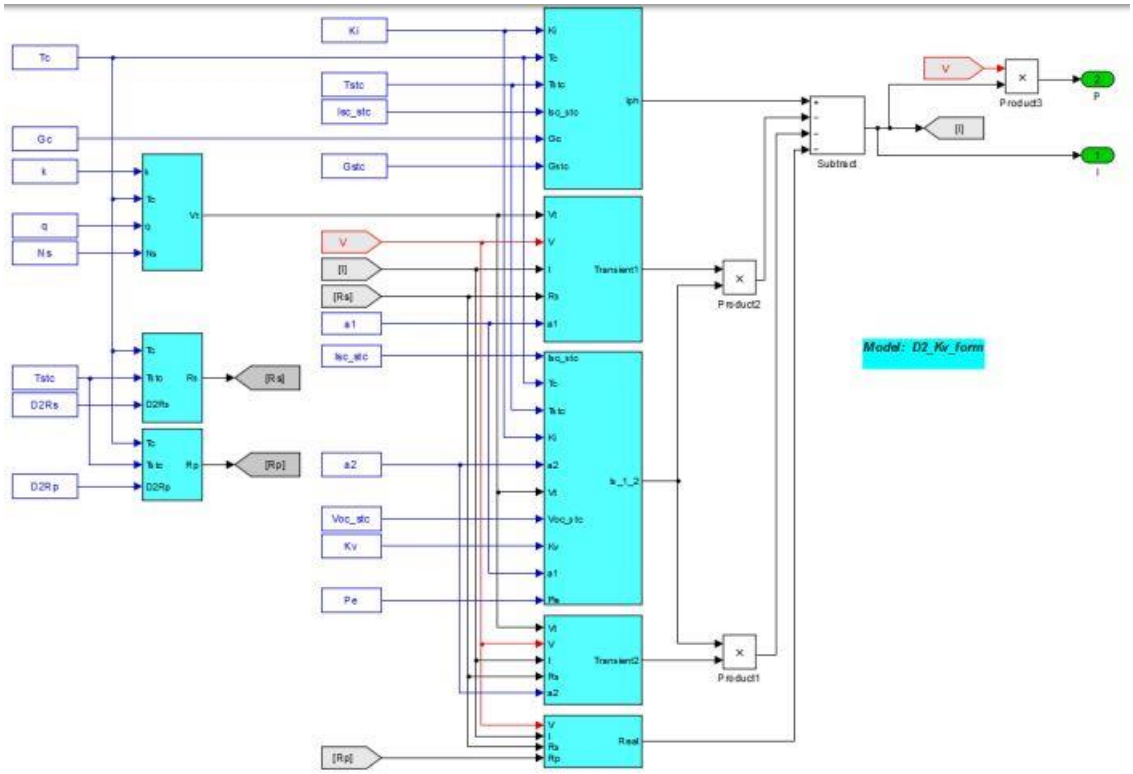

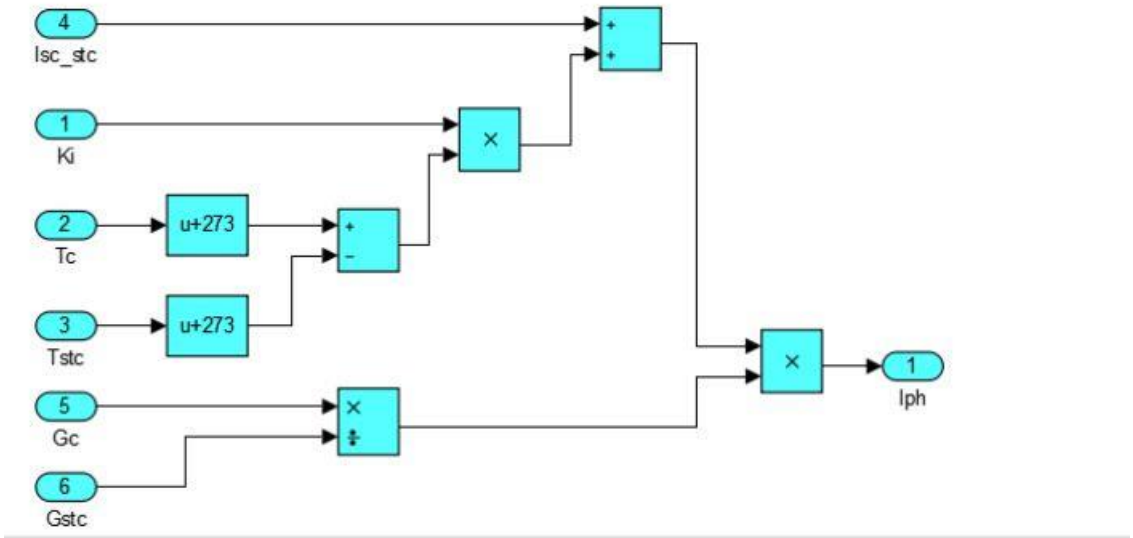

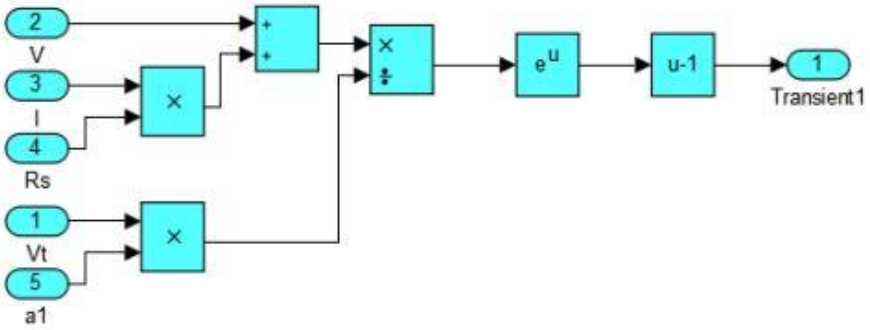
2
V
3
I
4
Rs
1
Vt
5
a1
e^u
u-1
1
Transient1

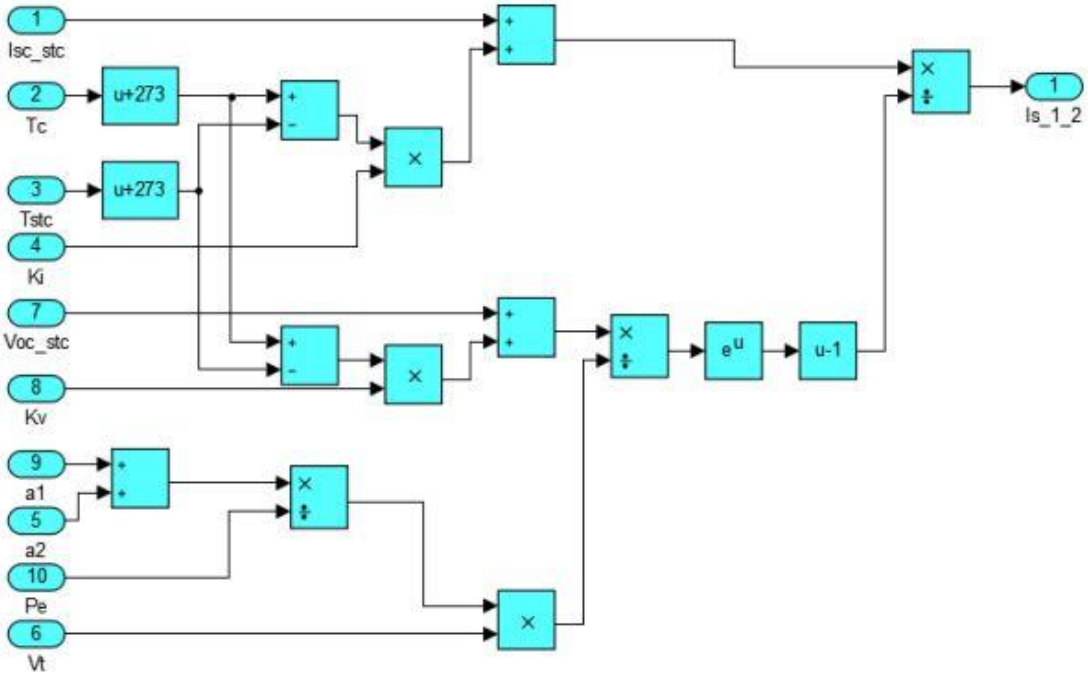
1
Isc_stc
2
Tc
u+273
3
Tstc
u+273
4
Ki
7
Voc_stc
8
Kv
9
a1
5
a2
10
Pe
6
Vt
e^u
u-1
1
Is_1_2

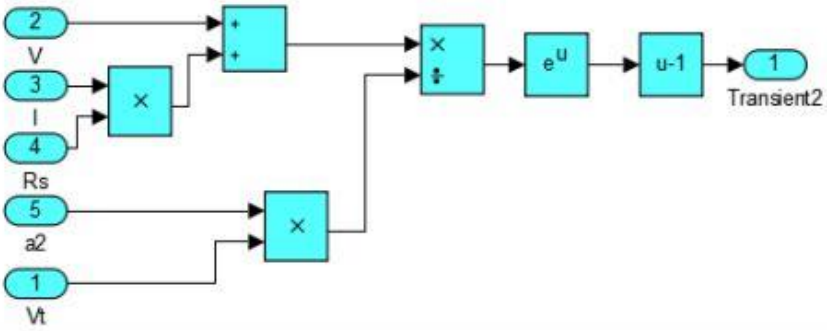
2
V
3
I
4
Rs
5
a2
1
Vt
e^u
u-1
1
Transient2

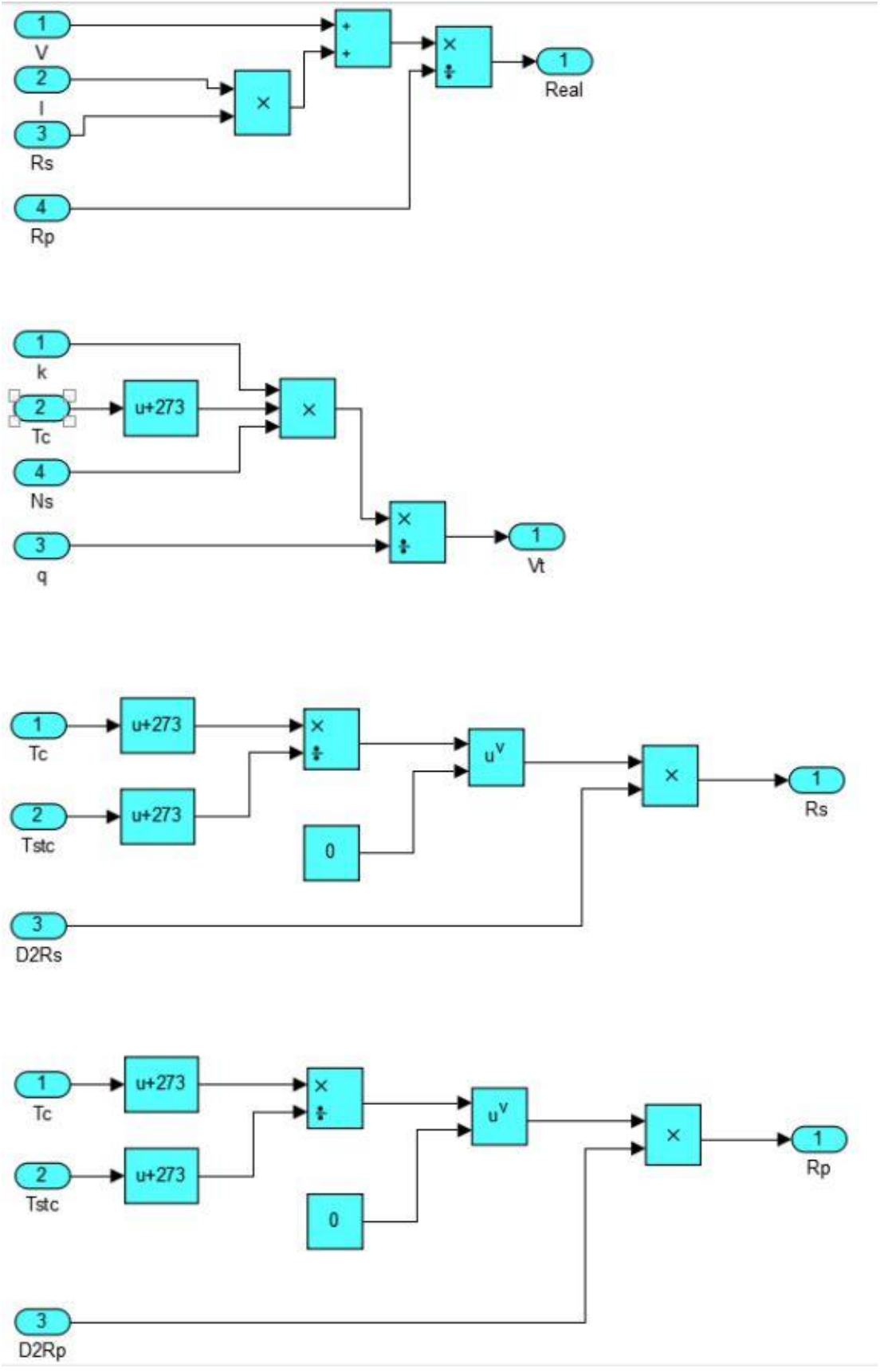
1
V
2
I
3
Rs
4
Rp
×
+
+
×
1
Real
1
k
2
Tc
u+273
×
4
Ns
3
q
×
1
Vt
1
Tc
u+273
2
Tstc
u+273
×
0
u^v
×
1
Rs
3
D2Rs
1
Tc
u+273
2
Tstc
u+273
×
0
u^v
×
1
Rp
3
D2Rp

Appendix 13 MATLAB script – Tvar Data

```
% Data Set for D1_Tvar model
% 26.04.16

% This code imports all data from the global workspace in relation to
% variations in temperature and then represents it in graphical form for
% further analysis.

Changing_Parameter = '(Gc=STC  Tc=Variable)';

DataSheet_Values = ...
{Model;Area;Pmpp_stc;Voc_stc;Isc_stc;Impp_stc;Vmpp_stc;' ';Ns;Ki;Kv;Tc;Gc;' '; ...
a;a1;a2;Pe;' ';D1Rs;D1Rp;D2Rs;D2Rp;Eg;};
xlswrite(Sim_Results,DataSheet_Values,'Tvar','C3')

tempVec = simout_D1_Tvar(1,10:13);
%Import the irradiance vectors from the sim model

VOC = zeros(1,4); %Row/column matrix to store Fill factor and efficiency data
ISC = zeros(1,4); %Row/column matrix to store Fill factor and efficiency data
Pmpp = zeros(1,4);%Row/column matrix to store Fill factor and efficiency data
Impp = zeros(1,4);%Row/column matrix to store Fill factor and efficiency data
Vmpp = zeros(1,4);%Row/column matrix to store Fill factor and efficiency data
FF = zeros(1,4);  %Row/column matrix to store Fill factor and efficiency data
ETA = zeros(1,4); %Row/column matrix to store Fill factor and efficiency data

i = 2;                      %Row Counter starts at 2 to allow for
j = 1;                      %Column counter starting at row 2

for Tc = tempVec

    P = simout_D1_Tvar(:,(i+4));
    %Vector containing the current out from positive current = zero to
    %current = zero crossing
    I = simout_D1_Tvar(:,i);
    %Vector containing the current out from positive current = zero to
    %current = zero crossing
    V = simout_D1_Tvar(:,1);
    %Vector containing the current out from positive current = zero to
    %current = zero crossing

    [Izero,row] = min(abs(I(:)));   %Find when I equals zero
    Voc = V(row);       %Voc at open current
    VOC(1,j) = Voc;     %Store the voc value to use in plot/table/legend

    Isc = I(1);         %I at short circuit
    ISC(1,j) = Isc;     %Store the Isc value to use in plot/table/legend

    [Pmax,roww]=max(P); %Value of the power at the maximum power point
    Pmpp(1,j) = Pmax;   %Store the Pmpp value to use in plot/table/legend

    Imax = I(roww);     %Value of the current at the maximum power point
    Impp(1,j) = Imax;   %Store the Impp value to use in plot/table/legend

    Vmax = V(roww);     %Value of the voltage at the maximum power point
    Vmpp(1,j) = Vmax;   %Store the Vmpp value to use in plot/table/legend

    FFn = (Vmax*Imax)/(Voc*Isc);%Fill factor
    FF(1,j) = FFn;      %Store the FF value to use in plot/table/legend

    Pmpp_stc = 1000*Area;           %Input power at (1000 W)/(Area m2)
    Eta = ((Voc*Isc*FFn)/Pmpp_stc)*100;  %Percent cell efficiency
    ETA(1,j) = Eta;     %Store the Eta value to use in plot/table/legend

    i=i+1;              %Increment counter
    j=j+1;              %Increment counter
```

```
P_array = simout_D1_Tvar(:,6:9);    %Power arrays to be plotted
I_array = simout_D1_Tvar(:,2:5);    %Current arrays to be plotted
V_array = simout_D1_Tvar(:,1);      %Voltage arrays to be plotted

PY = max(P_array);      %Find the highest value in each of the Pow arrays
IY = max(I_array);      %Find the highest value in each of the Pow arrays
PYmax = max(PY)*1.1;    %Value of the max Y-axis in VP plot
IYmax = max(IY)*1.1;    %Value of the max Y-axis in VI plot
VXmax = max(VOC)*1.1;   %Value of the max X-axis in VP plot

figure
plot(V_array, P_array,'LineWidth',1);
axis([0 VXmax 0 PYmax]);
grid on;
title({'Single Diode VP Plot (Gc=STC  Tc=Variable)'; Model});
xlabel('Output voltage, V');
ylabel('Output power, W');
legend( ...
['T = ',num2str(tempVec(1,1),'%.0f'),' C;','  Pmpp = ',num2str(Pmpp(1,1),'%.2f'),'
W'], ...
['T = ',num2str(tempVec(1,2),'%.0f'),' C;','  Pmpp = ',num2str(Pmpp(1,2),'%.2f'),'
W'], ...
['T = ',num2str(tempVec(1,3),'%.0f'),' C;','  Pmpp = ',num2str(Pmpp(1,3),'%.2f'),'
W'], ...
['T = ',num2str(tempVec(1,4),'%.0f'),' C;','  Pmpp = ',num2str(Pmpp(1,4),'%.2f'),'
W'], ...
'Location','NorthWest');

figure
plot(V_array, I_array,'LineWidth',1);
axis([0 VXmax 0 IYmax]);
grid on;
title({'Single Diode VI Plot (Gc=STC  Tc=Variable)'; Model});
xlabel('Output voltage, V');
ylabel('Output current, A');
legend( ...
['Tc = ',num2str(tempVec(1,1),'%.0f'),' C;','  Isc = ',num2str(ISC(1),'%.2f'),'
A;','  Voc = ',num2str(VOC(1),'%.2f'),' V;'], ...
['Tc = ',num2str(tempVec(1,2),'%.0f'),' C;','  Isc = ',num2str(ISC(2),'%.2f'),'
A;','  Voc = ',num2str(VOC(2),'%.2f'),' V;'], ...
['Tc = ',num2str(tempVec(1,3),'%.0f'),' C;','  Isc = ',num2str(ISC(3),'%.2f'),'
A;','  Voc = ',num2str(VOC(3),'%.2f'),' V;'], ...
['Tc = ',num2str(tempVec(1,4),'%.0f'),' C;','  Isc = ',num2str(ISC(4),'%.2f'),'
A;','  Voc = ',num2str(VOC(4),'%.2f'),' V;'], ...
'Location','SouthWest');

figure
EtaYmax = max(ETA)*1.1;                          %Y-axis maximum
TXmax = max(tempVec)+10;                        %X-axis maximum
TXmin = min(tempVec)-10;  %X-axis minimum
stem(tempVec(1),ETA(1),'LineWidth',1); hold on
stem(tempVec(2),ETA(2),'LineWidth',1); hold on
stem(tempVec(3),ETA(3),'LineWidth',1); hold on
stem(tempVec(4),ETA(4),'LineWidth',1); hold on
axis([TXmin TXmax 0 EtaYmax ])
grid on
title({'Single Diode Efficiency (Gc=STC  Tc=Variable)'; Model});
xlabel('Temperature (Tc)')
ylabel('Efficiency (Eta)')
legend( ...
['Eta = ',num2str(ETA(1),'%.2f'),' %','  @Tc = ',num2str(tempVec(1,1),'%.0f'),'
C'], ...
['Eta = ',num2str(ETA(2),'%.2f'),' %','  @Tc = ',num2str(tempVec(1,2),'%.0f'),'
C'], ...
['Eta = ',num2str(ETA(3),'%.2f'),' %','  @Tc = ',num2str(tempVec(1,3),'%.0f'),'
C'], ...
```

```
['Eta = ',num2str(ETA(4),'%.2f'),' %','  @Tc = ',num2str(tempVec(1,4),'%.0f'),'
C'], ...
'Location','NorthEast');

Results1 = ...
{Changing_Parameter;tempVec(1,1);tempVec(1,2);tempVec(1,3);tempVec(1,4);};
Results2 = {Pmpp(1,1);Pmpp(1,2);Pmpp(1,3);Pmpp(1,4);};
Results3 = {ETA(1);ETA(2);ETA(3);ETA(4);};
Results4 = {FF(1,1);FF(1,2);FF(1,3);FF(1,4);};
Results5 = {Vmpp(1,1);Vmpp(1,2);Vmpp(1,3);Vmpp(1,4);};
Results6 = {Impp(1,1);Impp(1,2);Impp(1,3);Impp(1,4);};
Results7 = {ISC(1,1);ISC(1,2);ISC(1,3);ISC(1,4);};
Results8 = {VOC(1,1);VOC(1,2);VOC(1,3);VOC(1,4);};

xlswrite(Sim_Results,Results1,'Tvar','E3');
xlswrite(Sim_Results,Results2,'Tvar','F4');
xlswrite(Sim_Results,Results3,'Tvar','G4');
xlswrite(Sim_Results,Results4,'Tvar','H4');
xlswrite(Sim_Results,Results5,'Tvar','I4');
xlswrite(Sim_Results,Results6,'Tvar','J4');
xlswrite(Sim_Results,Results7,'Tvar','K4');
xlswrite(Sim_Results,Results8,'Tvar','L4');

%_____________________________End of Code_____________________________
```

Appendix 14 MATLAB script – Gvar Data

```
% Data Set for D2_Gvar model
% 26.04.16

% This code imports all data from the global workspace in relation to
% variations in D2 irradiance and then represents it in graphical form for
% further analysis.

Changing_Parameter = '(Gc=Variable  Tc=STC)';

DataSheet_Values = ...
(Model;Area;Pmpp_stc;Voc_stc;Isc_stc;Impp_stc;Vmpp_stc;' ';Ns;Ki;Kv;Tc;Gc;' '; ...
a;a1;a2;Pe;' ';D1Rs;D1Rp;D2Rs;D2Rp;Eg;);
xlswrite(Sim_Results,DataSheet_Values,'Gvar','C30')

irradVec = simout_D2_Gvar(1,12:16);
%Import the irradiance vectors from the sim model

VOC = zeros(1,5);   %Row/column matrix to store Fill factor and efficiency data
ISC = zeros(1,5);   %Row/column matrix to store Fill factor and efficiency data
Pmpp = zeros(1,5);  %Row/column matrix to store Fill factor and efficiency data
Impp = zeros(1,5);  %Row/column matrix to store Fill factor and efficiency data
Vmpp = zeros(1,5);  %Row/column matrix to store Fill factor and efficiency data
FF = zeros(1,5);    %Row/column matrix to store Fill factor and efficiency data
ETA = zeros(1,5);   %Row/column matrix to store Fill factor and efficiency data

i = 2;                      %Row Counter starts at 2 to allow for
j = 1;                      %Column counter starting at row 2

for Gc = irradVec

    P = simout_D2_Gvar(:,(i+5));
%Vector containing the current out from positive current = zero to current
%= zero crossing
    I = simout_D2_Gvar(:,i);
%Vector containing the current out from positive current = zero to current
%= zero crossing
    V = simout_D2_Gvar(:,1);
%Vector containing the current out from positive current = zero to current
%= zero crossing
%Pin = simout_D2_Gvar_Pin(1);   %Input power

    [Izero,row] = min(abs(I(:)));   %Find when I equals zero
    Voc = V(row);       %Voc at open current
    VOC(1,j) = Voc;     %Store the voc value to use in plot/table/legend

    Isc = I(1);         %I at short circuit
    ISC(1,j) = Isc;     %Store the Isc value to use in plot/table/legend

    [Pmax,roww]=max(P); %Value of the power at the maximum power point
    Pmpp(1,j) = Pmax;   %Store the Pmpp value to use in plot/table/legend

    Imax = I(roww);     %Value of the current at the maximum power point
    Impp(1,j) = Imax;   %Store the Impp value to use in plot/table/legend

    Vmax = V(roww);     %Value of the voltage at the maximum power point
    Vmpp(1,j) = Vmax;   %Store the Vmpp value to use in plot/table/legend

    FFn = (Vmax*Imax)/(Voc*Isc);%Fill factor
    FF(1,j) = FFn;      %Store the FF value to use in plot/table/legend

    Pmpp_stc = 1000*Area;   %Input power at (1000 W)/(Area m2)
    Eta = ((Voc*Isc*FFn)/Pmpp_stc)*100;  %Percent cell efficiency
    ETA(1,j) = Eta;     %Store the Eta value to use in plot/table/legend

    i=i+1;              %Increment counter
```

```
    j=j+1;              %Increment counter
end

P_array = simout_D2_Gvar(:,7:11);   %Power arrays to be plotted
I_array = simout_D2_Gvar(:,2:6);    %Current arrays to be plotted
V_array = simout_D2_Gvar(:,1);      %Voltage arrays to be plotted

PY = max(P_array);      %Find the highest value in each of the Pow arrays
IY = max(I_array);      %Find the highest value in each of the Pow arrays
PYmax = max(PY)*1.1;    %Value of the max Y-axis in VP plot
IYmax = max(IY)*1.1;    %Value of the max Y-axis in VI plot
VXmax = Voc_stc*1.1;    %Value of the max X-axis in VP plot

figure
plot(V_array, P_array,'LineWidth',1);
axis([0 VXmax 0 PYmax]);
grid on;
title({'Double Diode VP Plot (Gc=Variable  Tc=STC)';Model});
xlabel('Output voltage, V');
ylabel('Output power, W');
legend( ...
['Gc = ',num2str(irradVec(1,1),'%.0f'),' W/m;','  Pmpp =
',num2str(Pmpp(1,1),'%.2f'),' W'], ...
['Gc = ',num2str(irradVec(1,2),'%.0f'),' W/m;','  Pmpp =
',num2str(Pmpp(1,2),'%.2f'),' W'], ...
['Gc = ',num2str(irradVec(1,3),'%.0f'),' W/m;','  Pmpp =
',num2str(Pmpp(1,3),'%.2f'),' W'], ...
['Gc = ',num2str(irradVec(1,4),'%.0f'),' W/m;','  Pmpp =
',num2str(Pmpp(1,4),'%.2f'),' W'], ...
['Gc = ',num2str(irradVec(1,5),'%.0f'),' W/m;','  Pmpp =
',num2str(Pmpp(1,5),'%.2f'),' W'], ...
'Location','NorthWest');

figure
plot(V_array, I_array,'LineWidth',1);
axis([0 VXmax 0 IYmax]);
grid on;
title({'Double Diode VI Plot (Gc=Variable  Tc=STC).',Model});
xlabel('Output voltage, V');
ylabel('Output current, A');
legend( ...
['Gc = ',num2str(irradVec(1,1),'%.0f'),' w/m;','  Isc = ',num2str(ISC(1),'%.2f'),'
A;','  Voc = ',num2str(VOC(1),'%.2f'),' V;'], ...
['Gc = ',num2str(irradVec(1,2),'%.0f'),' w/m;','  Isc = ',num2str(ISC(2),'%.2f'),'
A;','  Voc = ',num2str(VOC(2),'%.2f'),' V;'], ...
['Gc = ',num2str(irradVec(1,3),'%.0f'),' w/m;','  Isc = ',num2str(ISC(3),'%.2f'),'
A;','  Voc = ',num2str(VOC(3),'%.2f'),' V;'], ...
['Gc = ',num2str(irradVec(1,4),'%.0f'),' w/m;','  Isc = ',num2str(ISC(4),'%.2f'),'
A;','  Voc = ',num2str(VOC(4),'%.2f'),' V;'], ...
['Gc = ',num2str(irradVec(1,5),'%.0f'),' w/m;','  Isc = ',num2str(ISC(5),'%.2f'),'
A;','  Voc = ',num2str(VOC(5),'%.2f'),' V;'], ...
'Location','SouthWest');

figure
EtaYmax = max(ETA)*1.1;                          %Y-axis maximum
GcXmax = max(irradVec)+100;                      %X-axis maximum
GcXmin = min(irradVec)-100;                      %X-axis minimum
stem(irradVec(1),ETA(1),'LineWidth',1); hold on
stem(irradVec(2),ETA(2),'LineWidth',1); hold on
stem(irradVec(3),ETA(3),'LineWidth',1); hold on
stem(irradVec(4),ETA(4),'LineWidth',1); hold on
stem(irradVec(5),ETA(5),'LineWidth',1); hold on
axis([GcXmin GcXmax 0 EtaYmax ])
grid on
title({'Double Diode Efficiency (Gc=Variable  Tc=STC)';Model});
xlabel('Irradiance (Gc)')
ylabel('Efficiency (Eta)')
legend( ...
```

```
['Eta = ',num2str(ETA(1),'%.2f'),' %','  @Gc = ',num2str(irradVec(1,1),'%.0f'),'
w/m'], ...
['Eta = ',num2str(ETA(2),'%.2f'),' %','  @Gc = ',num2str(irradVec(1,2),'%.0f'),'
w/m'], ...
['Eta = ',num2str(ETA(3),'%.2f'),' %','  @Gc = ',num2str(irradVec(1,3),'%.0f'),'
w/m'], ...
['Eta = ',num2str(ETA(4),'%.2f'),' %','  @Gc = ',num2str(irradVec(1,4),'%.0f'),'
w/m'], ...
['Eta = ',num2str(ETA(5),'%.2f'),' %','  @Gc = ',num2str(irradVec(1,5),'%.0f'),'
w/m'], ...
'Location','NorthWest');

Results1 = ...
{Changing_Parameter;irradVec(1,1);irradVec(1,2);irradVec(1,3);irradVec(1,4);irradVe
c(1,5);};
Results2 = {Pmpp(1,1);Pmpp(1,2);Pmpp(1,3);Pmpp(1,4);Pmpp(1,5);};
Results3 = {ETA(1);ETA(2);ETA(3);ETA(4);ETA(5);};
Results4 = {FF(1,1);FF(1,2);FF(1,3);FF(1,4);FF(1,5);};
Results5 = {Vmpp(1,1);Vmpp(1,2);Vmpp(1,3);Vmpp(1,4);Vmpp(1,5);};
Results6 = {Impp(1,1);Impp(1,2);Impp(1,3);Impp(1,4);Impp(1,5);};
Results7 = {ISC(1,1);ISC(1,2);ISC(1,3);ISC(1,4);ISC(1,5);};
Results8 = {VOC(1,1);VOC(1,2);VOC(1,3);VOC(1,4);VOC(1,5);};

xlswrite(Sim_Results,Results1,'Gvar','E30');
xlswrite(Sim_Results,Results2,'Gvar','F31');
xlswrite(Sim_Results,Results3,'Gvar','G31');
xlswrite(Sim_Results,Results4,'Gvar','H31');
xlswrite(Sim_Results,Results5,'Gvar','I31');
xlswrite(Sim_Results,Results6,'Gvar','J31');
xlswrite(Sim_Results,Results7,'Gvar','K31');
xlswrite(Sim_Results,Results8,'Gvar','L31');

%_____________________________End of code_____________________________________
```

Appendix 15 D1_Kv form and D2_Kv form data

Single Diode Kv Form (D1-Kv) and Double Diode Kv Form (D2-Kv) model parameters.							
Initial Parameters (STC):	***Eg parameter not included.***						
Type of Cell:	Mono-crystalline Siemens SP70 PV Module (Kv).						
P_{mpp_stc} (W) =	70	N_s =	36	Area (m^2) =	0.5625	D1Rs =	0.406
I_{mpp_stc} (A) =	4.24	K_I (A/K) =	0.002	a =	1.3	D1Rp =	119
V_{mpp_stc} (V) =	16.5	K_V (V/K) =	-0.076	a1 =	1	D2Rs =	0.527
V_{oc_stc} (V) =	21.4	T_c (°C) =	25	a2 =	1.3	D2Rp =	89
I_{sc_stc} (A) =	4.7	G_c (W/m^2) =	1000	P_e =	2.3	**Eg =**	**N/A**

Measured Data:	***Taken from (Ishaque, Salam & Taheri 2011)***
	For Mono-crystalline SP-70 PV cell module

Single Diode Extracted parameters			
	Published	***D1_Kv***	***Error (%)***
I_{ph} (A) =	4.72	4.7	0.42%
a =	1.3	1.3	0.00%
R_p (ohm) =	122.1	149	22.03%
R_s (ohm) =	0.4	0.409	2.25%

Double Diode Extracted parameters			
	Published	***D2_Kv***	***Error (%)***
Iph (A) =	4.7	4.73	0.64%
a1 =	1	1	0.00%
a2 =	2	2	0.00%
Rs (ohm) =	91	85	6.59%
Rp (ohm) =	0.51	0.527	3.33%

Validation Data:

Taken from (Ishaque, Salam & Taheri 2011)

For Mono-crystalline SP-70 PV cell module

Single Diode Extracted parameters	
I_{ph} (A) =	4.72
a =	1.3
R_p (ohm) =	122.1
R_s (ohm) =	0.4
Double Diode Extracted parameters	
Iph (A) =	4.7
a1 =	1
a2 =	2
Rs (ohm) =	91
Rp (ohm) =	0.51

Relative errors on the maximum power point for D1 and D2 models against varying temperatures for a SP-70 mono-crystalline module.

Temp (°C)	Measured data	D1_Kv-Form	D2_Kv-Form	Expected Error (%)	Error D1 (%)	Error D2 (%)
50	P_{mpp} = 62.13	P_{mpp} = 61.37	P_{mpp} = 61.68	0.612	1.22	0.73
	V_{mpp} = 14.60	V_{mpp} = 14.61	V_{mpp} = 14.59	0.000	0.07	0.07
25	P_{mpp} = 70.00	P_{mpp} = 69.56	P_{mpp} = 69.73	0.014	0.63	0.38
	V_{mpp} = 16.50	V_{mpp} = 16.50	V_{mpp} = 16.50	0.000	0.00	0.00
0	P_{mpp} = 77.80	P_{mpp} = 77.71	P_{mpp} = 77.66	0.393	0.11	0.18
	V_{mpp} = 18.40	V_{mpp} = 18.45	V_{mpp} = 18.46	0.543	0.27	0.33
-25	P_{mpp} = 85.75	P_{mpp} = 85.79	P_{mpp} = 85.43	0.665	0.05	0.37
	V_{mpp} = 20.30	V_{mpp} = 20.44	V_{mpp} = 20.45	0.985	0.69	0.74
				0.40	0.38	0.35

D1_Kv-Form (Efficiency at varying temperatures.) (Irradiance: Gc = Gstc = 1000w/m²)							
Tc (°C)	P_{mpp}(W)	V_{mpp} (V)	I_{mpp} (A)	I_{sc} (A)	V_{oc} (V)	FF	Efficiency (%)
50	61.37	14.61	4.20	4.73	19.45	0.67	10.91
25	69.56	16.50	4.22	4.68	21.35	0.70	12.37
0	77.71	18.45	4.21	4.63	23.25	0.72	13.82
-25	85.79	20.44	4.20	4.58	25.15	0.74	15.25
							6.54

D2_Kv-Form (Efficiency at varying temperatures.) (Irradiance: Gc = Gstc = 1000w/m²)							
Tc (°C)	P_{mpp}(W)	V_{mpp} (V)	I_{mpp} (A)	I_{sc} (A)	V_{oc} (V)	FF	Efficiency (%)
50	61.68	14.59	4.23	4.72	19.44	0.67	10.96
25	69.73	16.50	4.23	4.67	21.35	0.70	12.40
0	77.66	18.46	4.21	4.62	23.25	0.72	13.81
-25	85.43	20.45	4.18	4.57	25.15	0.74	15.19
							6.54

D1_Kv-Form (Efficiency at varying irradiances) (Temperature: Tc = Tstc = 25(°C))							
Gc (W/m^2)	P_{mpp}(W)	V_{mpp} (V)	I_{mpp} (A)	I_{sc} (A)	V_{oc} (V)	FF	Efficiency (%)
1000	69.56	16.50	4.22	4.68	21.35	0.70	12.37
800	55.47	16.54	3.35	3.75	21.07	0.70	9.86
600	41.05	16.49	2.49	2.81	20.71	0.71	7.30
400	26.42	16.28	1.62	1.87	20.19	0.70	4.70
200	11.82	15.62	0.76	0.94	19.24	0.66	2.10
							4.54

D2_Kv-Form (Efficiency at varying irradiances) (Temperature: Tc = Tstc = 25(°C))							
Gc (W/m^2)	P_{mpp}(W)	V_{mpp} (V)	I_{mpp} (A)	I_{sc} (A)	V_{oc} (V)	FF	Efficiency (%)
1000	69.73	16.50	4.23	4.67	21.35	0.70	12.40
800	56.00	16.69	3.36	3.74	21.13	0.71	9.96
600	41.69	16.82	2.48	2.80	20.84	0.71	7.41
400	26.88	16.81	1.60	1.87	20.43	0.70	4.78
200	11.80	16.37	0.72	0.93	19.66	0.64	2.10
							4.58

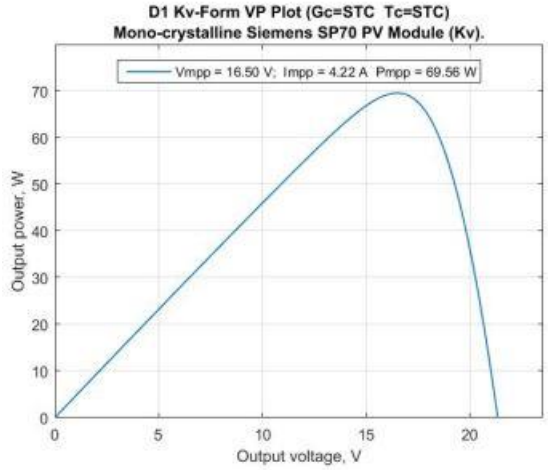
D1 Kv-Form VP Plot (Gc=STC Tc=STC)
Mono-crystalline Siemens SP70 PV Module (Kv).
Vmpp = 16.50 V; Impp = 4.22 A Pmpp = 69.56 W
Output power, W
Output voltage, V

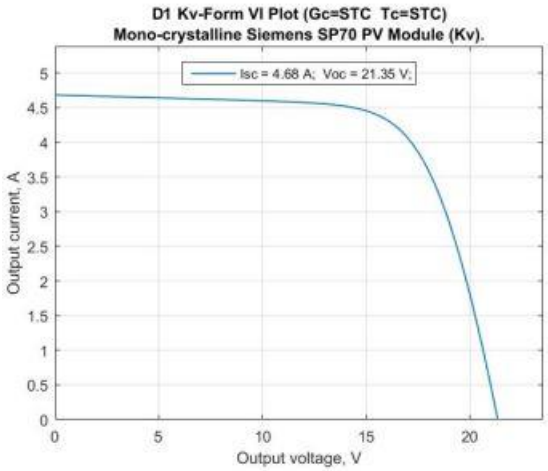
D1 Kv-Form VI Plot (Gc=STC Tc=STC)
Mono-crystalline Siemens SP70 PV Module (Kv).
Isc = 4.68 A; Voc = 21.35 V;
Output current, A
Output voltage, V

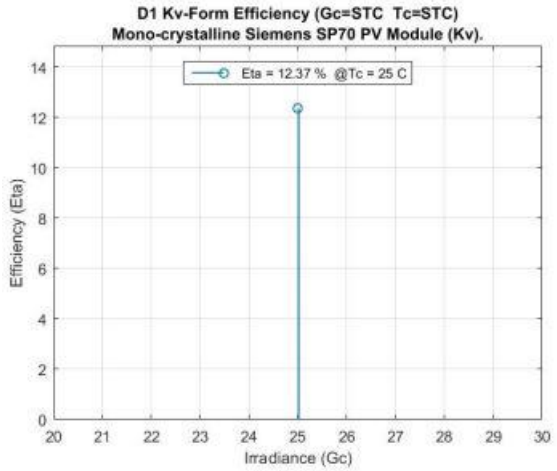
D1 Kv-Form Efficiency (Gc=STC Tc=STC)
Mono-crystalline Siemens SP70 PV Module (Kv).
Eta = 12.37 % @Tc = 25 C
Efficiency (Eta)
Irradiance (Gc)

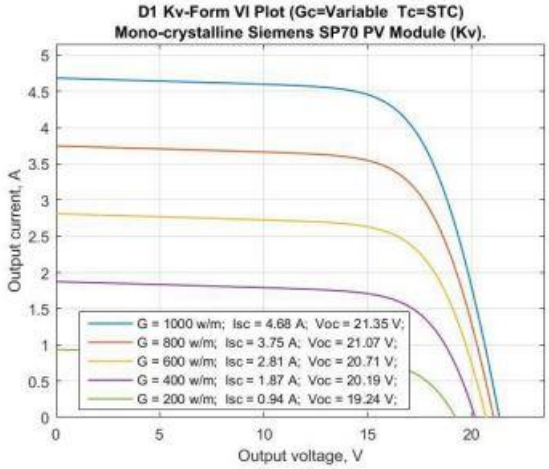
D1 Kv-Form VI Plot (Gc=Variable Tc=STC)
Mono-crystalline Siemens SP70 PV Module (Kv).
Output current, A
Output voltage, V
G = 1000 w/m; Isc = 4.68 A; Voc = 21.35 V;
G = 800 w/m; Isc = 3.75 A; Voc = 21.07 V;
G = 600 w/m; Isc = 2.81 A; Voc = 20.71 V;
G = 400 w/m; Isc = 1.87 A; Voc = 20.19 V;
G = 200 w/m; Isc = 0.94 A; Voc = 19.24 V;

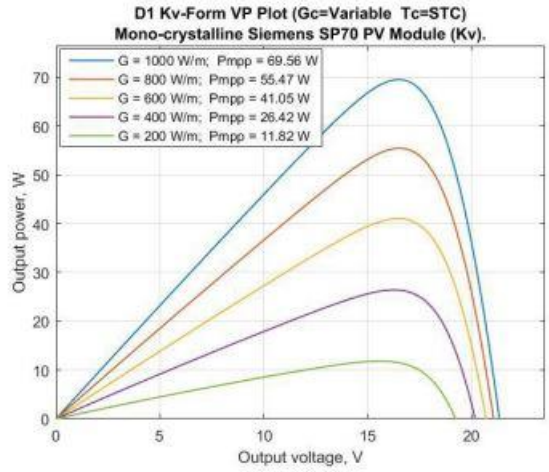
D1 Kv-Form VP Plot (Gc=Variable Tc=STC)
Mono-crystalline Siemens SP70 PV Module (Kv).
Output power, W
Output voltage, V
G = 1000 W/m; Pmpp = 69.56 W
G = 800 W/m; Pmpp = 55.47 W
G = 600 W/m; Pmpp = 41.05 W
G = 400 W/m; Pmpp = 26.42 W
G = 200 W/m; Pmpp = 11.82 W

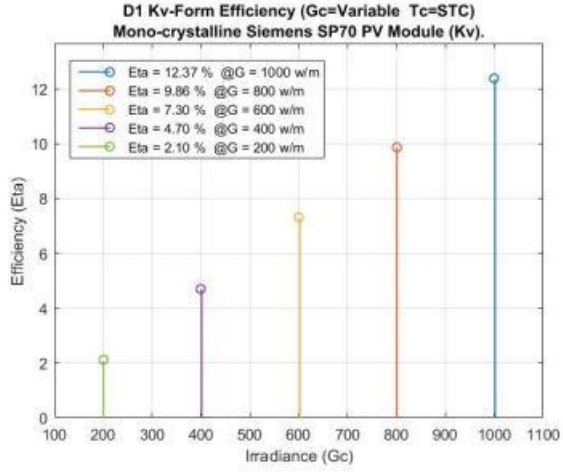
D1 Kv-Form Efficiency (Gc=Variable Tc=STC)
Mono-crystalline Siemens SP70 PV Module (Kv).
Efficiency (Eta)
Irradiance (Gc)
Eta = 12.37 % @G = 1000 w/m
Eta = 9.86 % @G = 800 w/m
Eta = 7.30 % @G = 600 w/m
Eta = 4.70 % @G = 400 w/m
Eta = 2.10 % @G = 200 w/m

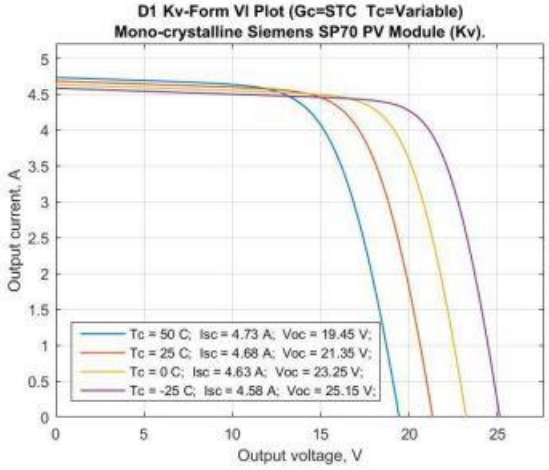
D1 Kv-Form VI Plot (Gc=STC Tc=Variable)
Mono-crystalline Siemens SP70 PV Module (Kv).
Output current, A
Output voltage, V
Tc = 50 C; Isc = 4.73 A; Voc = 19.45 V;
Tc = 25 C; Isc = 4.68 A; Voc = 21.35 V;
Tc = 0 C; Isc = 4.63 A; Voc = 23.25 V;
Tc = -25 C; Isc = 4.58 A; Voc = 25.15 V;

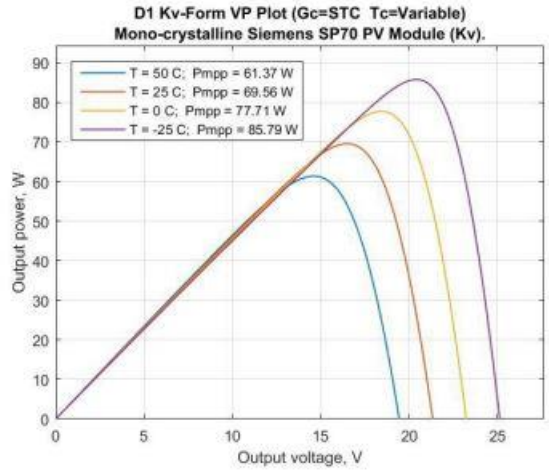
D1 Kv-Form VP Plot (Gc=STC Tc=Variable)
Mono-crystalline Siemens SP70 PV Module (Kv).
Output power, W
Output voltage, V
T = 50 C; Pmpp = 61.37 W
T = 25 C; Pmpp = 69.56 W
T = 0 C; Pmpp = 77.71 W
T = -25 C; Pmpp = 85.79 W

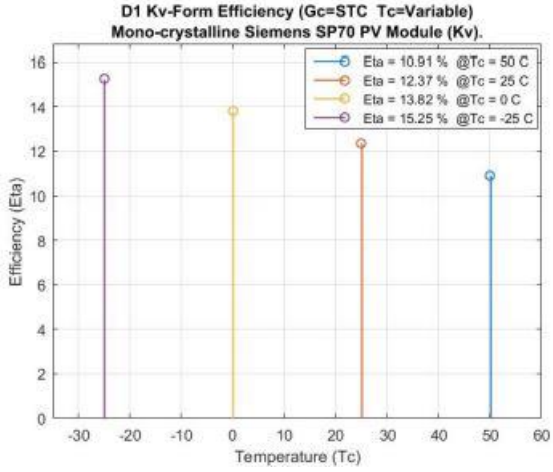
D1 Kv-Form Efficiency (Gc=STC Tc=Variable)
Mono-crystalline Siemens SP70 PV Module (Kv).
Efficiency (Eta)
Temperature (Tc)
Eta = 10.91 % @Tc = 50 C
Eta = 12.37 % @Tc = 25 C
Eta = 13.82 % @Tc = 0 C
Eta = 15.25 % @Tc = -25 C

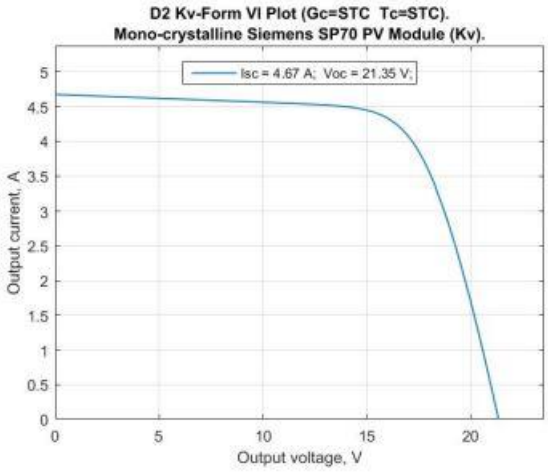
D2 Kv-Form VI Plot (Gc=STC Tc=STC).
Mono-crystalline Siemens SP70 PV Module (Kv).
Isc = 4.67 A; Voc = 21.35 V;
Output current, A
Output voltage, V

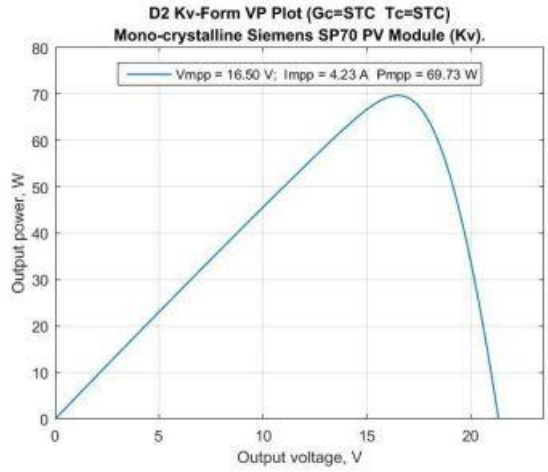
D2 Kv-Form VP Plot (Gc=STC Tc=STC)
Mono-crystalline Siemens SP70 PV Module (Kv).
Vmpp = 16.50 V; Impp = 4.23 A Pmpp = 69.73 W
Output power, W
Output voltage, V

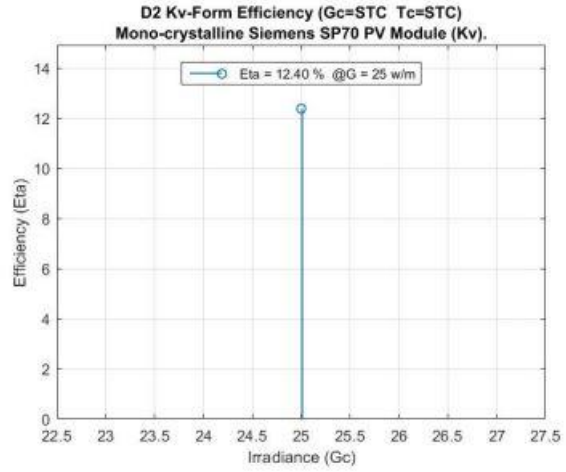
D2 Kv-Form Efficiency (Gc=STC Tc=STC)
Mono-crystalline Siemens SP70 PV Module (Kv).
Eta = 12.40 % @G = 25 w/m
Efficiency (Eta)
Irradiance (Gc)

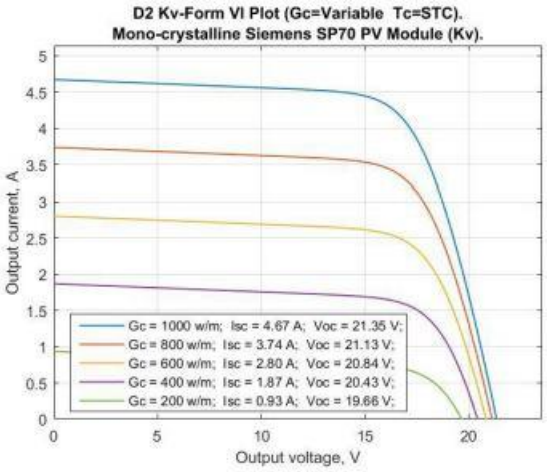
D2 Kv-Form VI Plot (Gc=Variable Tc=STC).
Mono-crystalline Siemens SP70 PV Module (Kv).
Output current, A
Output voltage, V
Gc = 1000 w/m; Isc = 4.67 A; Voc = 21.35 V;
Gc = 800 w/m; Isc = 3.74 A; Voc = 21.13 V;
Gc = 600 w/m; Isc = 2.80 A; Voc = 20.84 V;
Gc = 400 w/m; Isc = 1.87 A; Voc = 20.43 V;
Gc = 200 w/m; Isc = 0.93 A; Voc = 19.66 V;

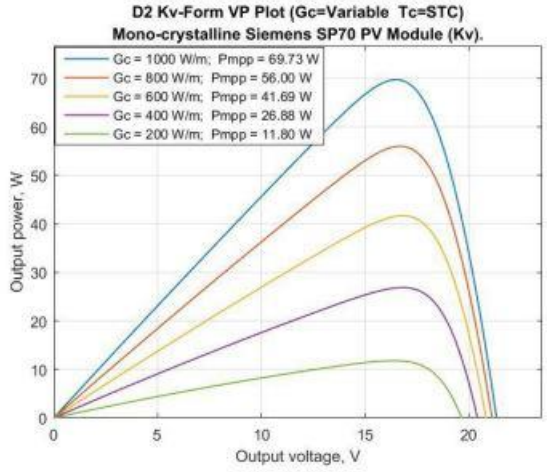
D2 Kv-Form VP Plot (Gc=Variable Tc=STC)
Mono-crystalline Siemens SP70 PV Module (Kv).
Output power, W
Output voltage, V
Gc = 1000 W/m; Pmpp = 69.73 W
Gc = 800 W/m; Pmpp = 56.00 W
Gc = 600 W/m; Pmpp = 41.69 W
Gc = 400 W/m; Pmpp = 26.88 W
Gc = 200 W/m; Pmpp = 11.80 W

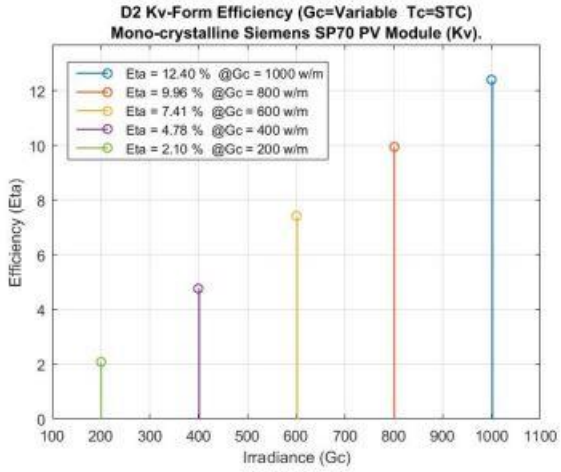
D2 Kv-Form Efficiency (Gc=Variable Tc=STC)
Mono-crystalline Siemens SP70 PV Module (Kv).
Efficiency (Eta)
Irradiance (Gc)
Eta = 12.40 % @Gc = 1000 w/m
Eta = 9.96 % @Gc = 800 w/m
Eta = 7.41 % @Gc = 600 w/m
Eta = 4.78 % @Gc = 400 w/m
Eta = 2.10 % @Gc = 200 w/m

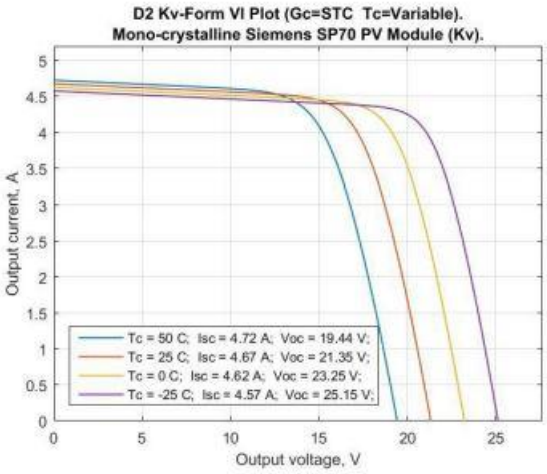
D2 Kv-Form VI Plot (Gc=STC Tc=Variable).
Mono-crystalline Siemens SP70 PV Module (Kv).
Output current, A
Output voltage, V
Tc = 50 C; Isc = 4.72 A; Voc = 19.44 V;
Tc = 25 C; Isc = 4.67 A; Voc = 21.35 V;
Tc = 0 C; Isc = 4.62 A; Voc = 23.25 V;
Tc = -25 C; Isc = 4.57 A; Voc = 25.15 V;

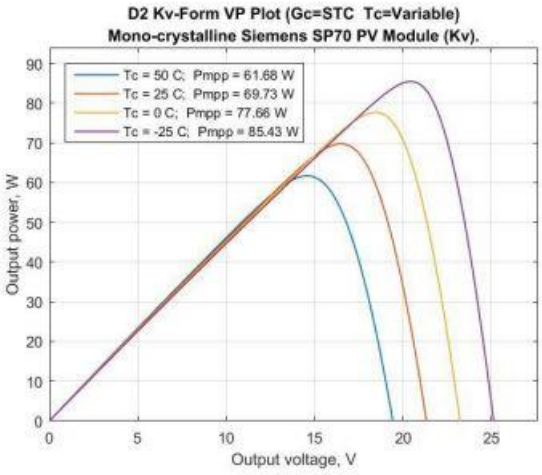
D2 Kv-Form VP Plot (Gc=STC Tc=Variable)
Mono-crystalline Siemens SP70 PV Module (Kv).
Output power, W
Output voltage, V
Tc = 50 C; Pmpp = 61.68 W
Tc = 25 C; Pmpp = 69.73 W
Tc = 0 C; Pmpp = 77.66 W
Tc = -25 C; Pmpp = 85.43 W

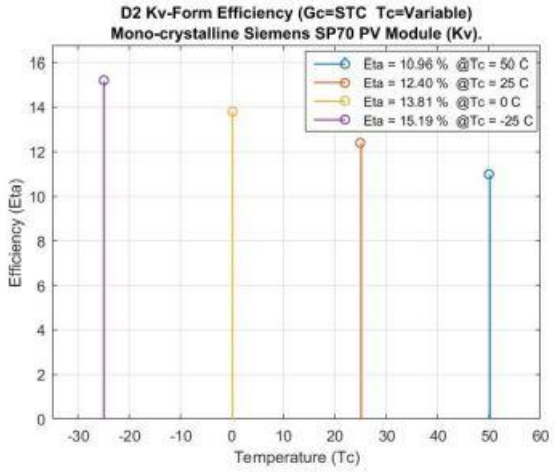
D2 Kv-Form Efficiency (Gc=STC Tc=Variable)
Mono-crystalline Siemens SP70 PV Module (Kv).
Efficiency (Eta)
Temperature (Tc)
Eta = 10.96 % @Tc = 50 C
Eta = 12.40 % @Tc = 25 C
Eta = 13.81 % @Tc = 0 C
Eta = 15.19 % @Tc = -25 C

Appendix 16 D1_Eg and D2_Eg data

Single Diode Bandgap Form (D1-Eg) and Double Diode Bandgap Form (D2-Eg) model parameters.

Initial Parameters (STC): *Includes bandgap energy.*

Type of Cell: Mono-crystalline Siemens SP70 PV Module (Kv).

P_{mpp_stc} (W) =	70	N_s =	36	Area (m^2) =	0.5625	D1Rs =	0.371
I_{mpp_stc} (A) =	4.24	K_I (A/K) =	0.002	a =	1.4	D1Rp =	158
V_{mpp_stc} (V) =	16.5	K_v (V/K) =	-0.076	a1 =	1	D2Rs =	0.527
V_{oc_stc} (V) =	21.4	T_c (°C) =	25	a2 =	1.4	D2Rp =	79
I_{sc_stc} (A) =	4.7	G_c (W/m^2) =	1000	P_e =	2.4	Eg =	1.12
I_{rs} (A) =	3.1E-07	$I_{rs1} = I_{rs2}$ (A) =	4.1E-10				

Measured Data: ***Taken from (Ishaque, Salam & Taheri 2011)***

For Mono-crystalline SP-70 PV cell module

Single Diode Extracted parameters

	Published	***D1_Eg***	***Error (%)***
I_{ph} (A) =	4.72	4.7	0.42%
a =	1.3	1.3	0.00%
R_p (ohm) =	122.1	131	7.29%
R_s (ohm) =	0.4	0.447	11.75%

Double Diode Extracted parameters

	Published	***D2_Eg***	***Error (%)***
Iph (A) =	4.7	4.73	0.64%
a1 =	1	1	0.00%
a2 =	1.2	1.2	0.00%
Rs (ohm) =	91	87	4.40%
Rp (ohm) =	0.51	0.52	1.96%

Relative errors on the maximum power point for D1_Eg and D2-Eg models against varying temperatures for a SP-70 mono-crystalline module.

Temp (°C)	Measured data	D1_Eg Model	D2_Eg Model	Expected Error (%)	Error D1 (%)	Error D2 (%)
50	P_{mpp} = 62.13	P_{mpp} = 61.54	P_{mpp} = 62.27	0.612	0.95	0.23
	V_{mpp} = 14.60	V_{mpp} = 14.59	V_{mpp} = 14.66	0.000	0.07	0.41
25	P_{mpp} = 70.00	P_{mpp} = 69.96	P_{mpp} = 69.98	0.014	0.06	0.03
	V_{mpp} = 16.50	V_{mpp} = 16.50	V_{mpp} = 16.50	0.000	0.00	0.00
0	P_{mpp} = 77.80	P_{mpp} = 78.27	P_{mpp} = 77.50	0.393	0.60	0.39
	V_{mpp} = 18.40	V_{mpp} = 18.43	V_{mpp} = 18.37	0.543	0.16	0.16
-25	P_{mpp} = 85.70	P_{mpp} = 86.42	P_{mpp} = 84.80	0.665	0.84	1.06
	V_{mpp} = 20.30	V_{mpp} = 20.39	V_{mpp} = 20.26	0.985	0.44	0.20
				0.40	0.39	0.31

D1_Eg (Efficiency at varying temperatures.) (Irradiance: Gc = Gstc = 1000w/m^2)

Tc (°C)	P_{mpp}(W)	V_{mpp} (V)	I_{mpp} (A)	I_{sc} (A)	V_{oc} (V)	FF	Efficiency (%)
50	61.54	14.59	4.22	4.75	19.46	0.67	10.94
25	69.96	16.50	4.24	4.70	21.37	0.70	12.44
0	78.27	18.43	4.25	4.65	23.25	0.72	13.91
-25	86.42	20.39	4.24	4.60	25.11	0.75	15.36
							6.58

D2_Eg (Efficiency at varying temperatures.) (Irradiance: Gc = Gstc = 1000w/m²)

Tc (°C)	P_{mpp}(W)	V_{mpp} (V)	I_{mpp} (A)	I_{sc} (A)	V_{oc} (V)	FF	Efficiency (%)
50	62.27	14.66	4.25	4.76	19.54	0.67	11.07
25	69.98	16.50	4.24	4.71	21.36	0.70	12.44
0	77.50	18.37	4.22	4.66	23.16	0.72	13.78
-25	84.80	20.26	4.19	4.61	24.94	0.74	15.07
							6.55

D1_Eg (Efficiency at varying irradiances) (Temperature: Tc = Tstc = 25(°C))

Gc (W/m²)	P_{mpp}(W)	V_{mpp} (V)	I_{mpp} (A)	I_{sc} (A)	V_{oc} (V)	FF	Efficiency (%)
1000	69.96	16.50	4.24	4.70	21.37	0.70	12.44
800	55.74	16.49	3.38	3.76	21.07	0.70	9.91
600	41.26	16.40	2.52	2.82	20.68	0.71	7.33
400	26.63	16.14	1.65	1.88	20.13	0.70	4.73
200	12.11	15.44	0.78	0.94	19.14	0.67	2.15
							4.57

D2_Eg (Efficiency at varying irradiances) (Temperature: Tc = Tstc = 25(°C))							
Gc (W/m^2)	P_{mpp}(W)	V_{mpp} (V)	I_{mpp} (A)	I_{sc} (A)	V_{oc} (V)	FF	Efficiency (%)
1000	69.98	16.50	4.24	4.71	21.36	0.70	12.44
800	56.13	16.70	3.36	3.77	21.14	0.70	9.98
600	41.70	16.82	2.48	2.83	20.85	0.71	7.41
400	26.76	16.80	1.59	1.88	20.43	0.70	4.76
200	11.55	16.33	0.71	0.94	19.64	0.62	2.05
							4.58

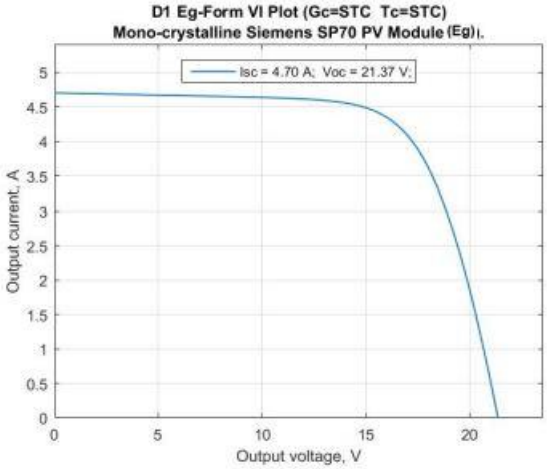
D1 Eg-Form VI Plot (Gc=STC Tc=STC)
Mono-crystalline Siemens SP70 PV Module (Eg)1.
Isc = 4.70 A; Voc = 21.37 V;
Output current, A
Output voltage, V

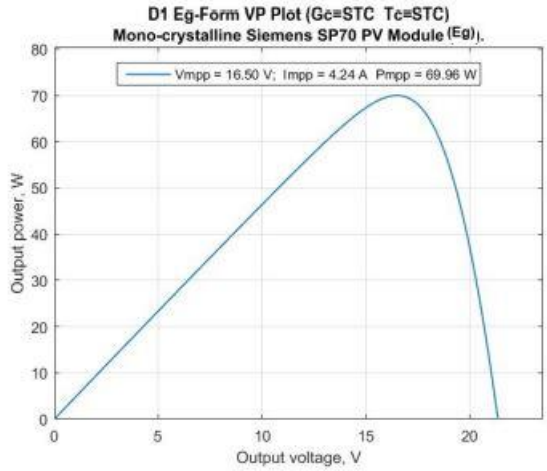
D1 Eg-Form VP Plot (Gc=STC Tc=STC)
Mono-crystalline Siemens SP70 PV Module (Eg)1.
Vmpp = 16.50 V; Impp = 4.24 A Pmpp = 69.96 W
Output power, W
Output voltage, V

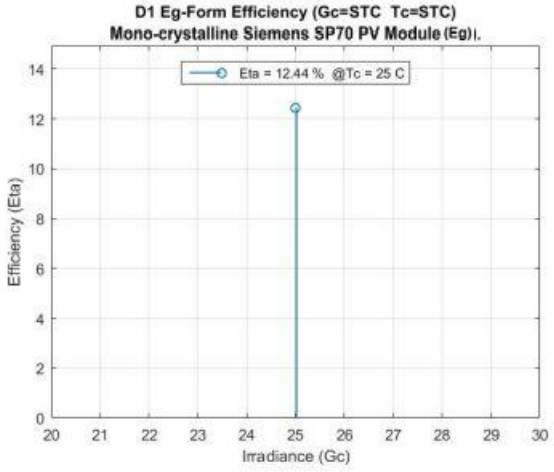
D1 Eg-Form Efficiency (Gc=STC Tc=STC)
Mono-crystalline Siemens SP70 PV Module (Eg)1.
Eta = 12.44 % @Tc = 25 C
Efficiency (Eta)
Irradiance (Gc)

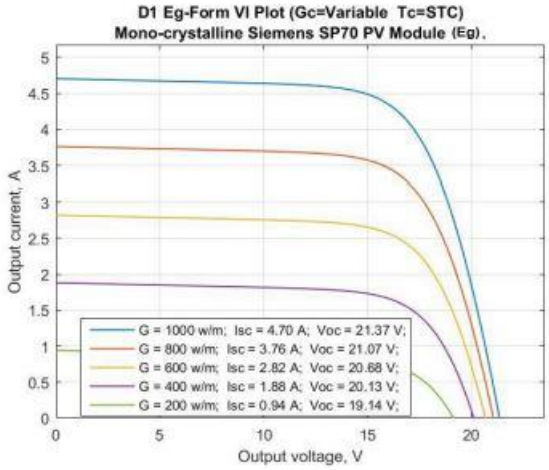
D1 Eg-Form VI Plot (Gc=Variable Tc=STC)
Mono-crystalline Siemens SP70 PV Module (Eg).
Output current, A
Output voltage, V
G = 1000 w/m; Isc = 4.70 A; Voc = 21.37 V;
G = 800 w/m; Isc = 3.76 A; Voc = 21.07 V;
G = 600 w/m; Isc = 2.82 A; Voc = 20.68 V;
G = 400 w/m; Isc = 1.88 A; Voc = 20.13 V;
G = 200 w/m; Isc = 0.94 A; Voc = 19.14 V;

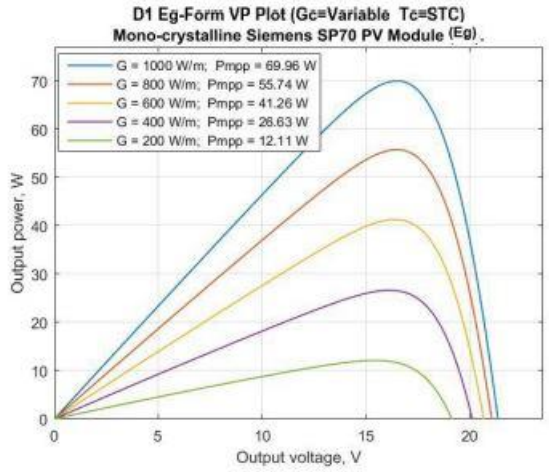
D1 Eg-Form VP Plot (Gc=Variable Tc=STC)
Mono-crystalline Siemens SP70 PV Module (Eg).
Output power, W
Output voltage, V
G = 1000 W/m; Pmpp = 69.96 W
G = 800 W/m; Pmpp = 55.74 W
G = 600 W/m; Pmpp = 41.26 W
G = 400 W/m; Pmpp = 26.63 W
G = 200 W/m; Pmpp = 12.11 W

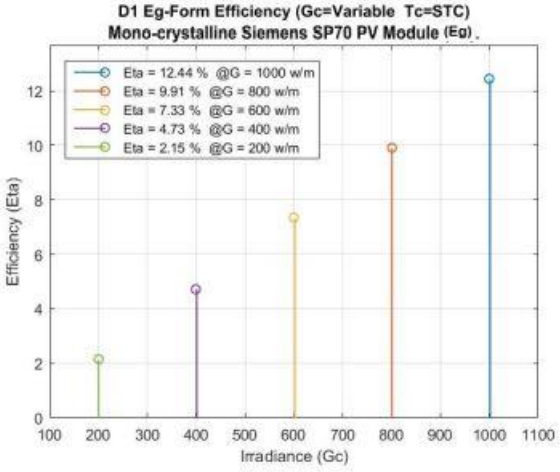
D1 Eg-Form Efficiency (Gc=Variable Tc=STC)
Mono-crystalline Siemens SP70 PV Module (Eg).
Efficiency (Eta)
Irradiance (Gc)
Eta = 12.44 % @G = 1000 w/m
Eta = 9.91 % @G = 800 w/m
Eta = 7.33 % @G = 600 w/m
Eta = 4.73 % @G = 400 w/m
Eta = 2.15 % @G = 200 w/m

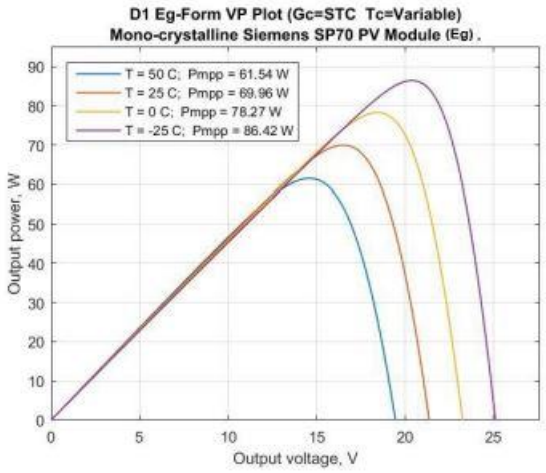
D1 Eg-Form VP Plot (Gc=STC Tc=Variable)
Mono-crystalline Siemens SP70 PV Module (Eg) .
T = 50 C; Pmpp = 61.54 W
T = 25 C; Pmpp = 69.96 W
T = 0 C; Pmpp = 78.27 W
T = -25 C; Pmpp = 86.42 W
Output power, W
Output voltage, V

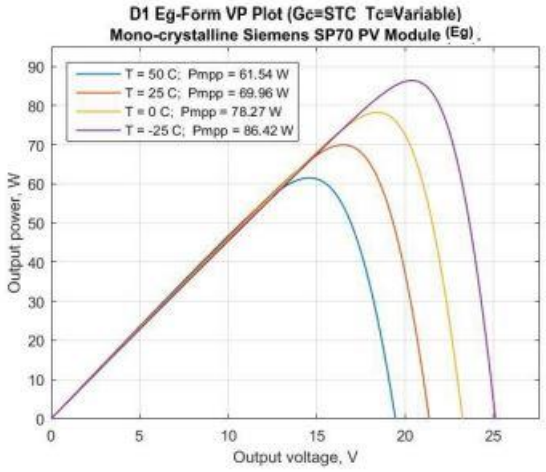
D1 Eg-Form VP Plot (Gc=STC Tc=Variable)
Mono-crystalline Siemens SP70 PV Module (Eg) .
T = 50 C; Pmpp = 61.54 W
T = 25 C; Pmpp = 69.96 W
T = 0 C; Pmpp = 78.27 W
T = -25 C; Pmpp = 86.42 W
Output power, W
Output voltage, V

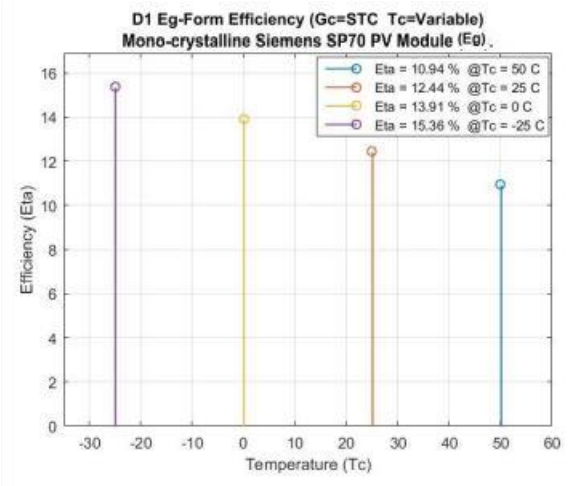
D1 Eg-Form Efficiency (Gc=STC Tc=Variable)
Mono-crystalline Siemens SP70 PV Module (Eg) .
Eta = 10.94 % @Tc = 50 C
Eta = 12.44 % @Tc = 25 C
Eta = 13.91 % @Tc = 0 C
Eta = 15.36 % @Tc = -25 C
Efficiency (Eta)
Temperature (Tc)

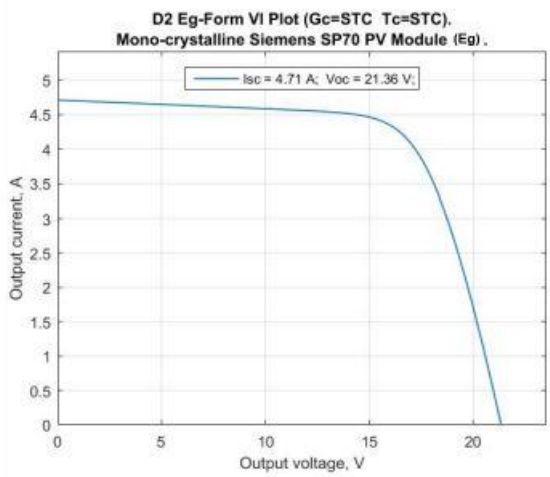
D2 Eg-Form VI Plot (Gc=STC Tc=STC).
Mono-crystalline Siemens SP70 PV Module (Eg).
Isc = 4.71 A; Voc = 21.36 V;
Output current, A
Output voltage, V

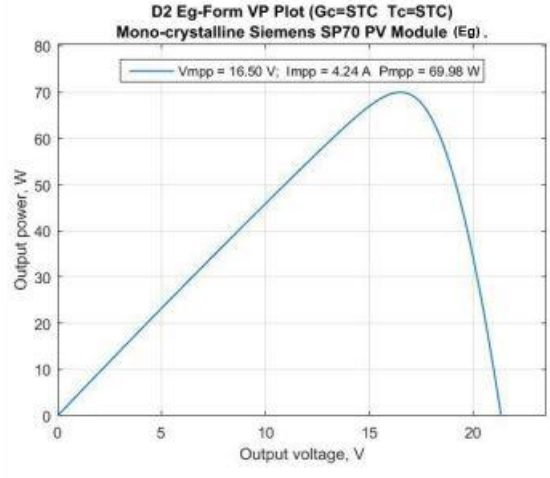
D2 Eg-Form VP Plot (Gc=STC Tc=STC)
Mono-crystalline Siemens SP70 PV Module (Eg).
Vmpp = 16.50 V; Impp = 4.24 A Pmpp = 69.98 W
Output power, W
Output voltage, V

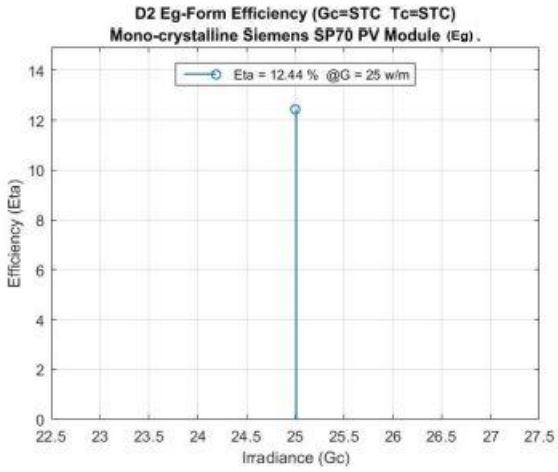
D2 Eg-Form Efficiency (Gc=STC Tc=STC)
Mono-crystalline Siemens SP70 PV Module (Eg).
Eta = 12.44 % @G = 25 w/m
Efficiency (Eta)
Irradiance (Gc)

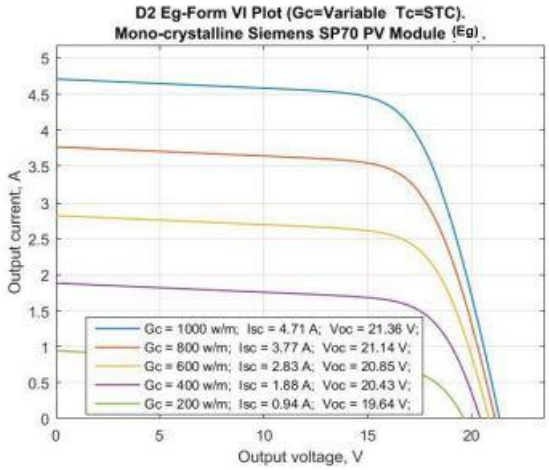
D2 Eg-Form VI Plot (Gc=Variable Tc=STC).
Mono-crystalline Siemens SP70 PV Module (Eg).
Output current, A
Output voltage, V
Gc = 1000 w/m; Isc = 4.71 A; Voc = 21.36 V;
Gc = 800 w/m; Isc = 3.77 A; Voc = 21.14 V;
Gc = 600 w/m; Isc = 2.83 A; Voc = 20.85 V;
Gc = 400 w/m; Isc = 1.88 A; Voc = 20.43 V;
Gc = 200 w/m; Isc = 0.94 A; Voc = 19.64 V;

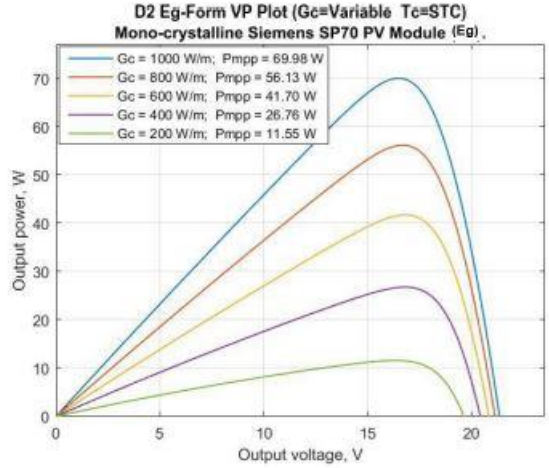
D2 Eg-Form VP Plot (Gc=Variable Tc=STC)
Mono-crystalline Siemens SP70 PV Module (Eg).
Output power, W
Output voltage, V
Gc = 1000 W/m; Pmpp = 69.98 W
Gc = 800 W/m; Pmpp = 56.13 W
Gc = 600 W/m; Pmpp = 41.70 W
Gc = 400 W/m; Pmpp = 26.76 W
Gc = 200 W/m; Pmpp = 11.55 W

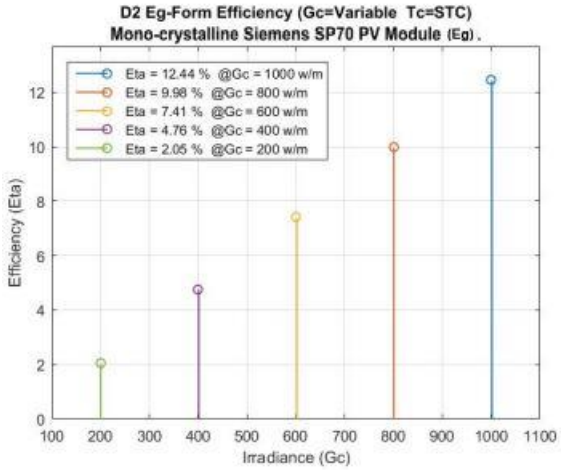
D2 Eg-Form Efficiency (Gc=Variable Tc=STC)
Mono-crystalline Siemens SP70 PV Module (Eg).
Efficiency (Eta)
Irradiance (Gc)
Eta = 12.44 % @Gc = 1000 w/m
Eta = 9.98 % @Gc = 800 w/m
Eta = 7.41 % @Gc = 600 w/m
Eta = 4.76 % @Gc = 400 w/m
Eta = 2.05 % @Gc = 200 w/m

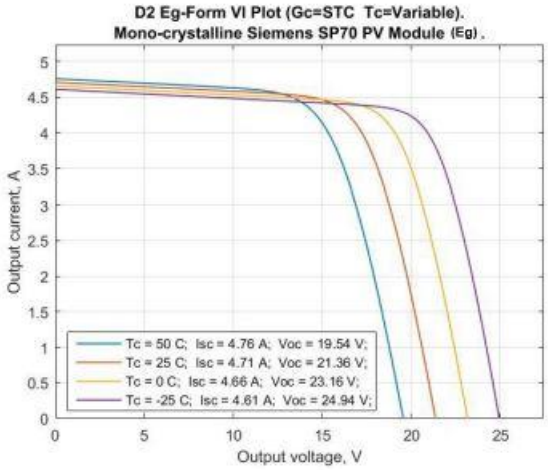
D2 Eg-Form VI Plot (Gc=STC Tc=Variable).
Mono-crystalline Siemens SP70 PV Module (Eg).
Output current, A
Output voltage, V
Tc = 50 C; Isc = 4.76 A; Voc = 19.54 V;
Tc = 25 C; Isc = 4.71 A; Voc = 21.36 V;
Tc = 0 C; Isc = 4.66 A; Voc = 23.16 V;
Tc = -25 C; Isc = 4.61 A; Voc = 24.94 V;

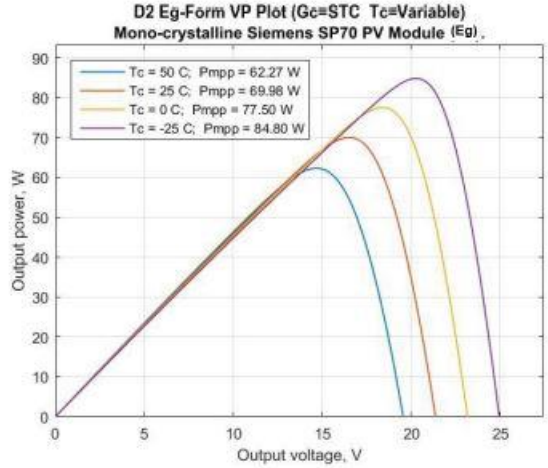
D2 Eg-Form VP Plot (Gc=STC Tc=Variable)
Mono-crystalline Siemens SP70 PV Module (Eg).
Output power, W
Output voltage, V
Tc = 50 C; Pmpp = 62.27 W
Tc = 25 C; Pmpp = 69.98 W
Tc = 0 C; Pmpp = 77.50 W
Tc = -25 C; Pmpp = 84.80 W

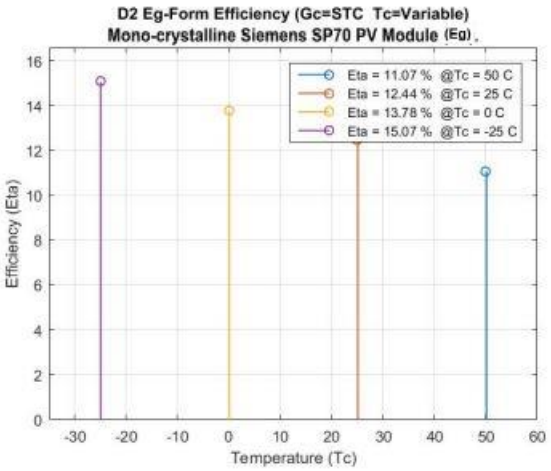
D2 Eg-Form Efficiency (Gc=STC Tc=Variable)
Mono-crystalline Siemens SP70 PV Module (Eg).
Efficiency (Eta)
Temperature (Tc)
Eta = 11.07 % @Tc = 50 C
Eta = 12.44 % @Tc = 25 C
Eta = 13.78 % @Tc = 0 C
Eta = 15.07 % @Tc = -25 C

Appendix 17 Interpolation and plotting code

```
%_____________________________________________________

% Written: October 2016
% Author : Anthony Laurent
% Input parameters for Datasheet Initial conditions for MJSC simulation

% Data taken from paper:

% Hussain, Abdulrahman Babiker, Abdalla, Abdelrahman S, Mukhtar, Abdellahi
% Sidi, Elamin, M, Alammari, R & Iqbal, A 2016, 'Modelling and simulation
% of single-and triple-junction solar cells using MATLAB/SIMULINK',
% International Journal of Ambient Energy, pp. 1-9.

% Note:
% D1 = Single diode model
% D2 = Double diode model

%_____________________________________________________________________
% ____________________ VI Characteristic curves      _________________

%_____________________________________________________________________
% Interpolate over the entire lines to get a better resolution:
%_____________________________________________________________________
Glob_Y = 0;
% Glob_Y = -0.02;
extra_indexes = 2;
% First interpolate the 3 Curves with 10,000 Points for better resolution
% 10,000 divisions...
V_divs = 10000;

[countA countAA]=size(MJSC_Bot_VI);
% x axis start for interpolation
VI_max_B = MJSC_Bot_VI(countA,1);
% The X-axis range of interpolation, from x=0 : (x,y=0)
VI_xq_B = (0: VI_max_B/V_divs :VI_max_B);

% Interpolate y values with respect to x divisions
VI_vq_B = interp1(MJSC_Bot_VI(:,1),MJSC_Bot_VI(:,2),VI_xq_B);
% Invert to fit in Bottom VI Array
VI_MJSC_interp_B = [VI_xq_B',VI_vq_B'];

[countB countBB]=size(MJSC_Mid_VI);
VI_M_divs_max_range = MJSC_Mid_VI(countB,1);
% x axis start for interpolation
VI_xq_M = (0: VI_M_divs_max_range/V_divs :VI_M_divs_max_range);
% The X-axis range of interpolation, from x=0 : (x,y=0)
VI_vq_M = interp1(MJSC_Mid_VI(:,1),MJSC_Mid_VI(:,2),VI_xq_M);
% Interpolate y values with respect to x divisions
VI_MJSC_interp_M = [VI_xq_M',VI_vq_M'];
% Invert to fit in Bottom VI Array

[countC countCC]=size(MJSC_Top_VI);
VI_T_divs_max_range = MJSC_Top_VI(countC,1);
% x axis start for interpolation
VI_xq_T = (0: VI_T_divs_max_range/V_divs :VI_T_divs_max_range);
% The X-axis range of interpolation, from x=0 : (x,y=0)
VI_vq_T = interp1(MJSC_Top_VI(:,1),MJSC_Top_VI(:,2),VI_xq_T);
% Interpolate y values with respect to x divisions
VI_MJSC_interp_T = [VI_xq_T',VI_vq_T'];
% Invert to fit in Bottom VI Array
```

```
%_____________________________________________________________________
% Find where y=0 is a give each line a max value for X axis to work to:
%_____________________________________________________________________

% The Bottom Bandgap curve:
VI_Bindex = min(find(VI_MJSC_interp_B(:,2)<0));
% What's the index number of the y=0 crossing
VI_curve_limit_B = VI_MJSC_interp_B((VI_Bindex+extra_indexes),1);
% ....Whats the corresponding value of the index number

% The Middle Bandgap curve:
VI_Mindex = min(find(VI_MJSC_interp_M(:,2)<0));
% What's the index number of the y=0 crossing
VI_curve_limit_M = VI_MJSC_interp_M((VI_Mindex+extra_indexes),1);          %
....Whats the corresponding value of the index number

% The Top Bandgap Curve
VI_Tindex = min(find(VI_MJSC_interp_T(:,2)<0));
% What's the index number of the y=0 crossing
VI_curve_limit_T = VI_MJSC_interp_T((VI_Tindex+extra_indexes),1);          %
....Whats the corresponding value of the index number


%_____________________________________________________________________
% Interpolate 3 curves again to y=0 with 10,000 divisions to get
% a better resolution
%_____________________________________________________________________

% Then interpolate the 3 Curves with 10,000 divisions to get a better
resolution
V_divs = 10000;
% 10,000 divisions...
VI_xq_BB = (0: VI_curve_limit_B/V_divs :VI_curve_limit_B);
% The X-axis range of interpolation, from x=0 : (x,y=0)
VI_vq_BB = interp1(MJSC_Bot_VI(:,1),MJSC_Bot_VI(:,2),VI_xq_BB);
% Interpolate y values with respect to x divisions
VI_MJSC_interp_BB = [VI_xq_BB',VI_vq_BB'];
% Invert to fit in Bottom VI Array

VI_xq_MM = (0: VI_curve_limit_M/V_divs :VI_curve_limit_M);
% The X-axis range of interpolation, from x=0 : (x,y=0)
VI_vq_MM = interp1(MJSC_Mid_VI(:,1),MJSC_Mid_VI(:,2),VI_xq_MM);
% Interpolate y values with respect to x divisions
VI_MJSC_interp_MM = [VI_xq_MM',VI_vq_MM'];
% Invert to fit in Bottom VI Array

VI_xq_TT = (0: VI_curve_limit_T/V_divs :VI_curve_limit_T);
% The X-axis range of interpolation, from x=0 : (x,y=0)
VI_vq_TT = interp1(MJSC_Top_VI(:,1),MJSC_Top_VI(:,2),VI_xq_TT);
% Interpolate y values with respect to x divisions
VI_MJSC_interp_TT = [VI_xq_TT',VI_vq_TT'];
% Invert to fit in Bottom VI Array

%_____________________________________________________________________
% _____________________Now Draw derive the total curve_______________

VI_Bbindex = min(find(VI_MJSC_interp_BB(:,2)<0));
% What's the index number of the y=0 crossing
```

```
VI_max_Bb = VI_MJSC_interp_BB((VI_Bbindex-1),1);
% ....Whats the corresponding value of the index number

VI_Mmindex = min(find(VI_MJSC_interp_MM(:,2)<0));
% What's the index number of the y=0 crossing
VI_max_Mm = VI_MJSC_interp_MM((VI_Mmindex-1),1);
% ....Whats the corresponding value of the index number

VI_Ttindex = min(find(VI_MJSC_interp_TT(:,2)<0));
% What's the index number of the y=0 crossing
VI_max_Tt = VI_MJSC_interp_TT((VI_Ttindex-1),1);
% ....Whats the corresponding value of the index number

%_____________________________________________________________________
% ____________________NJoin the individual curves_____________
VI_A = (VI_MJSC_interp_BB(:,1) + VI_MJSC_interp_MM(:,1) +
VI_MJSC_interp_TT(:,1));

VI_BMT_int_ratio = VI_max_Bb + VI_max_Mm + VI_max_Tt;
VI_B_int_ratio = VI_max_Bb/VI_BMT_int_ratio;
VI_M_int_ratio = VI_max_Mm/VI_BMT_int_ratio;
VI_T_int_ratio = VI_max_Tt/VI_BMT_int_ratio;

VI_BMT_ratio = VI_max_Bb + VI_max_Mm + VI_max_Tt;
VI_B_ratio = VI_max_Bb/VI_BMT_ratio;
VI_M_ratio = VI_max_Mm/VI_BMT_ratio;
VI_T_ratio = VI_max_Tt/VI_BMT_ratio;


%_____________________________________________________________________
% ____________________Check for error percentage     _____________
%_____________________________________________________________________
% MJSC_B_M_T = 0.5144,   MJSC_Int_Total = 0.5113,    Int_error = 5.7e-5
perc_error = -0.00312% Error
VI_BB = (VI_MJSC_interp_BB(:,2)*VI_B_ratio +
VI_MJSC_interp_MM(:,2)*VI_M_ratio + VI_MJSC_interp_TT(:,2)*VI_T_ratio);
VI_B = VI_BB(:);


VI_MJSC_Total_interp =[VI_A,VI_B];
VI_xq_Total = VI_A';
VI_vq_Total = VI_B';

Isc_max = max(VI_MJSC_Total_interp(:,2));
Voc_max = max(VI_MJSC_Total_interp(:,1));

%_____________________________________________________________________
% ____________________Plot the resultants     _____________
figure
VI_MJSC_Ymax = max(Isc_max)*1.3;
%Y-axis maximum
MJSC_Xmax = max(Voc_max)*1.1;

plot(VI_MJSC_Total_interp(:,1),VI_MJSC_Total_interp(:,2),'DisplayName','Tot
al VP characteristic curve','LineWidth',1.5,'Color',[0.380392163991928
0.380392163991928 0.380392163991928]),hold on;

plot(VI_MJSC_interp_TT(:,1),VI_MJSC_interp_TT(:,2),'DisplayName','Top GaInP
junction','LineWidth',1.5,'Color',[0.200000002980232 0.400000005960464 1]);
```

```
plot(VI_MJSC_interp_MM(:,1),VI_MJSC_interp_MM(:,2),'DisplayName','Middle
GaInAs junction','LineWidth',1.5,'Color',[0 0.800000011920929
0.200000002980232]);

plot(VI_MJSC_interp_BB(:,1),VI_MJSC_interp_BB(:,2),'DisplayName','Bottom Ge
junction','LineWidth',1.5,'Color',[1 0.200000002980232 0.200000002980232]);

axis([0 MJSC_Xmax Glob_Y VI_MJSC_Ymax ])
grid on

title({Model,'(D2) MJSC VI Characteristic curves.'});
xlabel('Voltage (V)')
ylabel('Current (A)')
legend('Total VI characteristic curve','Top GaInP junction','Middle GaInAs
junction','Bottom Ge junction'),'Location';'North';

PV_Xaxis = MJSC_Xmax;
VI_MJSC_Int_B = trapz(VI_MJSC_interp_BB(:,1),VI_MJSC_interp_BB(:,2));
%VI_MJSC_Int_B = trapz(VI_xq_BB,VI_vq_BB);
VI_MJSC_Int_M = trapz(VI_MJSC_interp_MM(:,1),VI_MJSC_interp_MM(:,2));
%VI_MJSC_Int_M = trapz(VI_xq_MM,VI_vq_MM);
VI_MJSC_Int_T = trapz(VI_MJSC_interp_TT(:,1),VI_MJSC_interp_TT(:,2));
%VI_MJSC_Int_T = trapz(VI_xq_TT,VI_vq_TT);

VI_MJSC_B_M_T = VI_MJSC_Int_B + VI_MJSC_Int_M + VI_MJSC_Int_T;
VI_MJSC_Int_Total = trapz(VI_xq_Total,VI_vq_Total);
VI_Int_error = VI_MJSC_B_M_T - VI_MJSC_Int_Total;
VI_Perc_error = VI_Int_error/VI_MJSC_B_M_T;


%_____________________________________________________________________
% _____________________ VP Characteristic curves      _______________

%_____________________________________________________________________
% Interpolate over the entire lines to get a better resolution:
%_____________________________________________________________________

% First interpolate the 3 Curves with 10,000 divisions to get a better
resolution

[countA countAA]=size(MJSC_Bot_VP);
VP_max_B = MJSC_Bot_VP(countA,1);
% x axis start for interpolation
VP_xq_B = (0: VP_max_B/V_divs :VP_max_B);
% The X-axis range of interpolation, from x=0 : (x,y=0)
VP_vq_B = interp1(MJSC_Bot_VP(:,1),MJSC_Bot_VP(:,2),VP_xq_B);
% Interpolate y values with respect to x divisions
VP_MJSC_interp_B = [VP_xq_B',VP_vq_B'];
% Invert to fit in Bottom VI Array

[countB countBB]=size(MJSC_Mid_VP);
VP_M_divs_max_range = MJSC_Mid_VP(countB,1);
% x axis start for interpolation
VP_xq_M = (0: VP_M_divs_max_range/V_divs :VP_M_divs_max_range);
% The X-axis range of interpolation, from x=0 : (x,y=0)
VP_vq_M = interp1(MJSC_Mid_VP(:,1),MJSC_Mid_VP(:,2),VP_xq_M);
% Interpolate y values with respect to x divisions
VP_MJSC_interp_M = [VP_xq_M',VP_vq_M'];
% Invert to fit in Bottom VI Array

[countC countCC]=size(MJSC_Top_VP);
```

```
VP_T_divs_max_range = MJSC_Top_VP(countC,1);
% x axis start for interpolation
VP_xq_T = (0: VP_T_divs_max_range/V_divs :VP_T_divs_max_range);
% The X-axis range of interpolation, from x=0 : (x,y=0)
VP_vq_T = interp1(MJSC_Top_VP(:,1),MJSC_Top_VP(:,2),VP_xq_T);
% Interpolate y values with respect to x divisions
VP_MJSC_interp_T = [VP_xq_T',VP_vq_T'];
% Invert to fit in Bottom VI Array

%_____________________________________________________________________
% Find where y=0 is a give each line a max value for X axis to work to:
%_____________________________________________________________________

% The Bottom Bandgap curve:
VP_Bindex = min(find(VP_MJSC_interp_B(:,2)<0));
% What's the index number of the y=0 crossing
%VP_max_Bb = VP_MJSC_interp_B((VP_Bindex-1),1);
% ....Whats the corresponding value of the index number
VP_curve_limit_B = VP_MJSC_interp_B((VP_Bindex+extra_indexes),1);          %
....Whats the corresponding value of the index number

% The Middle Bandgap curve:
VP_Mindex = min(find(VP_MJSC_interp_M(:,2)<0));
% What's the index number of the y=0 crossing
% VP_max_Mm = VP_MJSC_interp_M((VP_Mindex-1),1);
% ....Whats the corresponding value of the index number
VP_curve_limit_M = VI_MJSC_interp_M((VI_Mindex+extra_indexes),1);          %
....Whats the corresponding value of the index number

% The Top Bandgap Curve
VP_Tindex = min(find(VP_MJSC_interp_T(:,2)<0));
% What's the index number of the y=0 crossing
%VP_max_Tt = VP_MJSC_interp_T((VP_Tindex-1),1);
% ....Whats the corresponding value of the index number
VP_curve_limit_T = VI_MJSC_interp_T((VI_Tindex+extra_indexes),1);          %
....Whats the corresponding value of the index number

%_____________________________________________________________________
% Interpolate 3 curves agian to y=0 with 10,000 divisions to get
% a better resolution
%_____________________________________________________________________


% Then interpolate the 3 Curves with 10,000 divisions to get a better
resolution
V_divs = 10000;
% 10,000 divisions...
VP_xq_BB = (0: VP_curve_limit_B/V_divs :VP_curve_limit_B);
% The X-axis range of interpolation, from x=0 : (x,y=0)
VP_vq_BB = interp1(MJSC_Bot_VP(:,1),MJSC_Bot_VP(:,2),VP_xq_BB);
% Interpolate y values with respect to x divisions
VP_MJSC_interp_BB = [VP_xq_BB',VP_vq_BB'];
% Invert to fit in Bottom VI Array

VP_xq_MM = (0: VP_curve_limit_M/V_divs :VP_curve_limit_M);
% The X-axis range of interpolation, from x=0 : (x,y=0)
VP_vq_MM = interp1(MJSC_Mid_VP(:,1),MJSC_Mid_VP(:,2),VP_xq_MM);
% Interpolate y values with respect to x divisions
VP_MJSC_interp_MM = [VP_xq_MM',VP_vq_MM'];
% Invert to fit in Bottom VI Array
```

```
VP_xq_TT = (0: VP_curve_limit_T/V_divs :VP_curve_limit_T);
% The X-axis range of interpolation, from x=0 : (x,y=0)
VP_vq_TT = interp1(MJSC_Top_VP(:,1),MJSC_Top_VP(:,2),VP_xq_TT);
% Interpolate y values with respect to x divisions
VP_MJSC_interp_TT = [VP_xq_TT',VP_vq_TT'];
% Invert to fit in Bottom VI Array

%_____________________________________________________________________
% ________________________Now Draw derive the total curve_____________

VP_A = (VP_MJSC_interp_BB(:,1) + VP_MJSC_interp_MM(:,1) +
VP_MJSC_interp_TT(:,1));


% %_____________________________________________________________________
% % MJSC_B_M_T = 0.5144,   MJSC_Int_Total = 0.4919,    Int_error = 0.0195
perc_error = 3.81% Error
VP_BB = (VP_MJSC_interp_BB(:,2) + VP_MJSC_interp_MM(:,2) +
VP_MJSC_interp_TT(:,2));
VP_B = VP_BB(:);


VP_MJSC_Total_interp =[VP_A,VP_B];
VP_xq_Total = VP_A';
VP_vq_Total = VP_B';

[PMAX,Index] = max(VP_MJSC_Total_interp(:,2));

VMPP_max = VP_MJSC_Total_interp(Index,1);
IMPP_max = VI_MJSC_Total_interp(Index,2);
Impp_max = IMPP_max
Vmpp_max = VMPP_max
Pmax = Impp_max*Vmpp_max;
FF = (Impp_max*Vmpp_max)/(Isc_max*Voc_max);

figure
VP_MJSC_Ymax = Pmax*1.1;
%Y-axis maximum
MJSC_Xmax = max(VP_vq_Total)*1.1;

plot(VP_MJSC_Total_interp(:,1),VP_MJSC_Total_interp(:,2),'DisplayName','Tot
al VP characteristic curve','LineWidth',1.5,'Color',[0.380392163991928
0.380392163991928 0.380392163991928]),hold on;

plot(VP_MJSC_interp_TT(:,1),VP_MJSC_interp_TT(:,2),'DisplayName','Top GaInP
junction','LineWidth',1.5,'Color',[0.200000002980232 0.400000005960464 1]);

plot(VP_MJSC_interp_MM(:,1),VP_MJSC_interp_MM(:,2),'DisplayName','Middle
GaInAs junction','LineWidth',1.5,'Color',[0 0.800000011920929
0.200000002980232]);

plot(VP_MJSC_interp_BB(:,1),VP_MJSC_interp_BB(:,2),'DisplayName','Bottom Ge
junction','LineWidth',1.5,'Color',[1 0.200000002980232 0.200000002980232]);

axis([0 PV_Xaxis Glob_Y VP_MJSC_Ymax ])
grid on
title({Model,'(D2) MJSC VP Characteristic curves.'});
xlabel('Voltage (V)')
ylabel('Power (W)')
legend('Total VP characteristic curve','Top GaInP junction','Middle GaInAs
junction','Bottom Ge junction'),'Location';'North';
```

```
Pin = Gstc*Area;                %Input power at (1000 W)/(Area m2)
Eta = ((Vmpp_max*Impp_max*FF)/Pin);  %Percent cell efficiency

figure
Ymax = max(Eta)*1.2;                    %Y-axis maximum
Xmax = Gc+10;                           %X-axis maximum
Xmin = Gc-10;
stem(Gc,Eta,'LineWidth',1.5); hold on
axis([Xmin Xmax Glob_Y Ymax])
grid on
title({Model,'(D2) MJSC Efficiency'});
xlabel('Irradiance (Gc)')
ylabel('Efficiency (Eta)')
legend('GaInP/GaInAs/Ge efficiency'),'Location';'North';

Table_2 = {Pmax,Impp_max,Vmpp_max,Voc_max,Isc_max,Pin,FF,Eta};

xlswrite(Data_Hussain,Table_2,'Base','H29')
```

Appendix 18 Simulink D2 MJSC block model

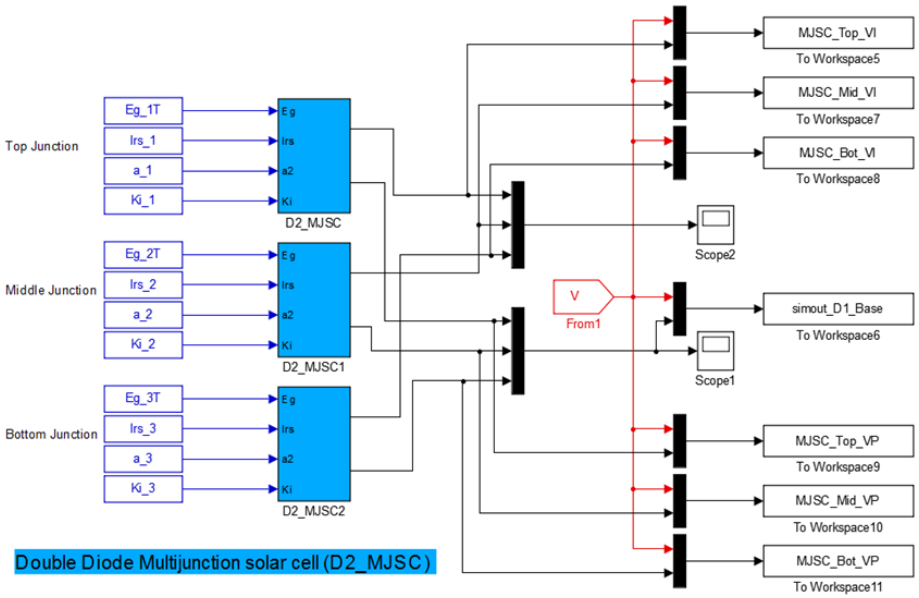

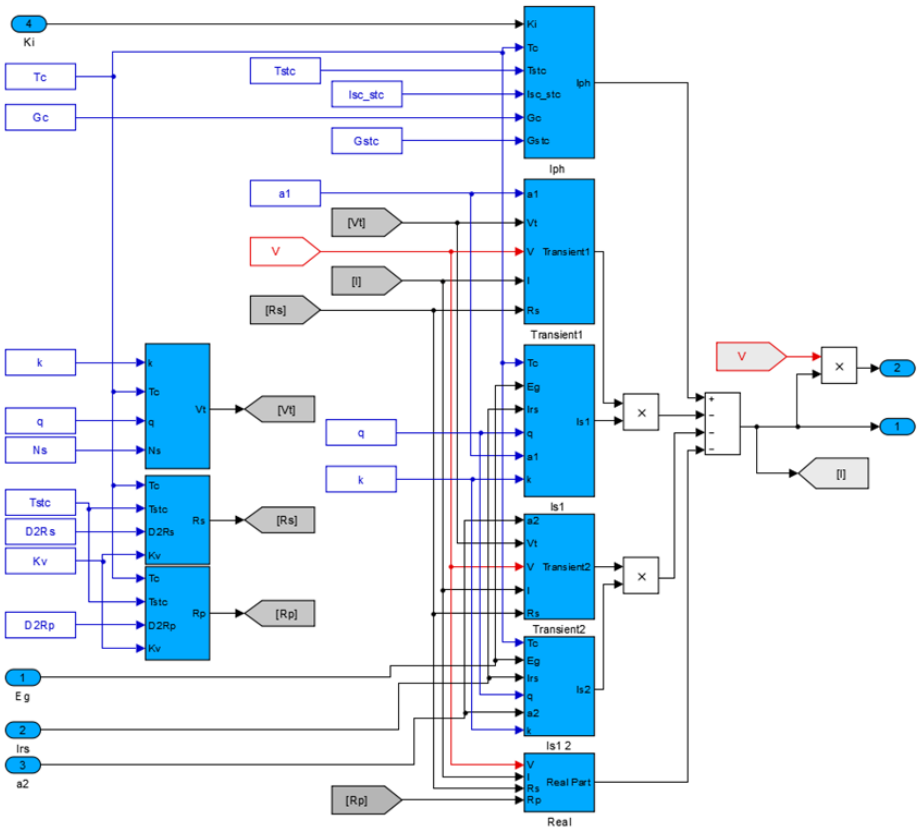

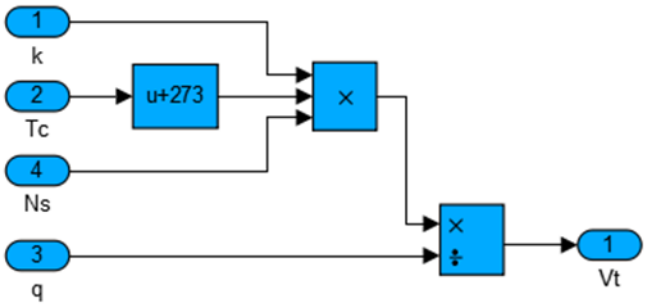
1
k
2
Tc
u+273
4
Ns
3
q
1
Vt

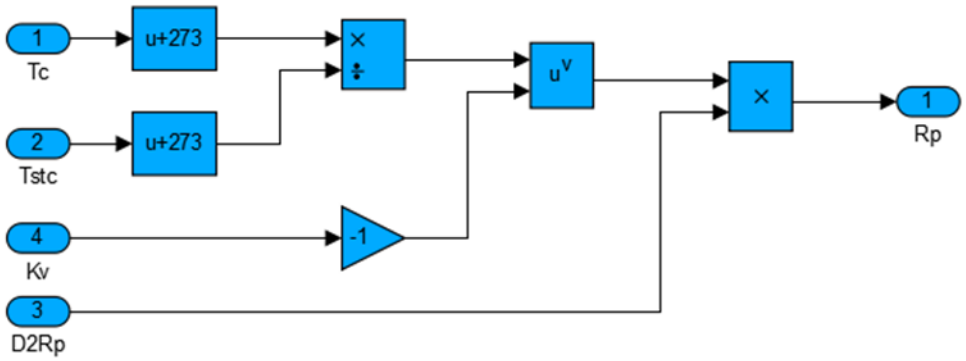
1
Tc
u+273
2
Tstc
u+273
4
Kv
-1
3
D2Rp
u^v
1
Rp

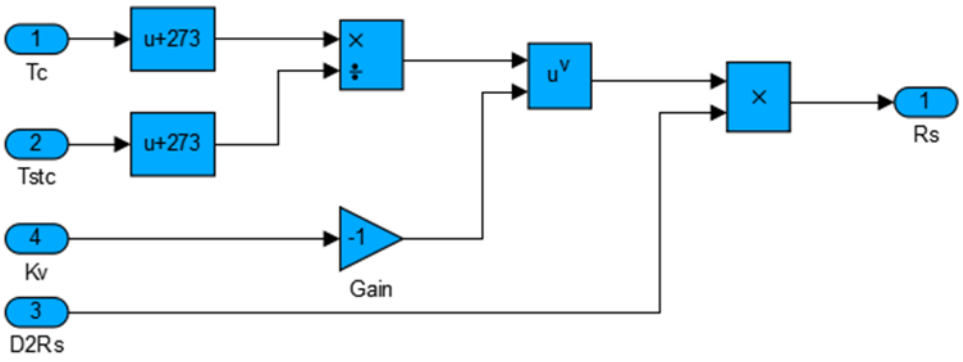
1
Tc
u+273
2
Tstc
u+273
4
Kv
-1
Gain
3
D2Rs
u^v
1
Rs

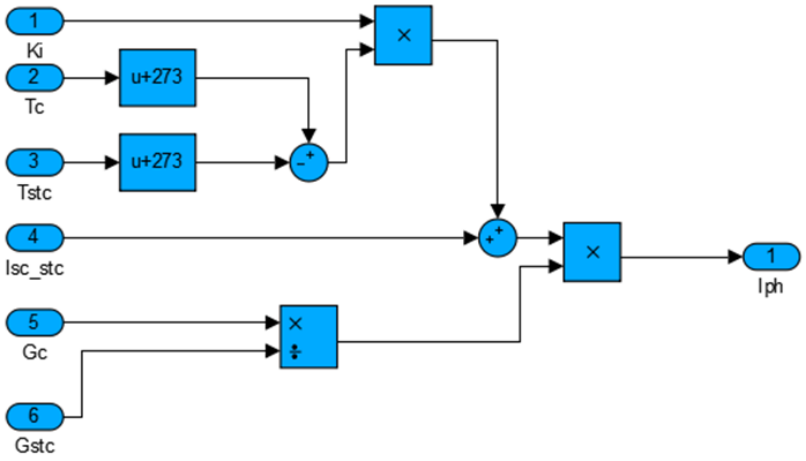
1
Ki
2
Tc
u+273
3
Tstc
u+273
4
Isc_stc
5
Gc
6
Gstc
1
Iph

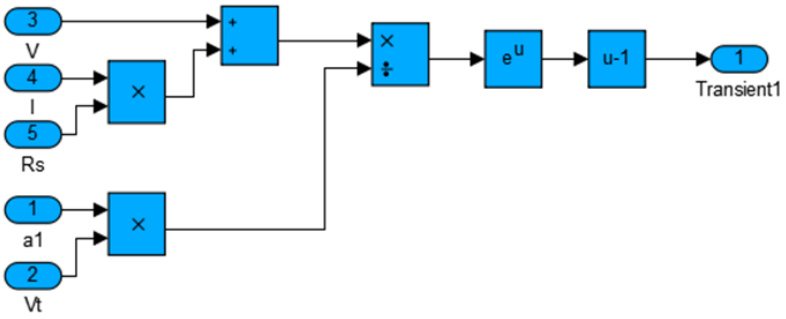
3
V
4
I
5
Rs
1
a1
2
Vt
e^u
u-1
1
Transient1

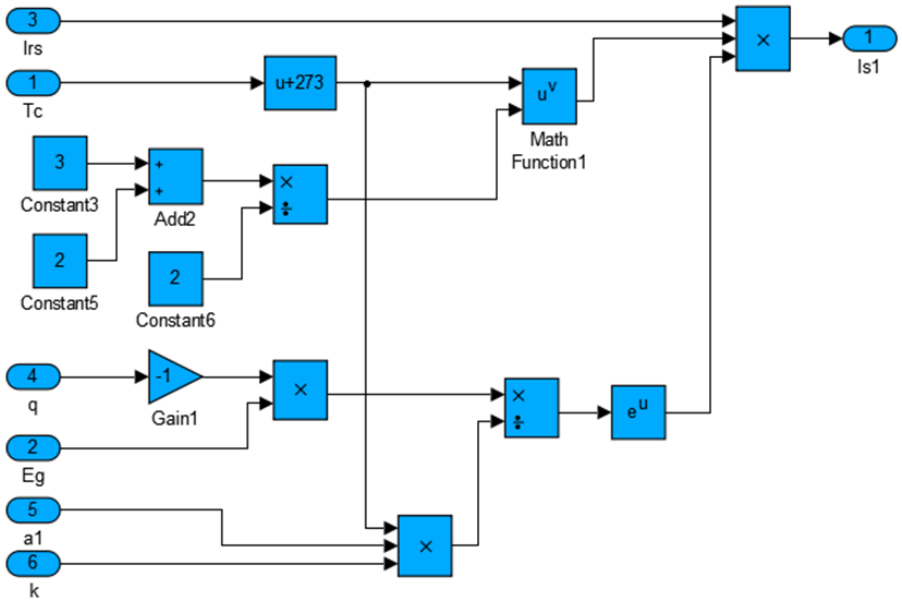
3
Irs
1
Tc
u+273
u^v
Math
Function1
3
Constant3
Add2
2
Constant5
2
Constant6
4
q
-1
Gain1
2
Eg
5
a1
6
k
e^u
1
Is1

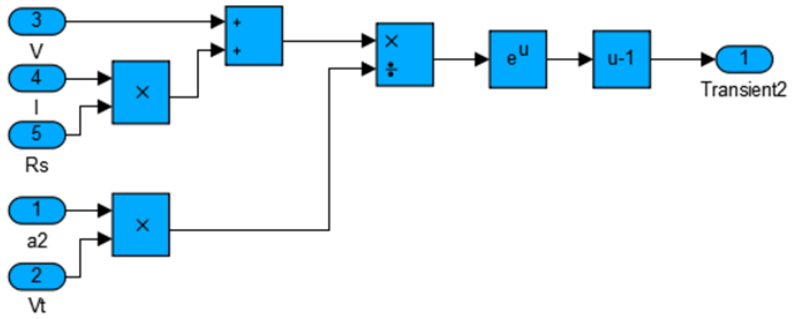
3
V
4
I
5
Rs
1
a2
2
Vt
e^u
u-1
1
Transient2

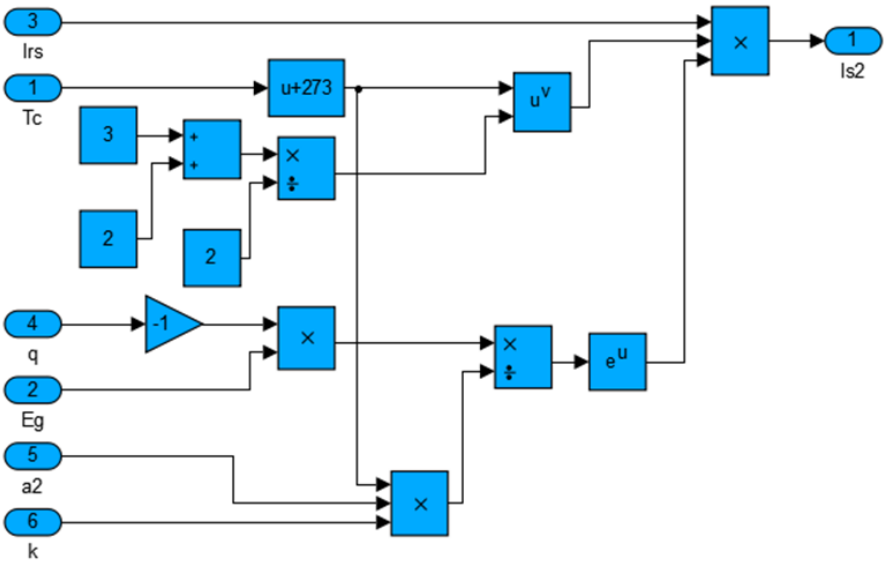
3
Irs
1
Tc
3
2
2
u+273
u^v
1
Is2
4
q
-1
2
Eg
5
a2
6
k
e^u

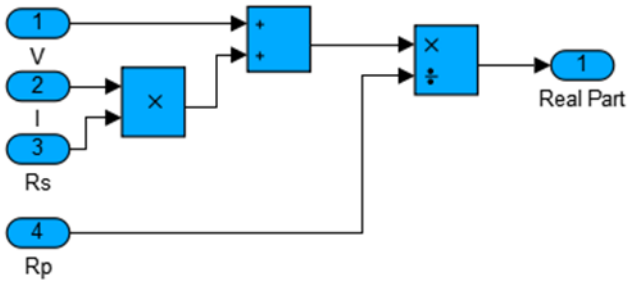
1
V
2
I
3
Rs
4
Rp
1
Real Part

Appendix 19 GaInP/GaInAs/Ge simulation results

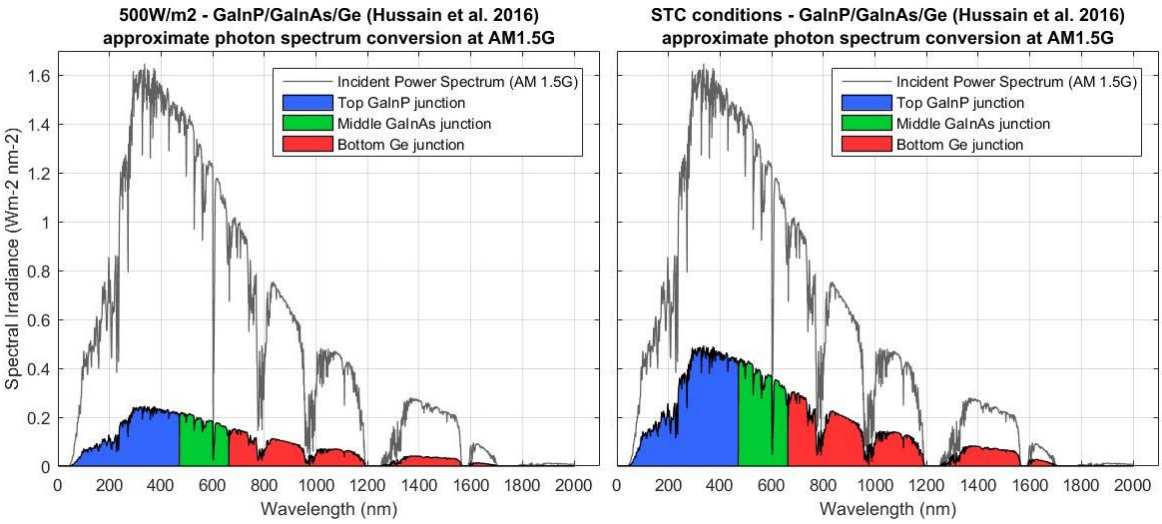

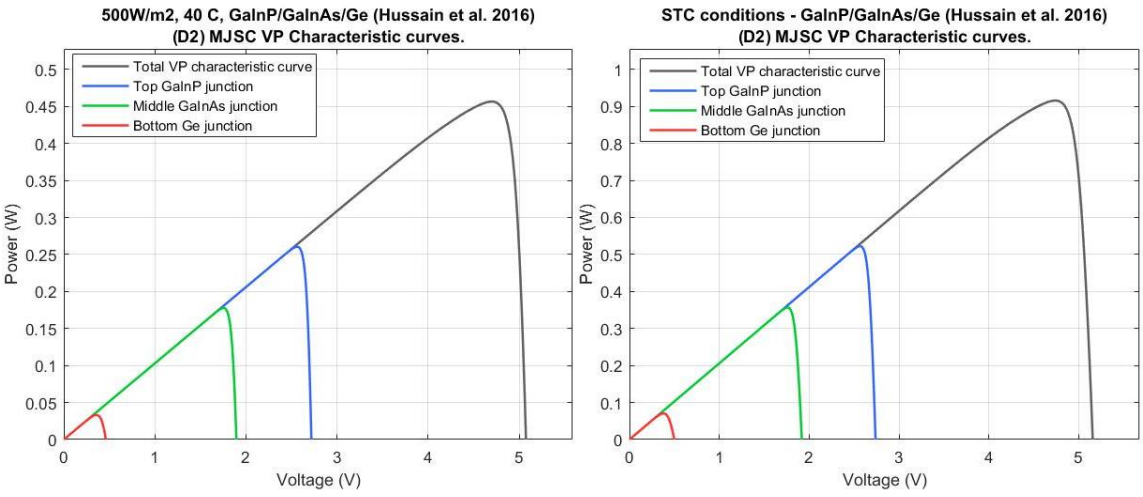

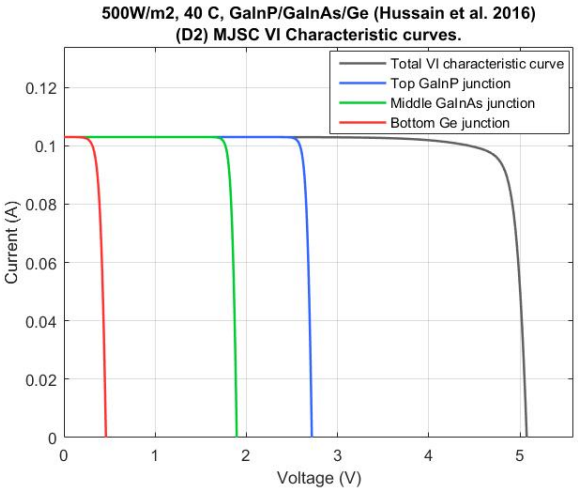
500W/m2, 40 C, GaInP/GaInAs/Ge (Hussain et al. 2016)
(D2) MJSC VI Characteristic curves.
Total VI characteristic curve
Top GaInP junction
Middle GaInAs junction
Bottom Ge junction
Current (A)
Voltage (V)

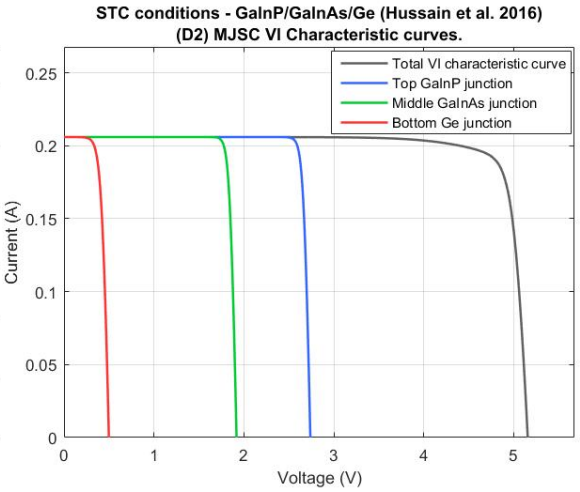
STC conditions - GaInP/GaInAs/Ge (Hussain et al. 2016)
(D2) MJSC VI Characteristic curves.
Total VI characteristic curve
Top GaInP junction
Middle GaInAs junction
Bottom Ge junction
Current (A)
Voltage (V)

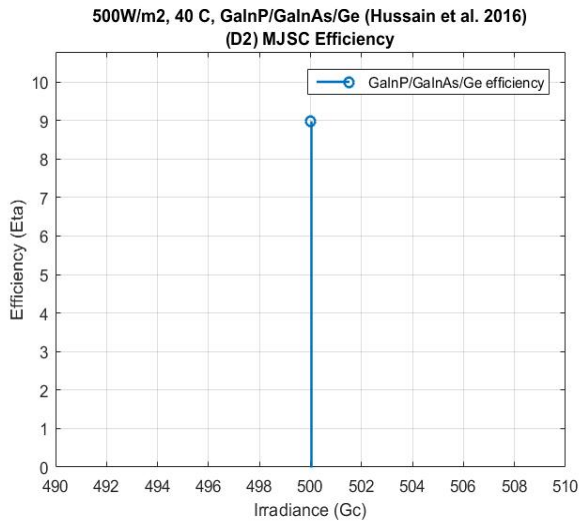
500W/m2, 40 C, GaInP/GaInAs/Ge (Hussain et al. 2016)
(D2) MJSC Efficiency
GaInP/GaInAs/Ge efficiency
Efficiency (Eta)
Irradiance (Gc)

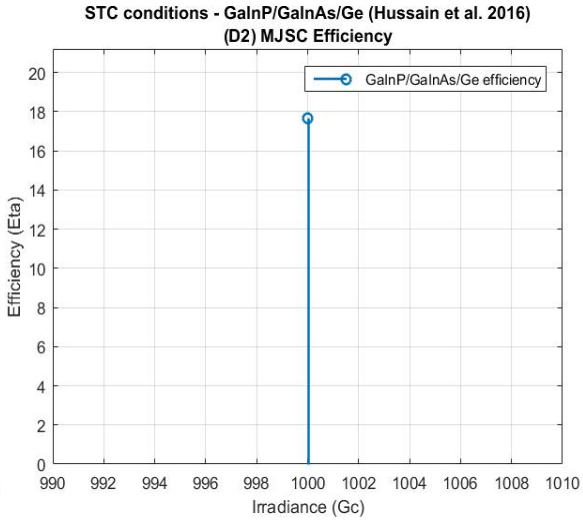
STC conditions - GaInP/GaInAs/Ge (Hussain et al. 2016)
(D2) MJSC Efficiency
GaInP/GaInAs/Ge efficiency
Efficiency (Eta)
Irradiance (Gc)

Appendix 20 Results of GaInP/GaAs/Ge (D2) simulation

Initial Parameters: GaInP/GaAs/Ge (Chen et al. 2015) (D2) triple MJSC.			
Parameter:	**Value**	**Parameter:**	**Value**
Voc_stc (V)	2.63	a3 (lower junct.)	1.96
Isc_stc (A)	0.01714	Spec1 (%) (top junct.)	
Vmpp_stc (V)	2.32	Spec2 (%) (mid junct.)	
Impp_stc (A)	0.0167	Spec3 (%) (lower junct.)	
Pmpp_stc (W)	0.038744	Irs_1 (A) (top junct.)	0.00002745
Irradiance (W/m2)	1000	Irs_2 (A) (mid junct.)	0.00002016
Temperature (‘C)	25	Irs_3 (A) (lower junct.)	0.00001863
Cell Area (m^2)	0.000116	KI1 (A) (top junct.)	0.00075
Number of cells	1	KI2 (A) (middle junct.)	0.000558
RS (Ω)	0.219	KI3 (A) (lower junct.)	0.0004774
RP (Ω)	2000000	β1 (K) (top junct.)	372
a1 (top junct.)	1.97	β2 (K) (mid junct.)	204
a2 (mid junct.)	1.75	β3 (K) (lower junct.)	235
Junction:	**Material**	**Bandgap (ev)**	**Wavelength (nm)**
Upper/top (Eg1)	GaInP	1.81	685
Middle (Eg2)	GaAs	1.405	882
Lower/bottom (Eg3)	Ge	0.69	1797

Simulation Results: GaInP/GaAs/Ge (Chen et al. 2015) (D2) triple MJSC.								
	Pmpp (W)	**Impp (A)**	**Vmpp (V)**	**Voc_stc (V)**	**Isc_stc (A)**	**Pin (W/m^2)**	**FF (%)**	**η (%)**
(Chen et al 2015) Results	0.0387	0.0167	2.32	2.63	0.01714	0.116	0.859	28.707
Simulation	0.038	0.016	2.413	2.630	0.017	0.116	0.846	28.303
% Error	1.619	3.646	-4.008	0.000	0.000	-	1.619	1.406

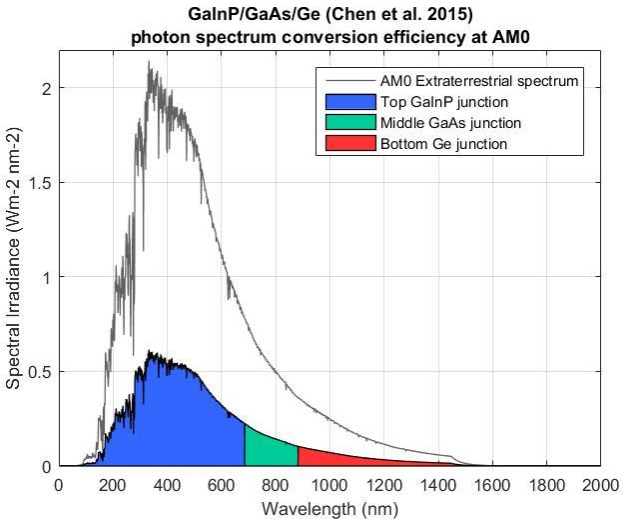
GaInP/GaAs/Ge (Chen et al. 2015)
photon spectrum conversion efficiency at AM0
AM0 Extraterrestrial spectrum
Top GaInP junction
Middle GaAs junction
Bottom Ge junction
Spectral Irradiance (Wm-2 nm-2)
Wavelength (nm)
0
0.5
1
1.5
2
0
200
400
600
800
1000
1200
1400
1600
1800
2000

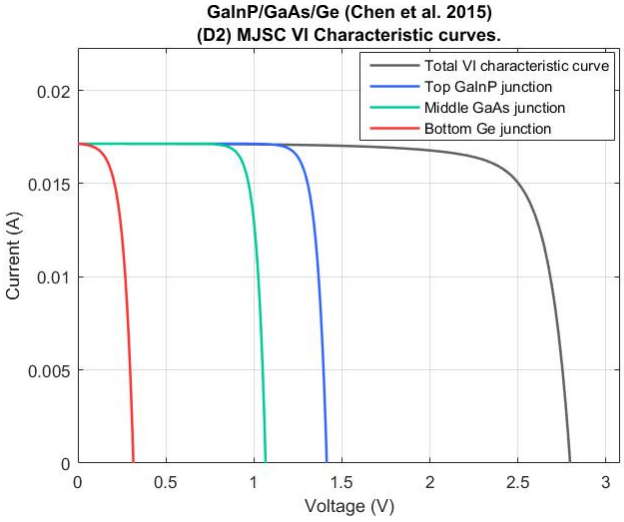
GaInP/GaAs/Ge (Chen et al. 2015)
(D2) MJSC VI Characteristic curves.
Total VI characteristic curve
Top GaInP junction
Middle GaAs junction
Bottom Ge junction
Current (A)
Voltage (V)
0
0.005
0.01
0.015
0.02
0
0.5
1
1.5
2
2.5
3

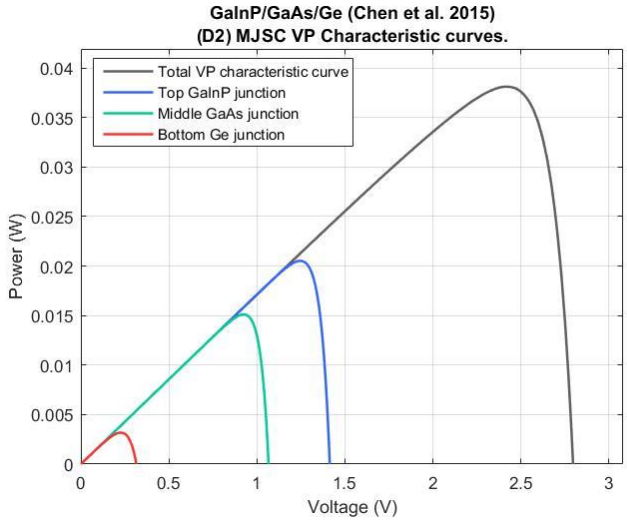
GaInP/GaAs/Ge (Chen et al. 2015)
(D2) MJSC VP Characteristic curves.
Total VP characteristic curve
Top GaInP junction
Middle GaAs junction
Bottom Ge junction
Power (W)
Voltage (V)
0.04
0.035
0.03
0.025
0.02
0.015
0.01
0.005
0
0.5
1
1.5
2
2.5
3

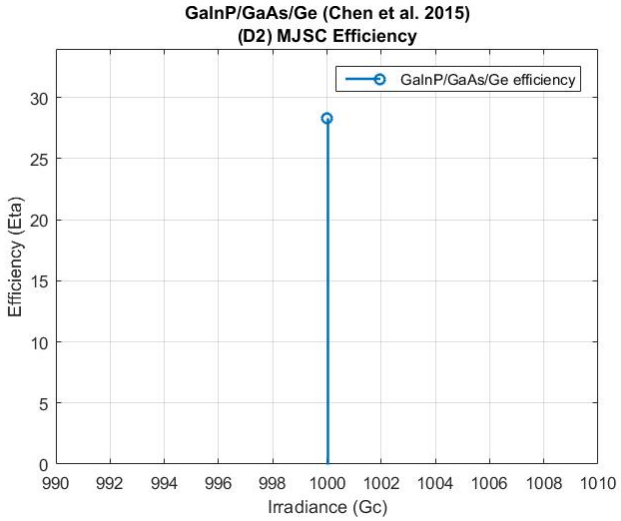
GaInP/GaAs/Ge (Chen et al. 2015)
(D2) MJSC Efficiency
GaInP/GaAs/Ge efficiency
Efficiency (Eta)
Irradiance (Gc)
30
25
20
15
10
5
0
990
992
994
996
998
1000
1002
1004
1006
1008
1010